การสังเคราะห์ไบพิริดิลพอร์ไฟรินเพื่อใช้เป็นสารไวแสงสีย้อมในเซลล์สุริยะ

นางสาวปรียานุช ดวงละออ

วิทยานิพนธ์นี้เป็นส่วนหนึ่งของการศึกษาตามหลักสูตรปริญญาวิทยาศาสตรดุษฎีบัณฑิต
สาขาวิชาเคมี ภาควิชาเคมี
คณะวิทยาศาสตร์ จุฬาลงกรณ์มหาวิทยาลัย
ปีการศึกษา 2555

SYNTHESIS OF BIPYRIDYLPORPHYRINS AS DYE-PHOTOSENSITIZERS FOR SOLAR CELLS

Miss Preeyanut Duanglaor

A Dissertation Submitted in Partial Fulfillment of the Requirements
for the Degree of Doctor of Philosophy Program in Chemistry
Department of Chemistry
Faculty of Science
Chulalongkorn University
Academic year 2012

Thesis Title	SYNTHESIS OF BIPYRIDYLPORPHYRINS AS DYE-PHOTOSENSITIZERS FOR SOLAR CELLS
By	Miss Preeyanut Duanglaor
Field of Study	Chemistry
Thesis Advisor	Associate Professor Buncha Pulpoka, Ph. D.

Accepted by the Faculty of Science, Chulalongkorn University in Partial Fulfillment of the Requirements for the Doctoral Degree

…….. Dean of the Faculty of Science
(Professor Supot Hannongbua, Dr.rer.nat)

THESIS COMMITTEE

…….. Chairman
(Associate Professor Sirirat Kokpol, Ph. D.)

……..……. Thesis Advisor
(Associate Professor Buncha Polpoka, Ph. D.)

…….. Examiner
(Associate Professor Nuanphun Chantarasiri, Ph. D.)

…….. Examiner
(Professor Orawon Chailapakul, Ph. D.)

…….. Examiner
(Associate Professor Nongnuj Muangsin, Ph. D.)

…….. External Examiner
(Assistant Professor Tienthong Thongpanchang, Ph. D.)

ปรียานุช ดวงละออ : การสังเคราะห์ไบพิริดิลพอร์ไฟรินเพื่อใช้เป็นสารไวแสงสีย้อมในเซลล์สุริยะ (SYNTHESIS OF BIPYRIDYLPORPHYRINS AS DYE-PHOTOSENSITIZERS FOR SOLAR CELLS) อ. ที่ปรึกษาวิทยานิพนธ์หลัก: รศ. ดร. บัญชา พูลโภคา, 128 หน้า.

สารประกอบไบพิริดิลพอร์ไฟรินได้ถูกออกแบบและสังเคราะห์สำหรับใช้เป็นสารสีย้อมไวแสงในเซลล์สุริยะ โดยสารสีย้อมไวแสงประกอบด้วยหมู่ให้อิเล็กตรอน (D) ต่อกับหมู่รับอิเล็กตรอน (A) ซึ่งมีส่วนพอร์ไฟรินทำหน้าที่เป็นหมู่ให้อิเล็กตรอน (D) และส่วนไบพิริดีนทำหน้าที่เป็นหมู่ดึงอิเล็กตรอน (A) สารที่สังเคราะห์ได้ถูกตรวจสอบเอกลักษณ์และยืนยันโครงสร้างของสาร ด้วยเทคนิค NMR, IR, Mass spectroscopy และ Elemental Analysis จากการศึกษาสมบัติเชิงไฟฟ้าประกอบกับสเปกตรัมการดูดกลืนแสงและการคำนวณทางทฤษฎีพบว่า ระดับพลังงานในชั้น HOMO และ LUMO ที่ได้จากการทดลองและการคำนวณทางทฤษฎีมีค่าระดับพลังงานที่เหมาะสม โดยค่าระดับพลังงานของชั้น HOMO มีค่าที่เหมาะสมกับแถบการนำไฟฟ้าของสารกึ่งตัวนำไทเทเนียมไดออกไซด์ ทำให้อิเล็กตรอนสามารถส่งผ่านจากสารสีย้อมไวแสงมาที่สารกึ่งตัวนำไทเทเนียมไดออกไซด์ได้ และระดับพลังงานของชั้น LUMO มีค่าที่เหมาะสมกับค่ารีด็อกซ์โพเทนเชียลของอิเล็กโทรไลท์ชนิด I^-/I_3^- ซึ่งทำให้สารสีย้อมไวแสงสามารถรับอิเล็กตรอนจากอิเล็กโทรไลท์ได้ ในการศึกษาประสิทธิภาพการเปลี่ยนพลังงานแสงอาทิตย์เป็นพลังงานไฟฟ้าของเซลล์สุริยะ ภายใต้ความเข้มแสง 1.5 AM และใช้ระบบ 0.10 M ลิเทียมไอโดด์, 0.05 M ไอโอดีน, 0.40 M พิริดีน และ 0.60 M TPAI เป็นอิเล็กโทรไลท์ในการประกอบเซลล์สุริยะ พบว่าให้ค่าประสิทธิภาพโดยรวมในการเปลี่ยนพลังงานแสงอาทิตย์เป็นพลังงานไฟฟ้า (η) ของสารประกอบไบพิริดิลพอร์ไพริน **A5**, **A6**, **A7** และ **A8** เท่ากับ 0.05, 0.28, 0.38 และ 0.05 % ตามลำดับ ซึ่งมีค่าต่ำกว่าสารไวแสงสีย้อมมาตรฐาน **N719** ที่ให้ค่าประสิทธิภาพเท่ากับ 5.97% จากค่าความหนาแน่นกระแสของสารสีย้อมไบพิริดิลพอร์ไฟรินมีค่าต่ำแสดงให้เห็นว่าความสามารถในการส่งผ่านอิเล็กตรอนจากสารสีย้อมไปสู่ไทเทเนียมไดออกไซด์เกิดขึ้นได้น้อยกว่าสารมาตรฐาน นอกจากนั้นพบว่าค่าประสิทธิภาพเพิ่มขึ้นเมื่อเติมกรดคีโนดีออกซีโคลลิคซึ่งใช้เป็นสารแข่งขันในการยึดเกาะพื้นผิวกับสารกึ่งตัวนำไทเทเนียมไดออกไซด์ในอัตราส่วนที่เหมาะสม

ภาควิชา เคมี ลายมือชื่อนิสิต.....

สาขาวิชา เคมี ลายมือชื่อ อ.ที่ปรึกษาวิทยานิพนธ์หลัก.....

ปีการศึกษา 2555

4872366423: MAJOR CHEMISTRY
KEYWORDS: DYE-SENSITIZED SOLAR CELLS / PHOTOSENSITIZER / PORPHYRIN / RUTHENIUM COMPLEX / DONOR-ACCEPTOR SYSTEM

PREEYANUT DUANGLAOR: SYNTHESIS OF BIPYRIDYL-PORPHYRINS AS DYE-PHOTOSENSITIZERS FOR SOLAR CELLS. ADVISOR: ASSOC. PROF. BUNCHA PULPOKA, Ph. D., 128 pp.

Bipyridylporphyrin derivatives were designed and synthesized for use as dye-sensitizer in dye-sensitized solar cells (DSSCs). Bipyridylporphyrin derivatives composed of Donor-Acceptor system (D-A) based on porphyrin moiety as the electron donor (D) and bipyridyl moiety as the electron-acceptor (A). All compounds were characterized and confirmed structures by NMR, IR, Mass spectroscopy and Elemental Analysis. From the experimental and the theoretical calculation, the HOMO and LUMO energy levels of all compounds are in range, which match well with the CB band of TiO_2 favoring electron injection from the exited dyes (s*) to TiO_2 and the redox potential of the I^-/I_3^-electrolyte favoring electron injection from the electrolyte to the cationic dyes (S^+). Upon the studies of the photovoltaic performance measurements, a overall solar-to-electric conversion efficiency under AM 1.5 irradiation and use 0.10 M LiI, 0.05 M I_2, 0.40 M pyridine and 0.60 M TPAI as electrolytic system of 0.05, 0.28, 0.38 and 0.05 % was achieved based on the bipyridylporphyrin dyes **A5**, **A6**, **A7** and **A8**, respectively, which were lower than the efficiency (5.97%) obtained from the standard dye **N719**. From the short circuit photocurrent density of the bipyridylporphyrin dyes **A5**, **A6**, **A7** and **A8**, showed lower than the standard dye **N719**, possibly due to poorer electron injection from bipyridylporphyrin dyes onto the TiO_2 surface. In addition, the efficiency of the dye was improved by adding chenodeoxycholic acid (CDCA) as the coadsorbant.

Department Chemistry Student's Signature .....
Field of Study Chemistry Advisor's Signature .....
Academic Year 2012

ACKNOWLEDGEMENTS

I am sincerely thankful to my advisor, Assoc. Prof. Dr. Buncha Pulpoka for guidance and support my thesis from the initial to the final stage to solve all of problem.

I would like to show gratitude to Assoc. Prof. Dr. Sirirat Kokpol, chairman of thesis defense committee, for her kind attention and suggestion. I am grateful to Assoc. Prof. Dr. Nuanphun Chantarasiri, Prof. Dr. Orawon Chailapakul, Assoc. Prof. Dr. Nongnuj Muangsin from Department of Chemistry, Faculty of Science, Chulalongkorn University and Assist. Prof. Dr. Tienthong Thongpanchang, thesis committe from Department of Chemistry, Faculty of Science, Mahidol University, for their kind attention and valuable recommendation.

I am delighted to express my pleasure to thank Assoc. Prof. Dr. Vinich Promarak, Assist. Prof. Dr. Taweesak Sudyoadsuk, Dr. Sayant Saengsuwan, Mr. Pongsathorn Tongkasee and all of Center for Organic Electronic and Alternative Energy's members for allowing me to use their facilities, doing my experiment on fabrication and photovoltaic experiment of dye sensitized solar cells and their warm-hearted friendship at Ubon Ratchathani University. I would like to thank Prof. Dr. Thawatchai Tuntulani and Assoc. Prof. Dr. Vithaya Ruangpornvisuti for invaluable suggestions in my thesis and computational studies. Moreover, it is my pleasure to thank everyone in Supramolecular Research Unit for their personal friendships, suggestions and support. Furthermore, my appreciation is also given to The Royal Golden Jubilee Ph.D. Program (Grant No. PHD/0226/2549; 3.C.CU/49/W.1) from the Thailand Research Fund (TRF) for financial support.

Finally, I would like to dedicate this thesis to my family who constantly present their understandings and encouragement to me during both of my pleasant and hard time. This thesis would not have been possible without their supports.

CONTENTS

Page

LIST OF TABLES

LIST OF FIGURES

Figures Page

LIST OF SCHEMES

LIST OF ABBREVIATIONS

^{1}H NMR	proton nuclear magnetic resonance
^{13}C NMR	carbon-13 nuclear magnetic resonance
$CDCl_3$	deuterated chloroform
$DMSO_{d6}$	deuterated dimethyl sulfoxide
DMSO	dimethylsulfoxide
DMF	*N*,*N*´-dimethylformamide
$MeOD_{d4}$	deuterated methanol
J	coupling constant
d	doublet (NMR)
dd	doublet of doublet (NMR)
m	multiplet (NMR)
t	triplet (NMR)
s	singlet (NMR)
Hz	hertz
ppm	parts per million
ATR-IR	attenuated total reflectance infrared spectroscopy
IR	infrared
MALDI-MS	matrix-assisted laser desorption/ionization mass spectrometry
m/z	mass per charge
UV	ultraviolet
TLC	thin layer chromatography
DFT	density functional theory
DSSC	dye sensitized solar cell
I_{sc}	photocurrent density
V_{oc}	open circuit voltage
FF	fill factor
η	efficiency
IPCE	incident photon to current conversion efficiency

AM	air mass
mA	milliampere
g	gram (s)
h	hour (s)
mg	milligram (s)
mL	milliliter (s)
mmol	millimole (s)
V	voltage (V)
I	current (A)
A	ampere
M	molar
RT	room temperature
FTO	fluorine-doped tin oxide
dcbp	4,4´-dicarboxy-2,2´-bipyridine
$TBAPF_6$	tetrabutylammonium hexafluorophosphate
$AgNO_3$	silver nitrate
CDCA	chenodeoxycholic acid
PMII	1-propyl-3-methylimdazolium iodide
TPAI	1,2-dimetyl-3-propyl imidazolium iodide
GBL	γ-butyrolactone
NMP	1-N-methyl-2-pyrrolidone
TBP	4-tert-butylpyridine
μM	micromolar
LiI	lithium iodide
I_2	iodine
δ	chemical shift
°c	degree celsius
%	yield percentage yield
HOMO	highest occupied molecular orbital
LUMO	lowest unoccupied molecular orbital
MLCT	metal-to-ligand charge transfer

CHAPTER I

INTRODUCTION

Nowadays, the energy crisis is the high potential problem due to increasing of the global energy demand and limitation of fossil fuel. From the energy report, the global will be confronted the energy crisis for the next few decades. Moreover, the processes for the conversion of the fuel to the usable energy can generate the pollutant into the environment. Hence, the renewable energies have become an important issue for overcoming the exhaustion of fuel energy resources [1].

It is clear that access to economically viable renewable energy sources is essential for the development of a globally sustainable society. Among all of the renewable energy resources such as solar, wind, water, and bioenergy, solar energy is the most attractive widespread attention due to a free huge amount of energy from the sun to the earth about 3×10^{34} J/year. Thus, if human can collect and convert the power from the sun into electricity in period of 0.1% with 10% an efficiency of device from the solar energy's crust on earth, the global will never confront of energy crisis [2]. In the other hand, the sunlight can convert to valuable electric power by photovoltaic device or solar cell. Most photovoltaic cells are made from silicon or heavy metals such as Indium, Copper and Cadmium but there are several disadvantages in using these inorganic materials. Moreover, solar cell that made from silicon is very expensive fabrication process and raw material and heavy metals are toxic and environmentally hazardous [1-3].

Thus, the other kind of solar cell called dye sensitized solar cells (DSSC) have been attracting widespread attention because of their high conversion of sunlight to electricity, easy preparation, environmentally friendly, and economically viable energy sources [4-7]. The best cells were investigated by Michael Gratzel and Brian O'regan in 1991 and are also known as Gratzel cells and presenting conversion efficiencies as high as 10-12% [1]. Although DSSCs cell showed the low efficiency than conventional silicon semiconductor (25%), the ease of fabrication and

application for flexible solar cell is very attractive enough to take the efforts in the development of this cell.

1.1 Dye-sensitized solar cells (DSSCs)

1.1.1 Introduction

The dye-sensitized solar cell (DSSC) is an alternative concept in solar energy after 40 years of the invention of silicon solar cell. Because the silicon must be extremely pure (99.9999%) and use a very high temperature for produce silicon from silica (SiO_2). This makes production of silicon solar cells very expensive. But the dye-sensitized solar cell is made from lower cost materials (TiO_2), easy to be fabricated, friendly to the environment and efficient to converse and storage sunlight to electricity. It is an efficiently concept to develop a solar cell [1].

1.1.2 Principle of dye-sensitized solar cells (DSSCs)

The dye-sensitized solar cells can be considered as a hybrid version of photogalvanic cells and solar cells based on semiconductor electrodes. The cell consists of 3 parts: dye-coated semiconductor electrode (anode), counter electrode (cathode) and electrolyte containing a redox mediator. In general in DSSC, it consists of 5 materials:

1) A fluorine-doped SnO_2 (FTO) conducting glass substrate
2) A nanocrystalline TiO_2 thin film as a semiconductor
3) A dye sensitizer
4) An electrolyte (redox mediator)
5) A platinum-coated glass substrate

On the anode, very porous layer of TiO_2 is constructed on the conducting glass. On the particles of TiO_2, a dye is adsorbed. Cathode is coated with Pt and (I^-/I_3^-) is the redox mediator [8].

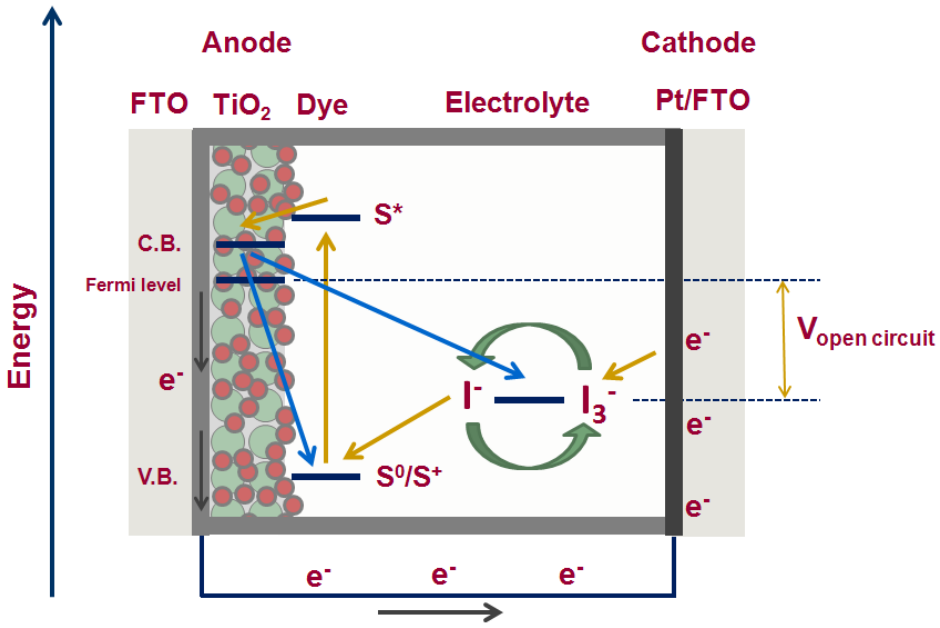

Figure 1.1 The principle of operation and energy level for the dye-sensitized solar cells.

A schematic presentation of the operating principles of the dye-sensitized solar cell is shown in Figure 1.1 When light falls onto the dye-sensitized solar cell, it is absorbed by the dye (S^0) with visible light and excite to an electronically excited state (S*). Photo-excitation of the dye is followed by electron injection into the conduction band of the TiO_2. The oxidized dye (S^+) is subsequently reduced back to the ground state (S^0) by the electron donation from the electrolyte (I^-). Then, I^- is generated in turn by reduction of I_3^- at the cathode. Finally, the circuit is completed via electron migration though the external circuit. The voltage generated under illumination corresponds to the difference between the Fermi level of the electron in the solid and the redox potential of the electrolyte. Consequently, the processes of electron injection from S* to CB band of TiO_2 and regeneration of the oxidized dye (S^+) by electrolyte must be kinetically more favourable than the recombination between dye S^+ and TiO_2 and also dark current in order to generate greater photocurrents and photovoltages [8].

Summary of the processes taking place during the regenerative cycle in the DSSCs.

Anode:

$S^0 + h\nu$	⟶	S^*	light absorption
S^*	⟶	$S^+ + e^-(TiO_2)$	electron injection
$2S^+ + 3I^-$	⟶	$2S^0 + I_3^-$	regenerate the dye

Cathode:

$I_3^- + 2e^-$	⟶	$3I^-$	regenerate the redox mediator

Other processes:

$2S^+ + e^-$ (on TiO_2)	⟶	S^0 (on TiO_2)	recombination
$I_3^- + e^-$ (on TiO_2)	⟶	$3I^-$	dark current

1.2 Materials

1.2.1 Mesoporous metal oxide electrode

In 1991, the breakthrough efficiency of DSSCs was achieved by the use of TiO_2 mesoporouse electrode coated on transparent conducting glass due to the high internal surface area to attack the dye-sensitizer. Although, TiO_2 still retains the highest efficiency, but other metal oxide such as ZnO, SnO_2, Nb_2O_5 and $SrTiO_3$ etc. have been investigated to improve the efficiency [9].

TiO_2 mesoporous electrode

TiO_2 mesoporous electrode is stable and nontoxic oxide, and is widely use in several kind of industrial product such as paint, toothpaste, self-cleaning materials and sunscreen etc. because of their high refractive index. Naturally, mesoporous TiO_2 can

be found in difference crystal structures: rutile, anatase, and brookite. Although rutile is a most stable form but anatase is suitable in DSSCs application because it has higher conduction band edge energy, E_c (3.2 vs 3.0 eV for rutile) [10]. This leads to the higher Fermi level and also higher open-circuit voltage in DSSCs application

The most common method to prepare TiO_2 nanoparticle is the hydrolysis of titanium (IV) alkoxide in a present of excess water by using acid or base as a catalyst followed by hydrothermal growth and crystallization. To deposit anatase particle onto conducting glass, the corresponding TiO_2 particle is formulated in paste with polymer additive. Deposition techniques can be doctor blading or screen printing. Finally, the coated conducting glass is sintered at about 450°C in air to eliminate all organic species and to make the electrical connection between the anatase particles [9].

1.2.2 Dye-sensitizers

The properties of dye-sensitizer should be achieved with some essential characteristics:

1) The dye-sensitizers for DSSCs should absorb across the entire visible and near-IR spectrum.

2) The dye-sensitizers must have at least one anchoring group for strongly binding onto electrode surface, has been achieved through a number of functional groups, such as carboxylic acid [11], sulphonic acid and phosphonic acid [12]. The most widely used and successful up to date is the carboxylic acid and phosphonic acid functionalities. The carboxylic acid group is easy to prepare, while ensuring efficient adsorption of the dye on the surface. The possible binding modes of chelation/derivatization was proposed by using IR and Raman spectroscopic data showing that the modes are ranging from electric interaction, chemical bonding (chelating or bridging mode) to H-bonding [9, 13-15] as shown in Figure 1.2.

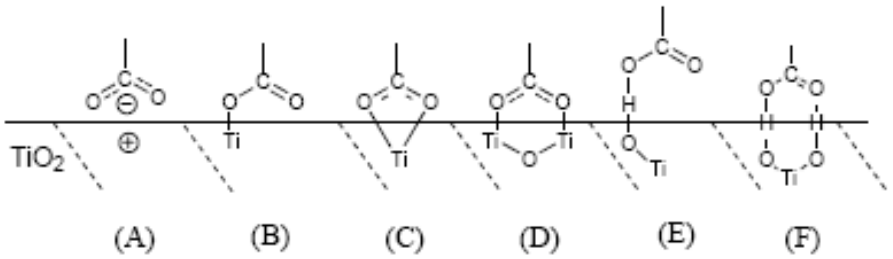

Figure 1.2 Possible binding modes for carboxylic acid group onto TiO_2 layer [14].

3) Efficient charge injection from the excited state of the dye into the conduction band of TiO_2 depends on the redox potential of the dye in the excited state. The excited state level of dye should be more negative than the conduction band edge of semiconductor to achieve the sufficient electron transfer process of electron from excited state of dye-sensitizer to the conduction band of semiconductor. In addition, the HOMO of the oxidized state level of the dye (S^+) should be more positive than the HOMO level of electrolyte to achieve the sufficient electron donation from the redox electrolyte.

4) The aggregation of dye-sensitizer on the semiconductor surface should be avoided by structured design or adding the coabsorbate to prevent dye-aggregation.

5) Stability of the dye is required over many years of exposure to sunlight.

Since, several dye-sensitizers including metal and metal-free compounds have been designed in several key criteria and applied to DSSCs.

1.2.3 Electrolyte

Nowadays, electrolytes have been applied and developed to fabricate DSSCs in many publication. To improve the conversion efficiency, electrolytic system was achieved by varying the redox electrolyte, the alternative solvent or adding coadsorbents.

1) Redox electrolyte

The most basic electrolyte is iodide/triiodide in polar organic solvent. Furthermore, lithium cation should be added to facilitate the electron transport in titania film. The study showed that the higher positive charge of cation and higher concentration in eletrolyte improve the dye absorption on semiconductor surface. Moreover, this iodide/triiodide electrolyte still keeps the highest efficiency for all DSSCs.

2) Additive

Since then a number of coadsorbents have been identified that increase the V_{OC}, the long term stability of the cell and/or suppress dye aggregation on the TiO_2-surface. There are two mechanisms by which the coadsorbent can alter the photovoltage of the DSSC. Firstly it may change the recombination rate between the TiO_2-conduction band and the electrolyte. Secondly the coadsorbent may alter the band edge position of the TiO_2-conduction band [9].

Additives play a central role in the enhancement of photoelectrochemical performance of DSSCs. Most additives are understood at a fairly phenomenological level, and their effects are often attributed to modification of redox couple potential, band shifts of the semiconducting electrode material, effects of surface blocking, or surface dye organization. Most additives that have been reported contain an electrondonating nitrogen heterocycle in a series of pyridine derivatives, such as 4-*tert*-butylpyridine, 2-propylpyridineor, pyridine etc. 4-*tert*-butylpyridine (TBP) was first applied in DSSC, demonstrating a remarkable increase in V_{oc} of these cells in combination with LiI-based electrolytes.

1.2.4 Counter Electrode

For counter electrode, the platinised conducting glass has been candidate for use as the material for efficient generation of I^-. Platinum is technically the best

material to construct the efficient devices. Due to the cost of Pt, many counter electrodes have been developed, including carbon cathode. Carbon cathodes have been a considerable candidates which can be used in many forms such as carbon black and carbon nanotube.

1.3 Efficiency measurement on solar cell performance

When the sun is directly overhead, the shortest path length between the sun and the earth is called called the *air mass* (AM) and can be calculated by following this equation; AM = 1/cos Θ_Z, where Θ_Z is the angle of elevation of the sun. The standard solar spectrum of AM 1.5 G (global) is used as the standard energy for efficiency measurements of solar cells, where is Θ_Z = 42°. This spectrum is normalized so that the integrated irradiance (the amount of radiant energy received from the sun per unit area per unit time) is 100 mW/cm^2. The spectrum is shown in Figure 1.3 as the irradiance of the sun as a function of wavelength [9].

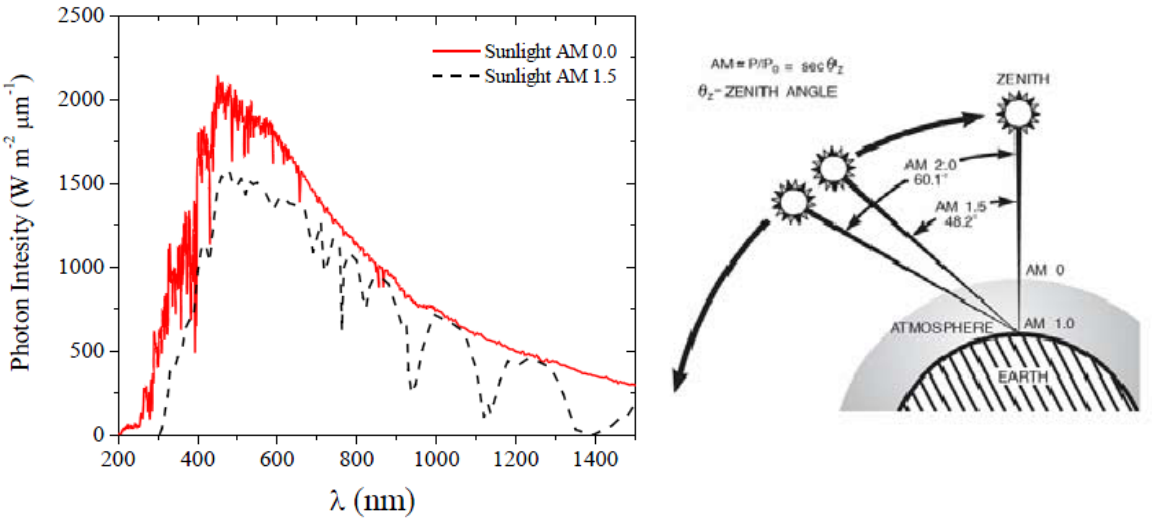

Figure 1.3 Spectra of sunlight at AM 0.0 and 1.5 [9].

Quantitative assessment of the solar cell performance is given by two key parameters: power conversion efficiency (η) and the incident photon-to-current conversion efficiency (IPCE) for monochromatic radiation [8].

1.3.1 Overall conversion efficiency of the photovoltaic cell (η)

The power conversion efficiency under white-light irradiation, η is calculated from the following equation:

$$\eta = FF \times J_{sc} \times V_{oc}/I_o$$

Where the fill factor (FF) is defined as $FF = P_{max} / (J_{sc}V_{oc})$, J_{sc} is the short circuit photocurrent density (mA/cm^2), V_{oc} is the open circuit photovoltage (V) and I_o is the intensity of the incident light (mW/cm^2).

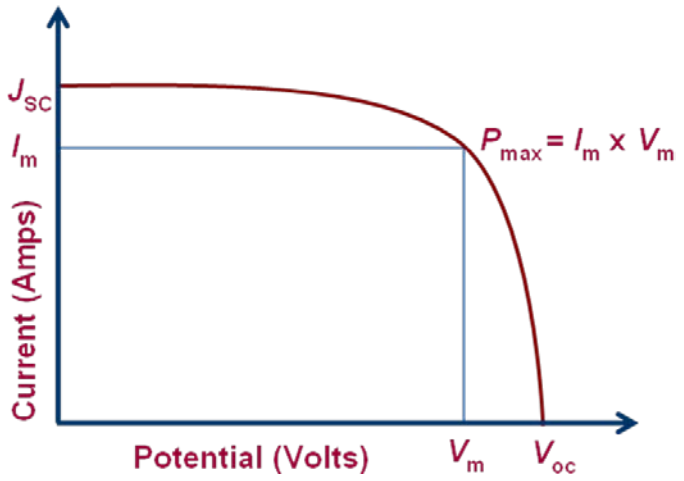

Figure 1.4 I-V Curve as function of light wavelength of solar cell tested under AM 1.5 conditions.

1.3.2 Incident photon to current conversion efficiency (IPCE)

The IPCE values are calculated by normalizing the photocurrent values for incident light energy and intensity for monochromatic radiation using:

$$\text{IPCE (\%)} = 1240 \times J_{sc}/(I_{inc} \times \text{wavelength})$$

Where J_{sc} is the short circuit photocurrent density (mA/cm^2), I_{inc} is the incident light intensity (mW/cm^2) and λ (nm) is the wavelength of the monochromatic light.

1.4 Literature reviews

1.4.1 Ruthenium as dye-sensitizers

Ruthenium complex come close to fulfilling their requirements for act as dye-sensitizer in DSSC due to their broad absorption according to metal to ligand charge transfer (MLCT) band in region of visible spectrum, bind strong to the semiconductor surface, have a suitable the HOMO-LUMO energy level, long-excited state lifetime and good stability. To date, the most successful DSSC is the commonly known Grätzel cell (1993) using Ru-polypyridyl based dyes adsorbed on nanocrystalline films of TiO_2. It has an overall solar light energy conversion efficiency (η) of 10.4% under AM 1.5 conditions [16-17].

The Ru complexes with bipyridine ligands were functionalized by thiocyanate to improve the electron injection into the TiO_2 conduction band and also reduced the recombination of charge from the electrode to the dye molecule via the result of the electron donating property of thiocynate ligand by shift the distribution of HOMO level of dye cation away from TiO_2 energy level and reducing the charge recombination process [18].

In 1999, the ruthenium dye **N719** has been developed by Nazeeruddin and coworkers. The effect of protons on anchoring group was investigated by replacing 2 proton of **N3** at a carboxylic position with 2 tetrabutylammonium ion and showed the higher overall conversion efficiency of 11.18% resulting in a factor of the short circuit photocurrent and the open circuit photovoltage of a DSSC [19].

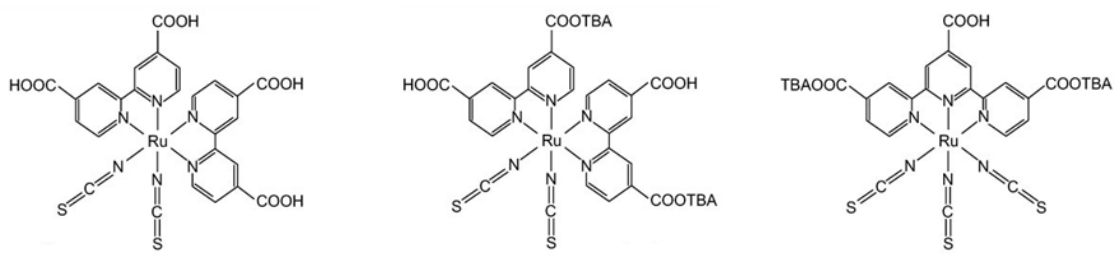

N 3
(10.4%)

N 719
(11.18%)

Black dye
(10.8%)

Figure 1.5 Ru-polypyridine photosensitizers used by Grätzel and coworker [19].

Moreover, the extended conjugated dye of terpyridil-Ru^{II} complex was investigated in 2001. Its extended absorption in the near infrared significantly enhances the overall conversion efficiency up to 10.4 % (1 cm^2 and 11.2 % for 0.26 cm^2) and call it as "**black dye**".

Since, the **N3** and **N719** have been used as a dye-reference and a building block for design of other dye-sensitizer by changing an ancillary ligand to improve the efficiency to convert sunlight to electricity.

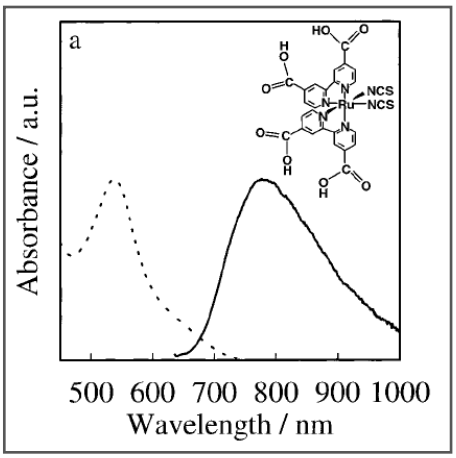

(….) absorption spectra

(—) emission spectra

Figure 1.6 Absorption and emission spectrum of **N3**.

1.4.2 Porphyrin as dye-sensitizers

For light harvesting in DSSCs, porphyrins are one of the most widely studied sensitizers because of their strong Soret band around 400–450 nm and moderate Q bands around 550–600 nm [20-34]. Furthermore, the porphyrin-based dyes have several intrinsic advantages, such as good photostability, their rigid molecular structures with large absorption and their many reaction sites for functionalization by variety of covalent or noncovalent compounds.

First time, DSSC based on Chlorophyll (Chl) derivatives and related porphyrins were modified by Grätzel and coworker to obtain IPCE and η of 80% and 2.6% for a TiO_2 electrode sensitized [20].

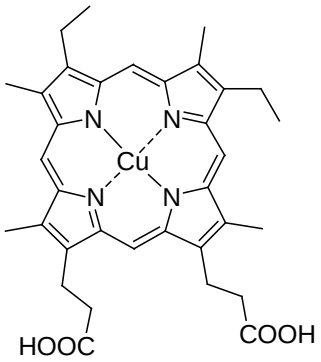

Figure 1.7 Structure of Chlorophyll (Chl) derivatives [20].

Dabestani *et al.* investigated sensitization of the Zn tetracarboxyphenyl porphyrin (ZnTCPP) on porous, nanocrystalline electrodes and obtained a maximum quantum efficiency of 9.5% (surface coverage 1.7 x 10^{-10} mol/cm^2) and 27 % (surface coverage 5.0 x 10^{-12} mol/cm^2) on an anatese TiO_2 and $SrTiO_2$ semiconductor electrode, respectively [13].

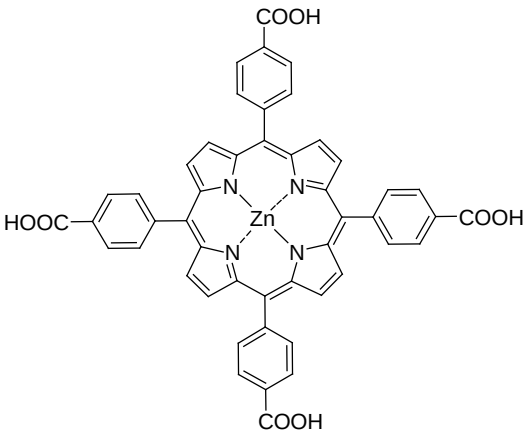

Figure 1.8 Structure of tetrakis(4-carboxyphenyl)porphyrins (**ZnTCPP**) [13].

In 2005, Gervaldo and coworkers synthesized a series of metalloporphyrin to investigate the effect of metallation on porphyrins (Free-base (P), Zn(II) (P_{Zn}), Cu(II) (P_{Cu}), Pd(II) (P_{Pd}), Ni(II) (P_{Ni}), and Co(II) (P_{Co}) 5-(4-carboxyphenyl)-10,15,20-tris(4-methylphenyl)porphyrins). The study showed that P(Ni) and P(Co) do not exhibit a photocurrent due to the HOMO level come close to VB of TiO_2 and lead to electron recombination from TiO_2 to dye S^+. In case of Free-base (P) and Zn(II) (P_{Zn}), photocurrent were occurred [22].

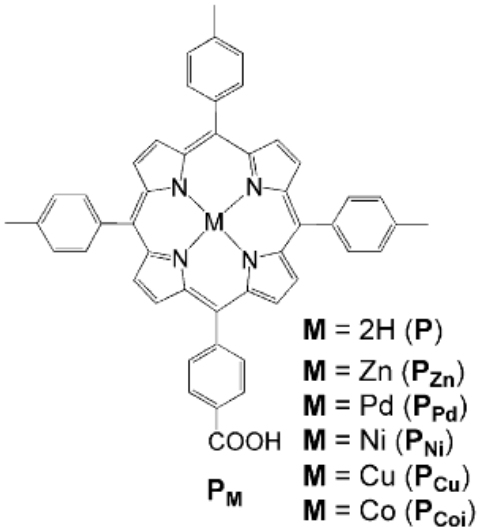

Figure 1.9 Structure of a series of metalloporphyrin [22].

Four *para*- and *meta*- Zn(II) tetra(carboxyphenyl)porphyrins [23] were studies to determine the effect of the spacer length and anchoring group position. The results from UV, IR, and solar efficiency suggest that the *meta* substitution favores a planar binding mode to the oxide surfaces. *Para* substitution favores a vertical binding to formation of H-aggregates. The greater efficiency of the shorter rigid planar *meta*-substituted systems was explained in terms of a greater charge injection into the TiO_2 semiconductor from rings that lie flat, and closer, to the surface.

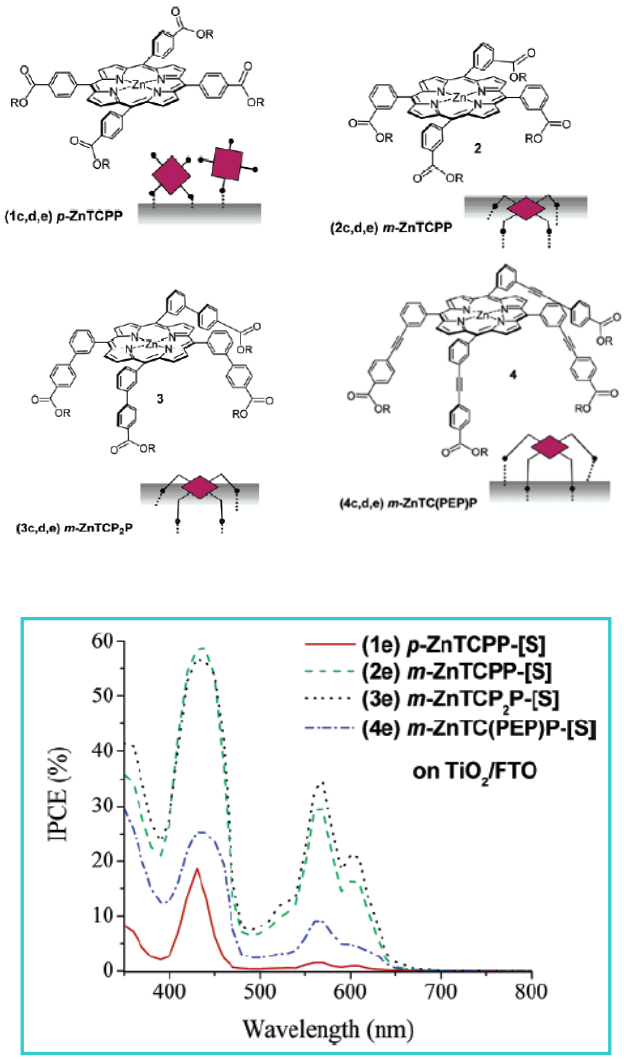

Figure 1.10 Model to determine influence of geometry binding and distance from surface and photocurrent action spectra of tetra(triethylammonium) carboxyporphyrin salts [23].

In 2007, porphyrin sensitizer containing the linker and anchor unit functionalized at the *β*-position has been developed by Campbell and coworkers [24]. The photovoltaic characteristics exhibited an excellent cell performance with a short-circuit photocurrent density ($J_{sc,}$), an open-circuit voltage (V_{oc}) and a fill factor (*FF*) and conversion efficiency as 14.0 mA/cm^2, 608 mV, 0.74 and 7.1%, respectively.

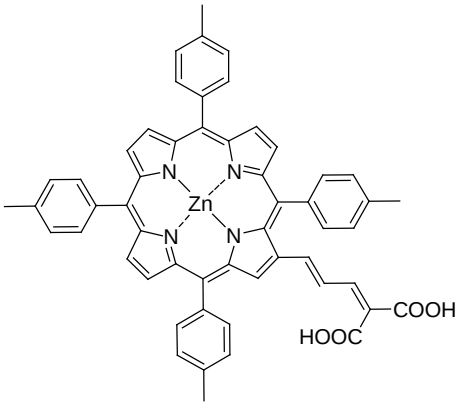

Figure 1.11 Structure and of porphyrin sensitizer [24].

In 2005, Hasobe *et al.* have synthesized quaternary self-organization of porphyrin and fullerene units by clusterization with gold nanoparticles as three-dimentional arrays onto nanostructured SnO_2. The composite cluster electrode exhibited an incident photon-to-photocurrent efficiency (IPCE) as high as 54 % and broad photocurrent action spectra (up to 1000 nm). The power conversion efficiency of the cluster reached as high as 1.5 % [25].

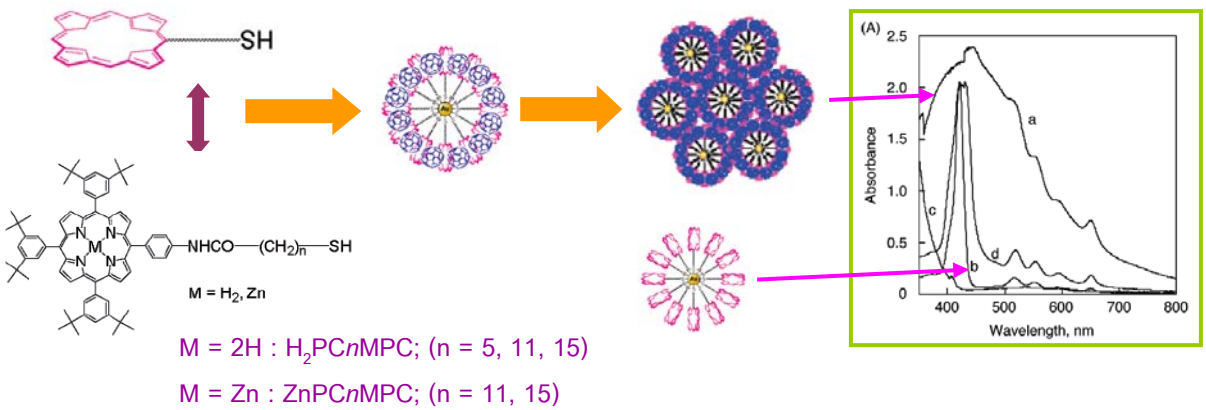

Figure 1.12 Structure and absorption spectra of quaternary self-organization cluster [25].

After the discovery of DSSCs, Donor-Acceptor system has become the subject of designing the dye-sensitizer to improving and tuning the overall conversion efficiency.

In 2009, Lee and coworker was success to synthesized novel *meso*-derivatized porphyrin composing *tert*-butyl groups onto phenyl rings as electron donating group, and decreasing of dye aggregation on semiconductor surface. The new dye showed the broad spectrum and red shift of the Soret and Q-bands and exhibited a short-circuit photocurrent density (J_{sc}) of 13.6 mA/cm^2, an open-circuit voltage (V_{oc}) of 0.70 V, and a fill factor (*FF*) of 0.63, resulting conversion efficiency (η) 6.0% under Air Mass (AM) 1.5 sunlight compared with **N3** dye ($J_{sc,}$ 12.1 mA/cm^2, V_{oc} 0.76 V, *FF* 0.67 and η 6.1%) under same conditions. Furthermore, the theoretical calculation from density functional theory (DFT) at the B3LYP/6-31G(d) of the dye showed electron distribution over HOMO-*tert*-butylphenyl and LUMO-porphyrin moisties due to electron push-pull system to increase the efficiency of power conversion [26].

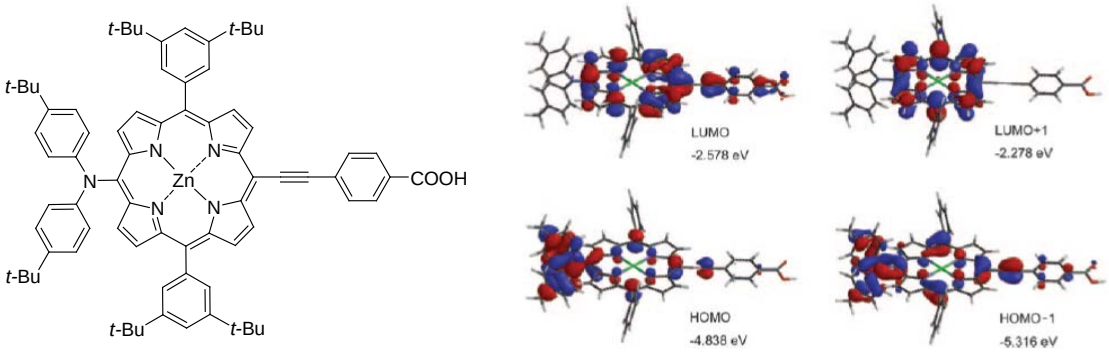

Figure 1.13 Structure and frontier molecular orbitals of *meso*-derivatized porphyrin [26].

In recent year, Kang Deuk Seo and coworker [27] synthesized the novel zinc porphyrin dyes which have a D-π-A system based on porphyrin derivatives containing

a triphenylamine (TPA) as electron-donating group and a phenyl carboxyl as anchoring group substituted at the meso position of the porphyrin ring, yielding the push-pull porphyrins as the most efficient green dye for dye-sensitized solar cell (DSSC) applications. A maximum photon-to photocurrent conversion efficiency of 3.36% was achieved with the DSSC based on **HKK-Por 5** dye ($J_{sc,}$ 9.04 mA/cm^2, V_{oc} 0.57 V, *FF* 0.66) under AM 1.5 irradiation (100 mW/cm^2).

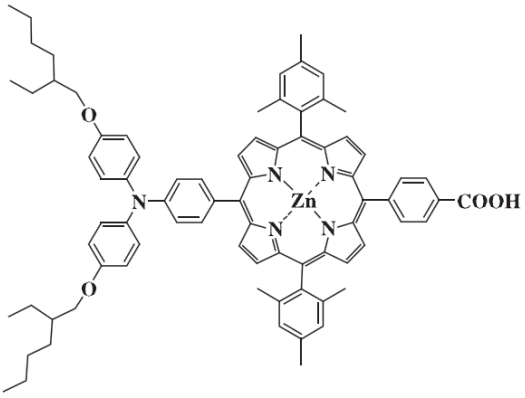

HKK-Por5

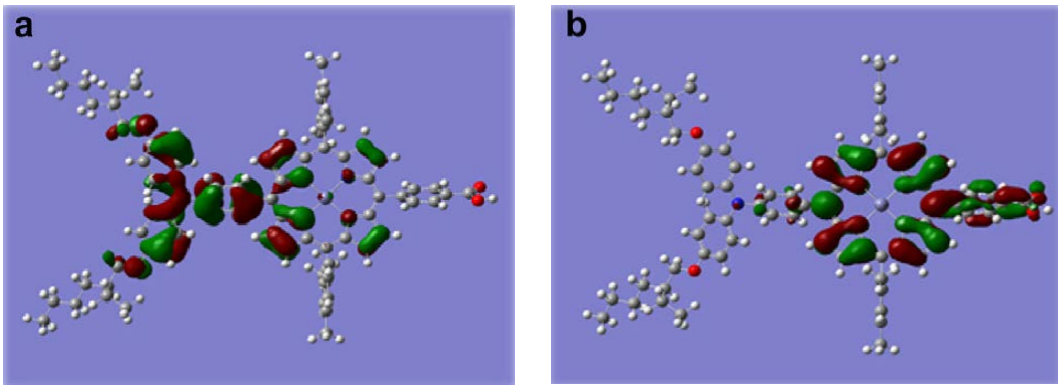

Figure 1.14 Structure and frontier molecular orbitals of **HKK-Por 5** dye [27].

Novel zinc porphyrin dyes that have a D-π-A system based on porphyrin derivatives containing a carbazole linked triphenylamine (TPA) electron-donating group as the second electron donor and a meso-substituted phenyl carboxyl anchoring group attached at the meso position of the porphyrin ring was synthesized. To

increase the electron-donating ability of the D-π-A system based on porphyrin derivatives. Under photovoltaic performance measurements, a maximum photon-to-electron conversion efficiency of 5.01% was achieved with the DSSC based on the dye **HKK-Por1** ($J_{sc,}$ = 10.7 mA/cm^2, V_{oc} = 0.67 V, *FF* = 0.70) under AM 1.5 irradiation (100 mW/cm^2) [28].

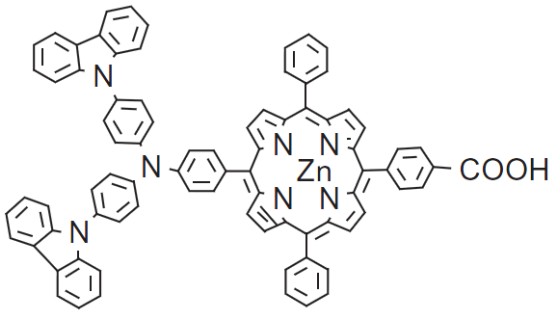

HKK-Por1

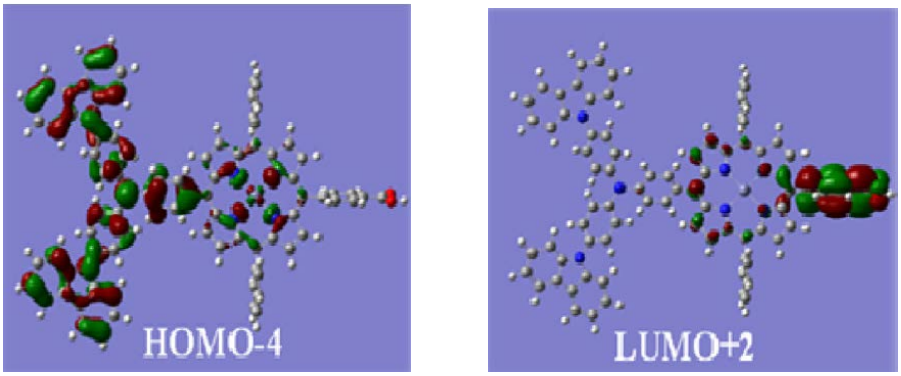

Figure 1.15 Structure and frontier molecular orbitals of **HKK-Por 1** dye [28].

Recently, Liu *et al.* have shown that the intramolecular electron transfer from the higher excited state S_2 of a Zn-porphyrin to a covalently linked ruthenium complex was possible. The result indicated that a long-live charge separation state was obtained in these assemblies [29-30].

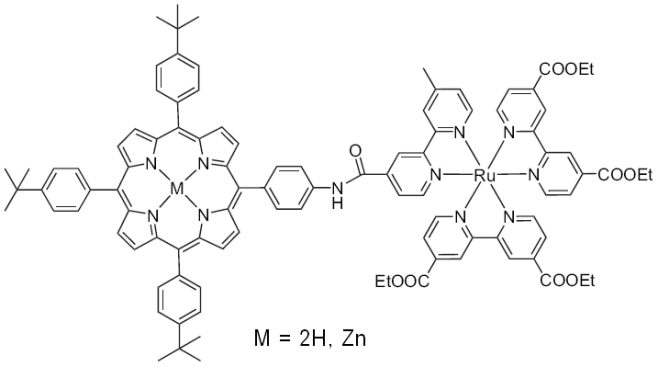

Figure 1.16 Structure of Zn-porphyrin connected ruthenium bipyridine complex by Liu *et al* [29].

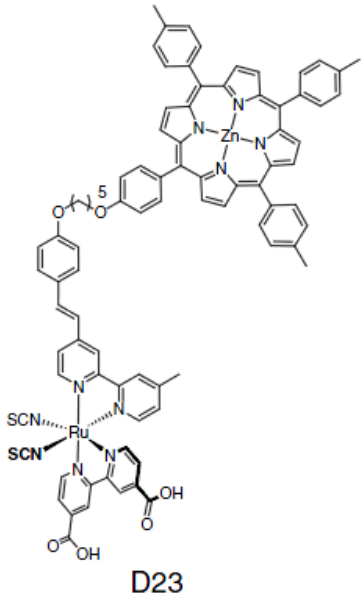

Figure 1.17 Structure of **D23** dye [31].

In 2007, Jung and coworker synthesized new ruthenium sensitizers containing styryl substituted bipyridine and antenna fragment (**D23**) for increase the extinction coefficient of sensitizer and stability of device performance the dye **D23** gave a short-

circuit photocurrent density of 6.45 mA/cm^2, an open-circuit voltage of 0.63 V, and a fill factor of 0.73, corresponding to an overall conversion efficiency of 2.98% [31].

1.5 Objectives and scope of the thesis

Nowadays, the most successful dye-sensitizer, bipyridyl-4,4′-dicarboxylate ruthenium(II), gave 10-12 % yield conversion efficiencies under air mass. However, the drawback of these ruthenium derivatives is hard to purify from the synthetic mixture. Furthermore, most of organic sensitizers applied in DSSCs exhibit the character with both the electron donor (D) and electron acceptor (A), which called the D-A structure to improve the electron transfer processes. To further design and develop the more efficient porphyrin dyes for DSSCs, the predominant light-harvesting abilities in visible and near-IR light of dyes are important to get a larger photocurrent response. Thus a combination of porphyrin and bipyridine complex as a D-A system provides an ideal system for fulfilling an enhance light-harvesting efficiency of photosensitized dyes.

Therefore, the objectives of this work are to synthesize bipyridylporphyrin derivatives **A5**, **A6**, **A7** and **A8** for dye-sensitized solar cells (DSSCs) possessing a Donor-Acceptor system (D-A) based on porphyrin moiety as the electron donor, bipyridyl moiety as the electron-acceptor and . The photophysical and electrochemical properties are investigated by absorption spectrometry and cyclic voltammetry. Density functional theory (DFT) is employed to study electron distribution. The conversion efficiency (η) and the incident photon-to-current conversion efficiency (IPCE) for monochromatic radiation are performed by photovoltaic measurements comparing to the reference dye (**N719**).

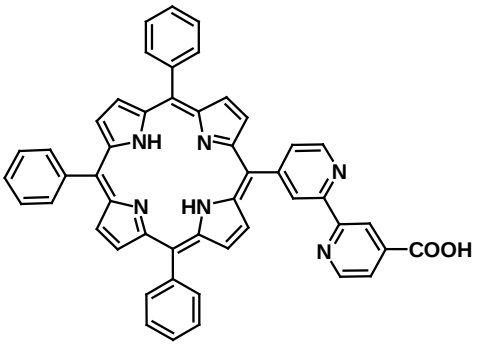
NH
N
N
HN
N
N
COOH

A5

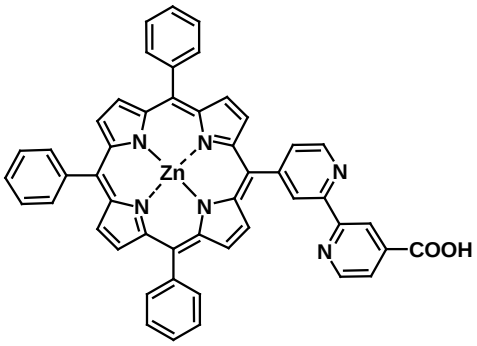
N
N
Zn
N
N
N
N
COOH

A6

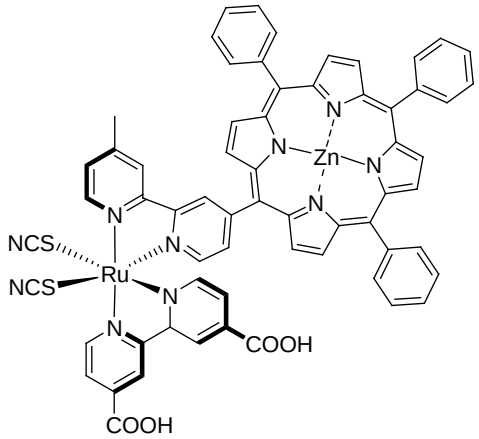
N
N
Zn
N
N
N
NCS
NCS
Ru
N
N
N
COOH
COOH

A7

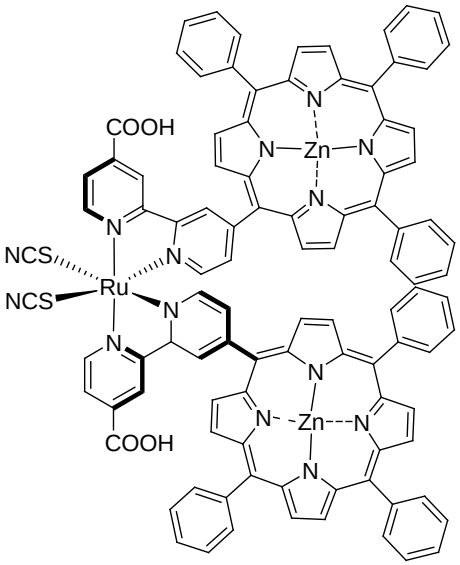
COOH
N
N
Zn
N
N
N
NCS
NCS
Ru
N
N
N
N
N
Zn
N
N
COOH

A8

Fugure 1.18 Structure of bipyridylporphyrin derivatives **A5**, **A6**, **A7** and **A8** as dye-photosensitizers for dye-sensitized solar cells (DSSCs).

CHAPTER II

MATERIALS AND EXPERIMENTAL PROCEDURES

2.1 Materials and analytical instruments

2.1.1 Materials

All reagents as analytical grade were purchased from Fluka, Sigma-aldrich and Merck and used as received without further purification. Commercial grade organic solvents were distilled prior to use. DMF was dried over CaH_2 and freshly distillation under nitrogen atmosphere. Column chromatography was performed using Merck silica gel 60 (70-230 mesh). Sephadex LH-20 was purchased from GE healthcare Bio Science. Thin layer chromatography (TLC) was performed on silica gel plates (Kieselgel 60 F_{254}, 1mm, Merck) using UV lamp. Fluorine-doped tin oxide (FTO: purchased from Dyesol Industries Pty Ltd) coated glass slides were purchased from Pilkington (Canada). Nanocrystalline titanium dioxide D/SP (Ti-Nanoxide D/SP, purchased from Solaronix) and thin adhesive polymeric film were purchased from Solaronix (Switzerland).

2.1.2 Analytical instruments

^{1}H NMR and ^{13}C NMR measurements were carried out on a Varian Mercury Plus 400 MHz (Varian Company, CA, USA) and Bruker 400 MHz NMR spectrometry (Bruker Company, Germany) using $CDCl_3$, DMSO-d_6 and Methanol-d_4 as a solvents.

The ATR-FTIR spectra were measured using Nicolet 6700 FT-IR spectrometer equipped (Fisher, USA) with Germanium crystal for contacting the sample. The FT-IR spectrometer was equipped with Schwarzschild Cassegrain infrared beam splitter and mercury cadmium-telluride (MCT) detector.

Mass spectra were performed by a Bruker Microflex MALDI-TOF Mass Spectrometer (Biflex Bruker Company, Germany) using 2-cyano-4-hydroxycinnamic acid (CCA) as a matrix.

Elemental analysis was analyzed by a Perkin Elmer CHON/S analyzer PE2400 series II (PerkinElmer Inc., USA).

UV-Vis and photoluminescence spectra were measured in a 1 cm path length quartz cell at 25 °C with Julabo F3 temperature controller using a Shimadzu Varian Cary 50 UV-Vis spectrophotometer and a Varian Cary Eclipse spectrofluorometer, respectively.

The cyclic voltammetry was performed on a μ-AUTOLAB potentiostat (AUTOLAB, Netherland) using a glassy carbon working electrode, a $Ag/AgNO_3$ (Sat.) reference electrode and a Pt wire counter electrode for all experiments.

Photovoltaic performance data were obtained using a Sun-simulator model 67005 Newport (Oriel instruments, U.S.A) and 1000 W ozone free xenon light source that gives intensity at the cell surface of 100 mW/cm^2 equivalent to one sun at Air Mass (AM) 1.5 and calibrated with a Si-based reference cell (VLSI standards, Oriel PN 91150V).

2.2 Synthesis

2.2.1 Overall of synthetic pathways

The synthetic pathways of the bipyridylporphyrin derivetives for use as dye-sensitizer were shown in Scheme 2.1. In the first step, porphyrin **A3** was synthesized from condensation between **A1** and **A2**. The pathway 1 started from bipyridylporphyrin **A3**, which converted to zinc complex **A4** after that coupling with [Ru(*p*-cymene)Cl_2]$_2$ complex then compound **A7** was occurred. The pathway 2, **A3** was transformed the methyl group to carboxylic acid one of **A5** and then metalation with zinc acetate to obtained **A6**. The compound **A8** was successfully after coupling with [Ru(*p*-cymene)Cl_2]$_2$ complex.

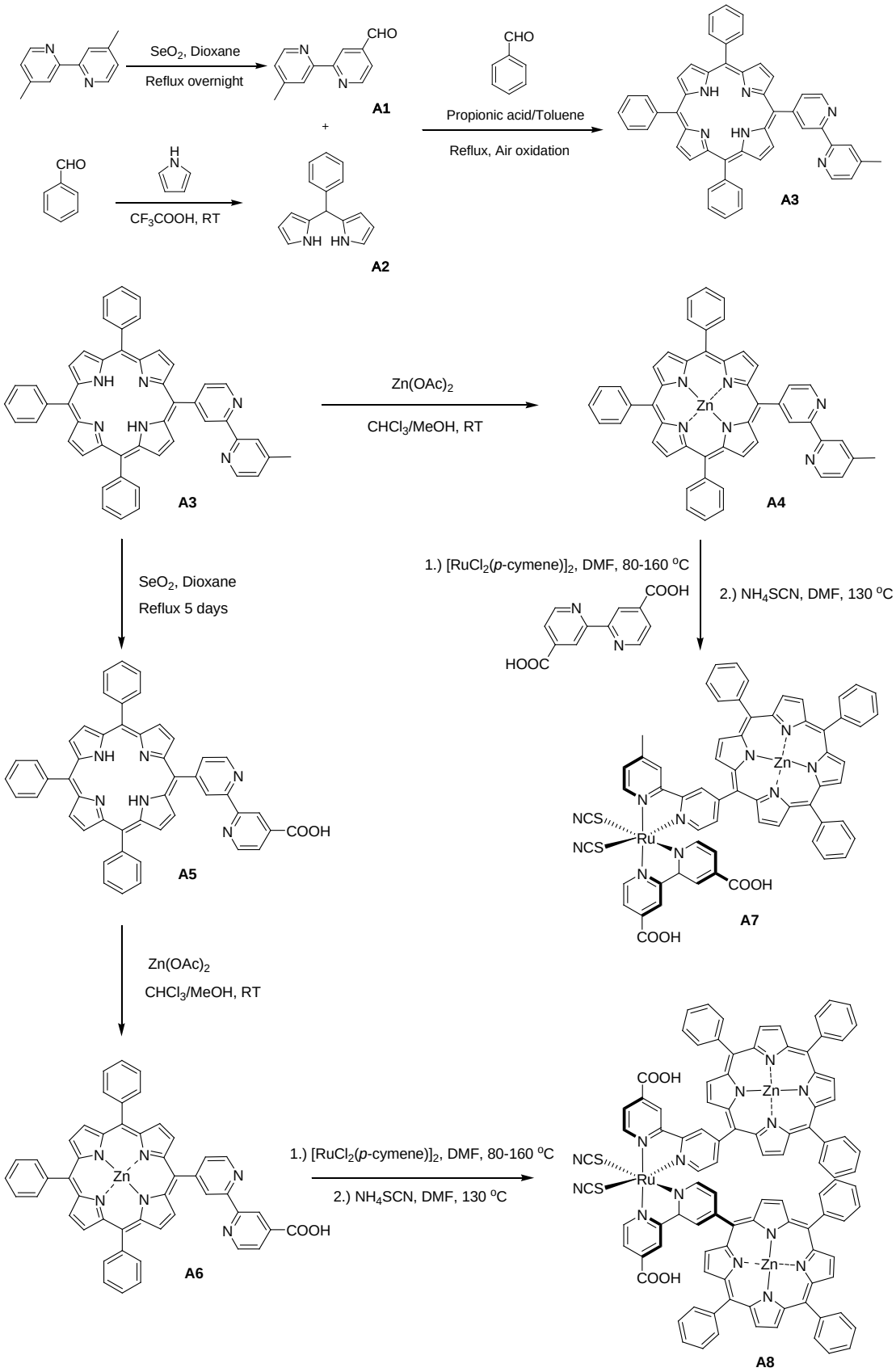

Scheme 2.1 Synthetic pathways of the bipyridylporphyrin derivetives.

2.2.2 4′-methyl-2,2′-bipyridine-4-carboxaldehyde (A1)

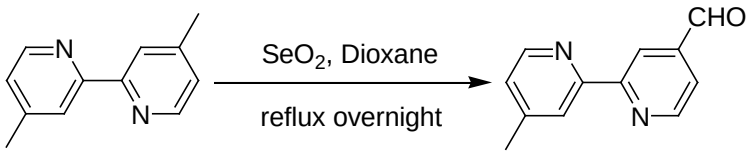

A1

A mixture of 4,4′-dimethyl-2,2′-bipyridine (1.00 g, 5.43 mmol) and SeO_2 (0.70 g, 5.97 mmol) in dioxane (28 mL) was stirred and refluxed under nitrogen atmosphere for 24 hours. The solid material was filtered off, and the dioxane was removed by a rotary evaporator. The obtained mixture was dissolved in dichloromethane (50 mL) and extracted with 1 M Na_2CO_3 (2 x 50 mL) to remove carboxylic acid residue and 0.3 M $Na_2S_2O_3$ (3 x 50 mL) to form the aldehyde bisulfite. The combined aqueous layer was adjusted to pH 10 with Na_2CO_3 and extracted with dichloromethane. The combined organic layer was dried over anhydrous Na_2SO_4 and filtered off. The solvent was removed to afford compound **A1** as white solid (0.72 g, 3.94 mmol, yield 67%) [35].

Characterization data for A1:

^{1}H NMR spectrum ($CDCl_3$, 400 MHz,): δ 10.17 (s, 1H, C***H***O), 8.90 (d, $J_{H\text{-}H}$ = 0.9 Hz, 1H, Bipy***H***), 8.83 (s, 1H, Bipy***H***), 8.58 (d, $J_{H\text{-}H}$ = 3.6 Hz, 1H, Bipy***H***), 8.28 (s, 1H, Bipy***H***), 7.72 (s, 1H, Py***H***), 7.20 (s, 1H, Bipy***H***), 2.47 (s, 3H, C***H***$_3$)

2.2.3 Phynyldipyrromethane (A2)

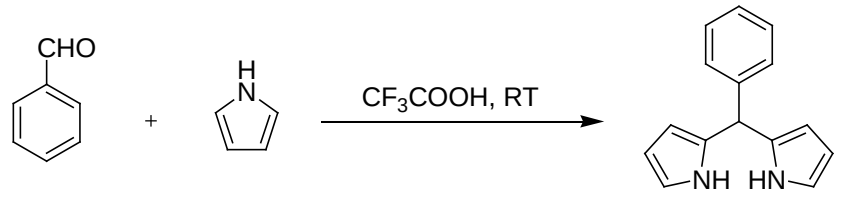

A2

Benzaldehyde (0.20 g, 1.00 mmol) and freshly distilled pyrrole (2.10 mL, 30 mmol) was stirred in a round-bottomed flask. The mixture was deoxygenated by flowing nitrogen though the solution for 15 minutes. Trifluoroacetic acid (0.0081 mL, 0.10 mmol) was added by a syringe, and the mixture was stirred for 15 minutes at room temperature. After removal of excess pyrrole, **A2** was separated by column chromatography (SiO_2, EtOAc:Hexane:triethylamine = 20:80:1) as white solid (0.11 g, 0.51 mmol, yield 51%). The progress of the reaction was monitored by TLC with bromine vapor, **A2** showed as bright pink spot in TLC.

Characterization data for A2:

^{1}H NMR spectrum ($CDCl_3$, 400 MHz): δ 7.87 (s, 2H, PyrN***H***), 7.46-7.31 (m, 5H, Ar***H***), 6.70-6.70 (d, $J_{H\text{-}H}$ = 0.8 Hz, 2H, Pyr***H***), 6.31-6.29 (dd, $J_{H\text{-}H}$ = 3.2, 2.4 Hz, 2H, Pyr***H***), 6.03 (s, 2H, Pyr***H***), 5.48 (s, 1H, C***H***)

2.2.4 5-(4′-methyl-bipyridine-4-yl)-10,15,20-triphenylporphyrin (A3)

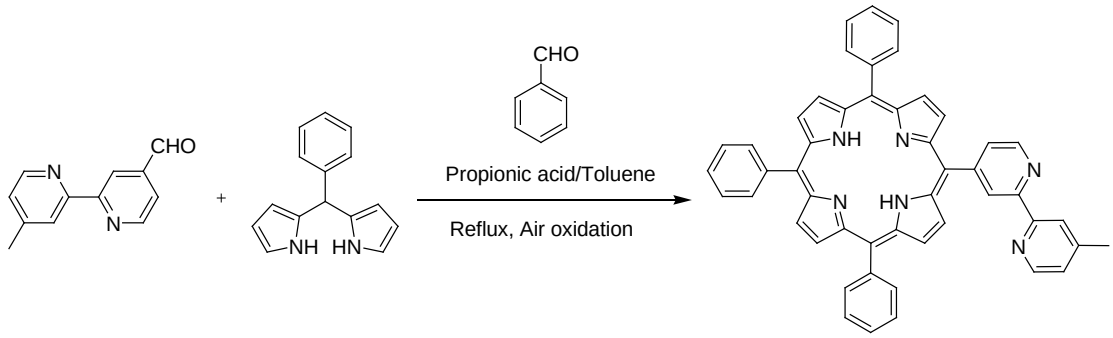

A1 **A2** **A3**

Compound **A1** (1.20 g, 3.84 mmol), **A2** (1.02 g, 3.84 mmol) and benzaldehyde (0.78 mL, 7.68 mmol) were dissolved in toluene (80 mL) and propionic acid (80 mL). The reaction mixture was stirred and refluxed in the open air for 3 hours. After the reaction completed, the mixture was extracted with $NaHCO_3$ and H_2O. The organic layer was dried over anhydrous Na_2SO_4 and solid was filtered off. After removal of the solvent, the product **A3** was separated by column chromatography (SiO_2, MeOH : CH_2Cl_2 = 2:98) and recrystallized with CH_2Cl_2:MeOH to obtain **A3** as a purple solid (0.87 g, 1.23 mmol, yield 32%).

Characterization data for A3:

^{1}H NMR spectrum ($CDCl_3$, 400 MHz): δ 9.30 (s, 1H, Bipy***H***), 9.08 (d, $J_{H\text{-}H}$ = 4.8 Hz, 1H, Bipy***H***), 8.87 (d, $J_{H\text{-}H}$ = 4.8 Hz, 8H Porphyrin***H***), 8.55 (s, 1H, Bipy***H***), 8.50 (d, $J_{H\text{-}H}$ = 4.8 Hz , 1H, Bipy***H***), 8.22 (m, 5H Ar***H***), 8.18 (d, $J_{H\text{-}H}$ = 4.8 Hz, 1H, Bipy***H***), 7.76 (m, 10H Ar***H***), 7.18 (d, $J_{H\text{-}H}$ = 4.8 Hz, 1H, Bipy***H***), 2.55 (s, 3H, C***H***$_3$), -2.79 (s, 2H, PorphyrinN***H***).

^{13}C NMR spectrum ($CDCl_3$, 400 MHz): δ 155.94, 154.94, 151.58, 149.28, 148.32, 147.63, 142.14, 142.08, 134.68, 129.62, 127.90, 127.10, 126.83, 125.00, 122.61, 120.99, 120.65, 116.90, 21.36.

IR spectrum (KBr pellet (cm^{-1})): 3315 (N-H st), 3053 (Aromatic C=H st), 3020 (Aliphatic C-H st), 1589 (N-H bend)

Elemental analysis:

Anal. Calcd. for $C_{49}H_{34}N_6$	C, 83.26; H, 4.85; N, 11.89
Found	C, 83.32; H, 4.86; N, 11.88

MALDI-TOF mass:

Anal. Calcd. for $C_{49}H_{34}N_6$	*m/z* = 706.83
Found	*m/z* = 707.2910 [M]

2.2.5 5-(4′-methyl-bipyridine-4-yl)-10,15,20-triphenylporphyrinatozinc (A4)

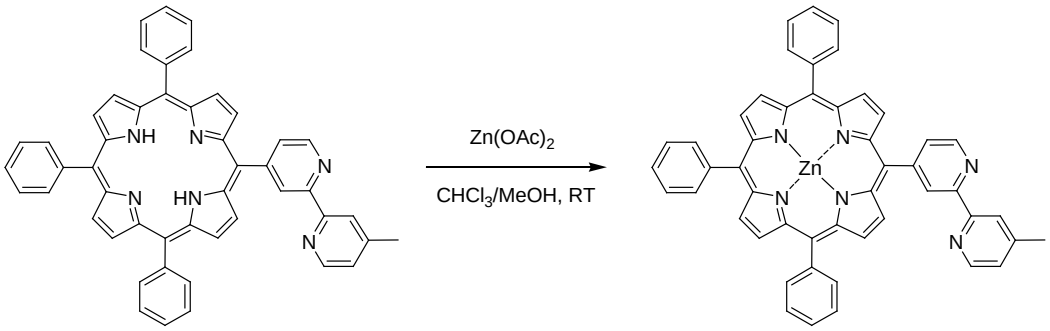

A3 **A4**

A mixture of compound **A3** (0.50 g, 0.68 mmol) and $Zn(OAc)_2$ (0.22 g, 1.02 mmol) in $CHCl_3$ (10 mL) and MeOH (10 mL) was stirred at room temperature for 24 hours. After removal the solvent under reduce pressure, the crude was dissolved in CH_2Cl_2 and then the mixture was extracted with water. The organic layer was separated and dried over anhydrous Na_2SO_4. The crude product was purified by a column chromatography (SiO_2, MeOH:CH_2Cl_2 = 5:95) to afford the compound **A4** as a purple solid (0.497 g, 0.65 mmol, yield 95%).

Characterization data for A4:

^{1}H NMR spectrum ($CDCl_3$, 400 MHz): δ 9.17 (s, 1H, Bipy***H***), 8.92-8.97 (m, 8H, Porphyrin***H***), 8.82-8.94 (d, $J_{H\text{-}H}$ = 5.2 Hz , 1H, Bipy***H***), 8.27 (s, 1H, Bipy***H***), 8.23 (s, 5H, Ar***H***), 8.22 (d, 1H, Bipy***H***), 8.16-8.17 (d, $J_{H\text{-}H}$ = 1.2 Hz, 1H, Bipy***H***), 7.73-7.76 (m, 10H, Porphyrin***H***), 6.98-7.00 (d, $J_{H\text{-}H}$ = 4.0 Hz, 1H, Bipy***H***), 2.40 (s, 3H, C***H***$_3$)

^{13}C NMR spectrum ($CDCl_3$, 400 MHz): δ 155.78, 154.43, 152.20, 150.43, 150.27, 149.11, 149.04, 148.14, 147.22, 142.76, 142.71, 143.50, 143.45, 132.58, 132.22, 132.12, 131.35, 129.25, 127.55, 127.02, 126.56, 124.73, 122.34, 121.71, 121.39, 117.64, 110.00, 21.22

IR spectrum (KBr pellet (cm^{-1})): 3635 (N-H st), 3048 (Aromatic C=H st), 3020 (Aliphatic C-H st), 1589 (C=N st)

Elemental analysis:

Anal. Calcd. for $C_{49}H_{32}N_6Zn$	C, 76.41; H, 4.19; N, 10.91
Found	C, 76.10; H, 4.19; N, 10.92

MALDI-TOF mass:

Anal. Calcd. for $C_{49}H_{32}N_6Zn$	*m/z* = 770.21
Found	*m/z* = 770.371 [M]

2.2.6 5-(4′-carboxy-2,2′-bipyridine-4-yl)-10,15,20-triphenylporphyrin (A5)

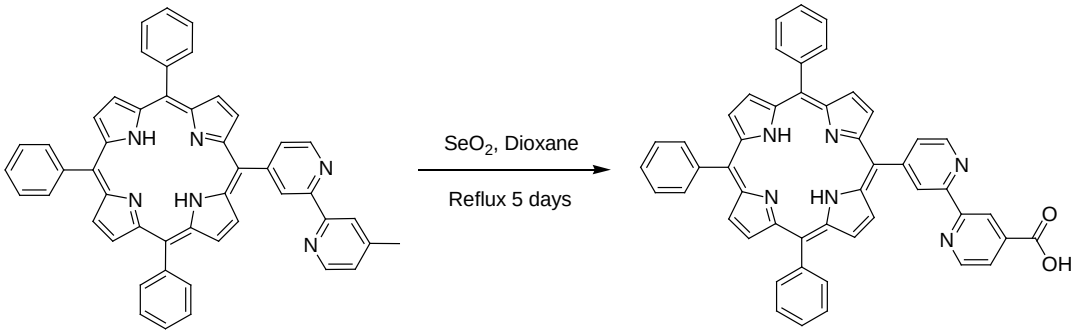

A3 **A5**

A mixture of compound **A3** (0.20 g, 0.28 mmol) and SeO_2 (1.65 g, 14.16 mmol) in dioxane (30 mL) was stirred and refluxed under nitrogen atmosphere for 5 days. The solid was filtered off. Dioxane was removed by a rotary evaporator. Compound **A5** was purified by column chromatography on siliga gel with MeOH/CH_2Cl_2 (5:95) as eluent and obtained as a purple solid (92.84 mg, 0.13 mmol, yield 45%).

Characterization data for A5:

^{1}H NMR spectrum ($CDCl_3$, 400 MHz): δ 9.63 (s, 1H, Bipy***H***), 9.47 (s, 1H, Bipy***H***), 8.91 (s, 1H, Bipy***H***), 8.87-8.90 (m, 8H, Porphyrin***H***), 8.35 (s, 1H, Bipy***H***), 8.22-8.23 (d, $J_{H\text{-}H}$ = 6.0 Hz, 5H, Ar***H***), 8.04 (s, 1H, Bipy***H***), 7.76-7.78 (m, 10H, Ar***H***), -2.78 (s, 2H, PorphyrinN***H***).

^{13}C NMR spectrum (DMSO-*d6*, 400 MHz): δ 194.00, 166.90, 150.14, 148.18, 141.09, 141.04, 134.22, 131.49, 129.38, 128.14, 127.00, 125.83, 123.65, 120.66, 120.31, 116.78

IR spectrum (KBr pellet (cm^{-1})): 3422 (O-H st), 3310 (N-H st), 1713 (C=O st), 1592 (N-H bend)

Elemental analysis:

Anal. Calcd. for $C_{49}H_{32}N_6O_2$	C, 79.87; H, 4.38; N, 11.41
Found	C, 79.88; H, 4.52; N, 11.58

MALDI-TOF mass:

Anal. Calcd. for $C_{49}H_{32}N_6O_2$	*m/z* = 736.82
Found	*m/z* = 736.984 [M]

2.2.7 5-(4′-carboxy-2,2′-bipyridine-4-yl)-10,15,20-triphenylporphyrinatozinc (A6)

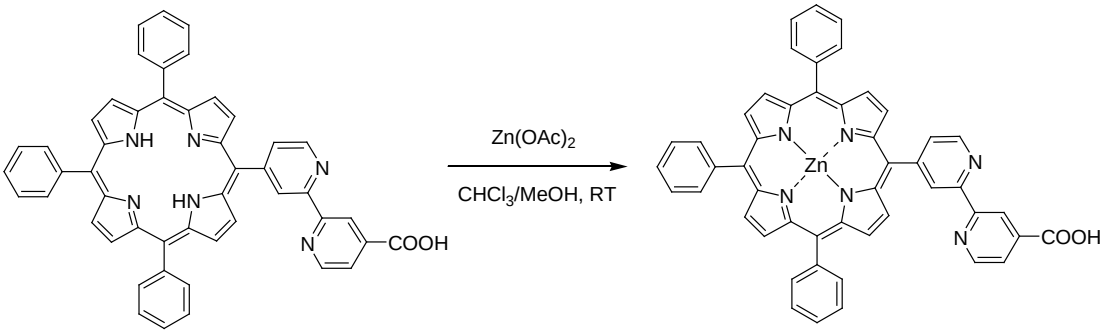

A5 **A6**

A mixture of compound **A5** (0.50 g, 0.68 mmol) and $Zn(OAc)_2$ (0.22 g, 1.02 mmol) in $CHCl_3$ (10 mL) and MeOH (10 mL) was stirred at room temperature for 24 hours. The solvent was removed by a rotary evaporator and the residue was extracted with water. The organic layer was separated and dried over anhydrous Na_2SO_4. The crude product was purified by a column chromatography on siliga gel with MeOH/CH_2Cl_2 (10:90) as eluent to afford the compound **A6** as a purple solid (0.52 g, 0.65 mmol, yield 95%).

Characterization data for A6:

^{1}H NMR spectrum (DMSO-*d6*, 400 MHz): δ 9.15 (s, 1H, Bipy***H***), 9.10 (s, 2H, Bipy***H***), 8.78-8.86 (dd, $J_{H\text{-}H}$ = 4.8, 28.8 Hz, 4H, Porphyrin***H***), 8.77 (s, 4H, Ar***H***), 8.53-8.54 (d, $J_{H\text{-}H}$ = 4.4 Hz, 1H, Bipy***H***), 8.25-8.26 (d, $J_{H\text{-}H}$ = 3.2 Hz, 1H, Bipy***H***), 8.20 (m, 6H, 1H-Bipy***H*** + 5H-Porphyrin***H***), 7.78-7.79 (m, 10H, Ar***H***).

^{13}C NMR spectrum (DMSO-*d6*, 400 MHz): δ 174.95, 167.39, 155.10, 154.07, 151.55, 149.53, 149.51, 149.41, 149.32, 148.89, 148.35, 147.62, 142.66, 142.63, 134.15, 132.11, 131.74, 131.63, 131.09, 129.19, 127.49, 126.58, 125.94, 123.86, 120.97, 120.91, 120.56, 117.17

IR spectrum (KBr pellet (cm^{-1})): 3363 (O-H st), 3051 (Aromatic C=H st), 2924 (Alipatic C-H st), 1599 (C=O st)

Elemental analysis:

Anal. Calcd. for $C_{49}H_{30}N_6O_2Zn$	C, 73.55; H, 3.78; N, 10.50
Found	C, 73.50; H, 3.79; N, 10.65

MALDI-TOF mass:

Anal. Calcd. for $C_{49}H_{30}N_6O_2Zn$	*m/z* = 800.19
Found	*m/z* = 799.1735 [M - H^+]

2.2.8 Bipyridylporphyrin ruthenium complex (A7)

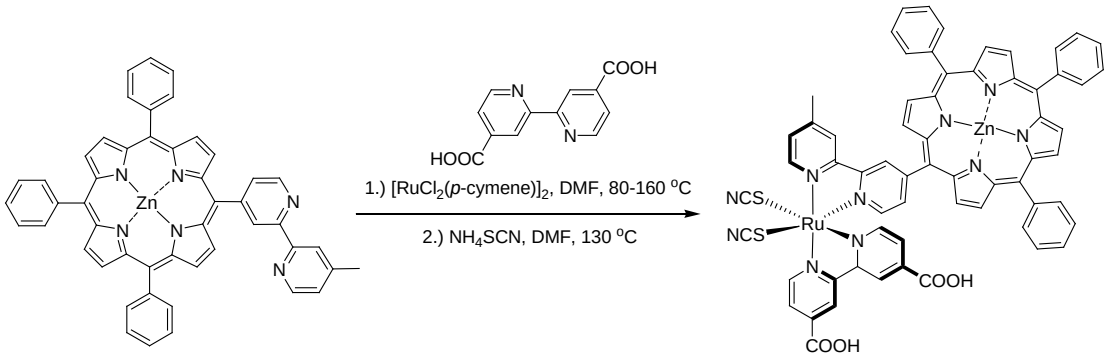

A4 **A7**

A mixture of $[RuCl_2(p\text{-cymene})]_2$ (0.10 g, 0.17 mmol) and compound **A4** (0.13 g, 0.17 mmol) was added to DMF (10 mL). The reaction mixture was heated at 80 °C under nitrogen for 6 hours and then 2,2′-bipyridyl-4,4′-dicarboxylic acid (0.04 g, 0.17 mmol) was added into the solution. The reaction mixture was refluxed at 160 °C for another 6 hours under dark condition to avoid light induced *cis* to *trans* isomerisation. Excess of NH_4SCN (0.14 g, 1.83 mmol) was then added to the reaction and heated at 130 °C for further 6 hours. Water was added to the mixture reaction and the water insoluble product was collected on a sintered glass crucible by suction filtration, washed with distilled water and diethyl ether and dried. The crude product **A7** was purified by a Sephadex LH-20 column eluted with methanol. The red product of **A7** was collected (122.92 mg, 0.10 mmol, yield 58%).

Characterization data for A7:

^{1}H NMR spectrum (DMSO-*d6*, 400 MHz): 9.42 (d, 1H), 9.12 (d, 1H), 8.96 (s, 1H), 8.83 (s, 1H), 8.82 (d, 1H), 8.76 (s, 8H), 8.60 (d, *J* = 4.8 Hz, 1H), 8.53 (d, *J* = 4.8 Hz, 1H), 8.38 (d, 1H), 8.36 (s, 1H), 8.21 (s, 1H), 8.05 (d, *J* = 7.8 Hz, 8H), 7.75 (d, 1H), 7.59 (d, *J* = 7.8 Hz, 6H), 7.50 (d, *J* = 8.7 Hz, 2H), 2.40 (s, 3H, C***H***$_3$)

IR spectrum: 3382 (O-H st), 3054 (Aromatic C=H st), 2924 (Aliphatic C-H st), 2850 (Aliphatic C-H st), 2102 (N=CS st), 1969 (N=CS st), 1610 (C=O st)

Elemental analysis:

Anal. Calcd. for $C_{63}H_{41}N_{10}O_4RuS_2Zn$	C, 61.39; H, 3.35; N, 11.36
Found	C, 61.44; H, 3.32; N, 11.46

MALDI-TOF mass:

Anal. Calcd. for $C_{49}H_{32}N_6O_2$	*m/z* = 1232.65
Found	*m/z* = 1233.91 [M + H^+].

2.2.9 Bipyridylporphyrin ruthenium complex (A8)

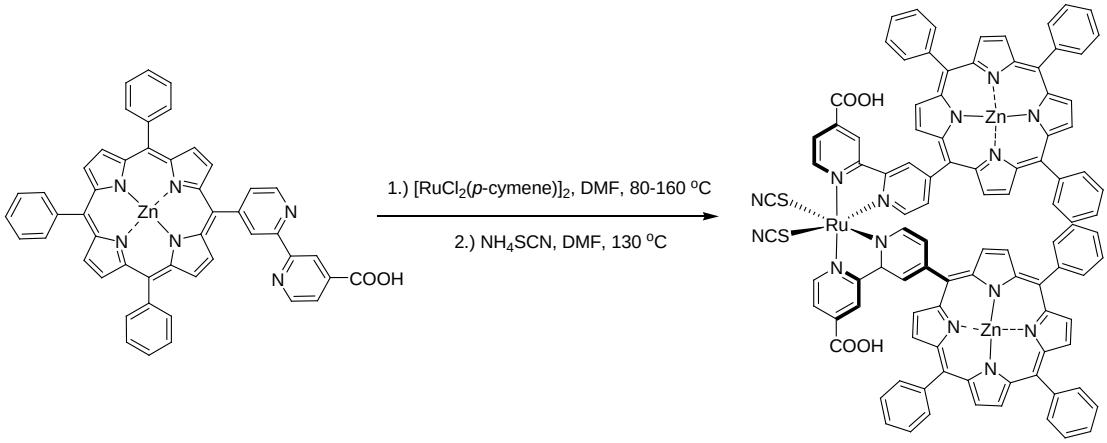

A6 **A8**

A mixture of $[RuCl_2(p\text{-cymene})]_2$ (0.001 g, 0.02 mmol) and compound **A6** (0.01 g, 0.02 mmol) was added to DMF (10 mL). The reaction mixture was heated at 80 °C under nitrogen for 6 hours and then **A6** (0.01 g, 0.02 mmol) was added to the solution. The reaction mixture was refluxed at 160 °C for another 6 hours under dark condition to avoid light induced *cis* to *trans* isomerisation. Excess NH_4NCS (0.03 g, 0.37 mmol) was added to the reaction mixture and heated at 130 °C for further 6 hours. Water was added to the mixture and the water insoluble product was collected on a sintered glass crucible by suction filtration and washed with distilled water and diethyl ether. After that the crude product was purified by a Sephadex LH-20 column eluted with methanol. The red product of **A8** was collected (190.59 mg, 0.01 mmol, yield 52%).

Characterization data for A8:

^{1}H NMR spectrum (DMSO, 400 MHz): δ 9.08 (s, 2H), 9.06 (s, 2H), 8.83 (s, 2H), 8.71 (s, 2H), 8.35-8.52 (m, 16H), 7.70 (s, 2H), 7.30-7.42 (m, 12H) 7.25 (s, 2H), 7.14-7.21 (m, 18H)

IR spectrum (KBr pellet (cm^{-1})): 3363 (O-H st), 3051 (Aromatic C=H st), 2924 (Alipatic C-H st), 2102 (N=CS st), 1969 (N=CS st), 1599 (C=O st)

MALDI-TOF mass:

Anal. Calcd. for $C_{100}H_{61}N_{14}O_4RuS_2Zn_2$	*m/z* = 1818.63
Found	*m/z* = 1819.73 [$M + H^+$]

2.3 UV-Visible spectroscopy and Fluorescence spectrophotometry

The characterization of absorption properties were performed on a Varian Cary 50 Probe UV-Visible spectrometer. The spectrum of all dyes were collected in dried DMF at room temperature with the concentration between 10^{-6}-10^{-5} M. Their absorbance were recorded extending from 350-800 nm.

The characterization of emission properties were investigated by Varian Cary Eclipse spectrofluorometer. The spectrum of all dyes were performed in dried DMF at room temperature with the concentration 10^{-6} M. Each dye was excited at the soret wavelength absorption.

2.4 Electrochemical measurement

The cyclic voltammetry was performed on a μ-AUTOLAB potential using a glassy carbon working electrode, a Pt wire counter electrode and a $Ag/AgNO_3$ (Sat.) reference electrode at room temperature for all experiments. The supporting electrolyte was 0.1 M $TBAPF_6$ in freshly distilled DMF and the concentration of analyzes were 1.0 mM. The solutions were purged with nitrogen. All samples were measured with a scan rate of 100 mV/sec.

2.5 Theoretical calculation

Geometry optimization and electronic structure calculations were optimized by Density Functional Theory (DFT) calculations on the bipyridylporphyrin dyes using the B3LYP functional and 6-31 G(d) or LanL2DZ as basis set methods in the Gaussian 03 program package. Molecular orbitals were visualized by GaussView 3.0 software.

2.6 Fabrication of DSSCs

The preparation of TiO_2 electrodes and the fabrication of the DSSCs were performed by following the procedures previously reported by Grätzel and co-workers.

For preparation of the working electrodes, a transparent conducting fluorine-doped tin oxide (FTO) coated glass plates were cleaned using an ultrasonic bath about 30 minutes for each step in detergent solution, water, agua regia solution, water, ethanol and acetone, respectively. The FTO glass plates were immersed into a 40 mM $TiCl_4$ solution at 70 °C for 30 minutes in the oven and washed with water and ethanol. Two types of nanocrystalline-TiO_2 paste, nanocrystalline-TiO_2 20 nm for transparent layer and submicronanocrystalline-TiO_2 70 μm for light-scattering layer were used as working electrode. A layer of nanocrystalline-TiO_2 paste were coated on the FTO plate by screen-printing method, dried on the hotplate at 120 °C for 10 minutes and repeated this step for triple layer. A layer of submicronanocrystalline-TiO_2 paste was coated by the same method for a single layer. Finally, the working electrode was heated step by step at 325 °C for 5 minutes, at 375 °C for 5 minutes, at 450 °C for 5 minutes and at 500 °C for 30 minutes. The electrode was treated again with 40 mM $TiCl_4$ solution and washed with water and ethanol and sintered at 450 °C for 30 minutes. Before dipping into the dye solution, the working electrode was heated at 80 °C to avoid the absorption of water on TiO_2 surface, then the electrode was dipped into a dye solution (5×10^{-4} M in ethanol) and maintained under dark for 24 hours. The dye-coated electrode was rinsed with ethanol.

For a counter electrode, FTO plates were drilled (radius = 1 mm) and cleaned by the previous method. After heating at 80 °C for 30 minutes, the Pt catalyst was deposited on FTO by dropping of H_2PtCl_4 solution (2 mg Pt in 2-methoxy ethanol/acetylacetone), and the solvent was dried at room temperature for 12 hrs.

A sandwich cell was performed by assembly the counter Pt-electrode with the dye-coated working electrode, which separated by thin adhesive polymeric film sheets. The sandwiched electrodes were tightly held, and then heated around the thin film sheets to attach the two electrodes. The electrolyte was introduced into the inter-electrode space. Then, the cells were sealed with a cover glass to avoid leakage of the

electrolyte solution. Pt foil was clipped onto the top of surface of the electrodes and silver paint was covered onto the conductive side for correcting electron.

2.7 Photocurrent-voltage measurement

Photovoltaic performance data were measured using a 1000 W ozone free xenon light source that gives intensity at the cell surface of 100 mW/cm^2 equivalent to one sun at Air Mass (AM) 1.5 and calibrated with a Si-based reference cell (VLSI standards, Oriel PN 91150V).

2.7.1 The photovoltaic properties of N719 in the various electrolytes.

The optimized conditions for all experiments were determined to be $5x10^{-4}$ M of **N719** dye in dried ethanol. The TiO_2 working electrodes were dipped into the 25.0 mL of dye solution and maintained under dark for 24 hours. The various electrolytes were filled into the sandwiched electrodes. For the electrolyte conditions, **E1**, **E2**, **E3**, **E4** and **E5** were prepared according to Table 2.1.

Table 2.1 Amount of components in various electrolytes for photovoltaic properties studies.

Component	**E1** **(M)**	**E2** **(M)**	**E3** **(M)**	**E4** **(M)**	**E5** **(M)**
LiI	0.50	0.10	0.10	0.10	0.10
I_2	0.05	0.05	0.05	0.05	0.05
TBP	-	0.40	0.40	0.40	-
Pyridine	0.40	-	-	-	0.40
PMII	-	-	0.60	-	-
TPAI	-	-	-	0.60	0.60
Solvent	70:30 ; GBL:NMP	50:50 ; CH_3CN: Valeronitrile	50:50 ; CH_3CN: Valeronitrile	50:50 ; CH_3CN: Valeronitrile	50:50 ; CH_3CN: Valeronitrile

2.7.2 The photovoltaic properties of bipyridylporphyrin derivatives and N719.

The dye solutions were prepared at concentrations of 5 x 10^{-4} M in dried ethanol. The TiO_2 working electrodes were dipped into the 25.0 mL of dye solution and maintained under dark for 24 hours. The optimized electrolyte **E5** was filled into the sandwiched electrodes for all conditions. The photovoltaic performances were recorded at room temperature.

2.7.3 Solubility and dye adsorption on TiO_2

2.7.3.1 Solubility test

Dissolve **A6** in various solvent: EtOH, DMF, THF, $CHCl_3$, MeOH and toluene in concentration of 5 x 10^{-4} M. The mixture was stirred for 30 minutes, and then solubility test of compound **A6** was observed.

2.7.3.2 Dye adsorption on TiO_2

Stock solutions of dye **A6** with approximate concentrations of 5 x 10^{-4} M has been prepared and dissolved in various solvent: EtOH, DMF, THF, $CHCl_3$, MeOH and toluene. The TiO_2 working electrode was dipped into 25.0 mL of the stock solution **A6** in difference solvent for 3 hours under dark condition. After cleaning TiO_2 working electrode with solvent and dried, observed the result on working electrode's surface.

2.7.4 The effect of CDCA concentration on the photovoltaic performance.

The mixed dye-CDCA solutions were prepared from the **A6** dye at concentrations of 3 x 10^{-4} M in ethanol with addition of a variety of CDCA portions according to Table 2.2. The TiO_2 working electrodes were dipped into 5.0 mL of mixed dye-CDCA solution and maintained under dark for 24 hours. The optimized electrolyte **E6** was filled into the sandwiched electrodes for all experiments. The photovoltaic performances were recorded at room temperature.

Table 2.2 Amount of CDCA in the stock solution of **A6** for photovoltaic properties studies.

	Equivalent of A6	**Volume of A6 stock solution (mL)**	**Equivalent of CDCA**	**Weight of CDCA (g)**
CDCA 0.5	1.0	5.0	0.5	0.059
CDCA 1.0	1.0	5.0	1.0	0.118
CDCA 2.0	1.0	5.0	2.0	0.236
CDCA 5.0	1.0	5.0	5.0	0.588
CDCA 10.0	1.0	5.0	10.0	1.177

CHAPTER III

RESULTS AND DISCUSSION

This chapter showed the result and discussion of synthesis and characterization of the bipyridylporphyrin derivatives and followed by their photophysical and electrochemical properties. The photovoltaic performances of the photovoltaic cells using the bipyridylporphyrin derivatives as photosensitizers are presented at the final part of this chapter.

3.1 Design and synthesis of bipyridylporphyrin derivatives

The bipyridylporphyrin derivatives were designed and synthesized for use as dye-sensitizer in dye-sensitized solar cells (DSSCs). Bipyridylporphyrin derivatives composed of Donor-Acceptor system (D-A) based on porphyrin moiety as the electron donor (D) and bipyridyl moiety as the electron-acceptor (A). All bipyridylporphyrin derivatives composed of the carboxylic part in the compound which act as the anchoring group to bind with TiO_2 surface on the FTO electrode, and the thiocynate ligand was used to fine tune the energy level via the result of the electron donating property of thiocynate ligand by shift the distribution of HOMO level of the oxidized dye (S^+) away from CB energy level of TiO_2 and reducing the charge recombination process. Thus the designing of D-A system provides an ideal system for fulfilling a light-harvesting efficiency of photosensitized dyes.

All compounds were synthesized according to Scheme 2.1. The compound 4,4′-dimethyl-2,2′-bipyridine was oxidized with SeO_2 in refluxing dioxane to afford monoaldehyde **A1**. Bispyrrole **A2** was condensed between freshly distilled pyyrole with benzaldehyde in TFA using acid catalytic. Then bipyridylporphyrin **A3** was obtained from condensation reaction between **A1**, **A2** and benzaldehyde in refluxing propionic acid/toluene using air-oxidation and used as the porphyrin-based for synthetic of the other bipyridylporphyrin derivatives in the next pathway. For the pathway 1 started from bipyridylporphyrin **A3**, which converted to zinc complex **A4**

via metalation after that coupling with [Ru(*p*-cymene)Cl_2]$_2$ complex and 4,4′-dicarboxyl-2,2′-bipyridine, and then exchanged choro ligand with a large excess of ammonium thiocyanate ligand to afford the bipyridylporphyrin ruthenium complex **A7**.then compound **A7** was occurred.

For the pathway 2, the methyl group of **A3** was transformed to carboxylic acid one of **A5** using SeO_2 as oxidant in dioxane. Treatment of **A5** with zinc acetate gave zinc porphyrin complex **A6**. Finally, the bipyridylporphyrin was transformed to bipyridylporphyrin ruthenium complex **A8** by a reaction of [Ru(*p*-cymene)Cl_2]$_2$ complex with **A6**.

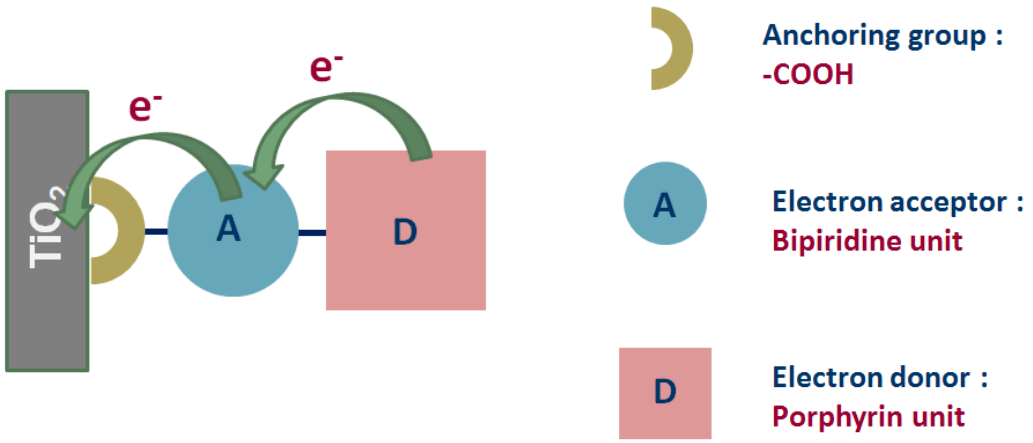

Figure 3.1 The molecular designing of D-A system in bipyridylporphyrin complex.

3.1.1 Synthesis and characterization of 5-(4′-methyl-bipyridine-4-yl)-10,15,20-triphenylporphyrin (A3)

The synthetic pathways of the 5-(4′-methyl-bipyridine-4-yl)-10,15,20-triphenylporphyrin **(A3)** in Scheme 3.1 start with a preparation of compound **A1** and **A2**. **A1** was provided by the oxidation between 4,4′-dimethyl-2,2′-bipyridine and SeO_2 in reflexing dioxane for 24 hours. The white solid of monoformyl-bipyridine **A1** was occurred in 67% yield by extracted with Na_2CO_3 to remove the carboxylic acid residue of 4,4′-dicarboxyl-2,2′-bipyridine. The ^{1}H NMR spectrum of compound **1** showed characteristic peaks of formyl groups at 10.17 ppm and also the singlet proton of C***H***$_3$ at 2.47 ppm in 1:3 of proton ratio.

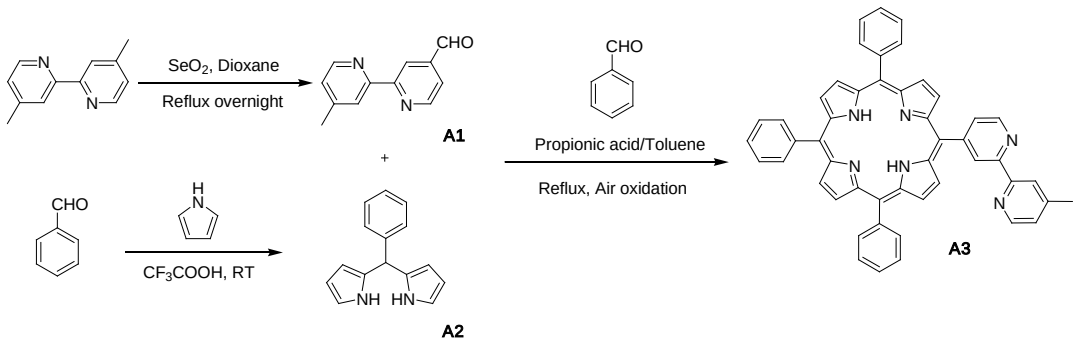

Scheme 3.1 Synthetic pathways of 5-(4′-methyl-bipyridine-4-yl)-10,15,20-triphenyl porphyrin **(A3)**

Bispyrrole **A2** was carried out by condensation between benzaldehyde and excess pyrrole (30 equiv.) in the presence of TFA as acid catalytic for 15 minutes according to conventional proceduce [36]. After purification by column chromatography (SiO_2, EtOAc:Hexane:triethylamine = 20:80:1) and the reaction was monitored by TLC with bromine vapor, The bispyrrole **A2** showed as bright pink spot in TLC and gave the white solid in 51% yield. The ^{1}H NMR spectrum of compound **A2** exhited characteristic peaks of pyrrole-N***H*** as a broad singlet at 7.87 and the three

signals of *β*-pyrrolic protons at signal of 6.70 (J_{H-H} = 0.8 Hz), 6.31-6.29 (dd, J_{H-H} = 3.2, 2.4 Hz) and 6.03 ppm, respectively. The aromatic proton of phenyl group appeared at 7.46-7.31 ppm. Additional, the singlet proton at 5.48 ppm showed that the condensation between benzaldehyde and pyrrole was occurred.

Bipyridylporphyrin **A3** was obtained from condensation between **A1**, **A2** and benzaldehyde in refluxing propionic acid/toluene using air-oxidation for 3 hours. **A3** was separated by column chromatography (SiO_2, MeOH : CH_2Cl_2 = 2:98) and recrystallized with CH_2Cl_2:MeOH to obtain product as a purple solid in 32% yield. The ^{1}H NMR spectrum of bipyridylporphyrin **A3** showed characteristic peaks of *β*-pyrrolic protons in porphyrin ring at 8.87 (J_{H-H} = 4.8 Hz), and the aromatic proton of meso position at 8.22, 8.18 ppm, respectively. Furthermore, The upfield singlet proton at -2.79 ppm showed the free base of porphyrin-N***H*** due to the anisotropic effect of porphyrin. The signals of bipyridine-***H*** appeared at 9.30, 9.08 (d, J_{H-H} = 4.8 Hz), 8.55, 8.50, 8.18 (d, J_{H-H} = 4.8 Hz) and 7.18 (d, J_{H-H} = 4.8 Hz) ppm. The MALDI-TOF mass analysis of bipyridylporphyrin **A3** revealed signals of *m/z* = 736.984, correspondind to the molecular ion [M] as the major signal (Anal. Calcd. *m/z* = 706.83).

In addition, the ^{1}H NMR spectra of the first 3 factions in the purple color from column chromatography showed that the condensation between **A1**, **A2** and benzaldehyde provided at least 3 compounds of porphyrin with in the proposed structures (Figure 3.1).

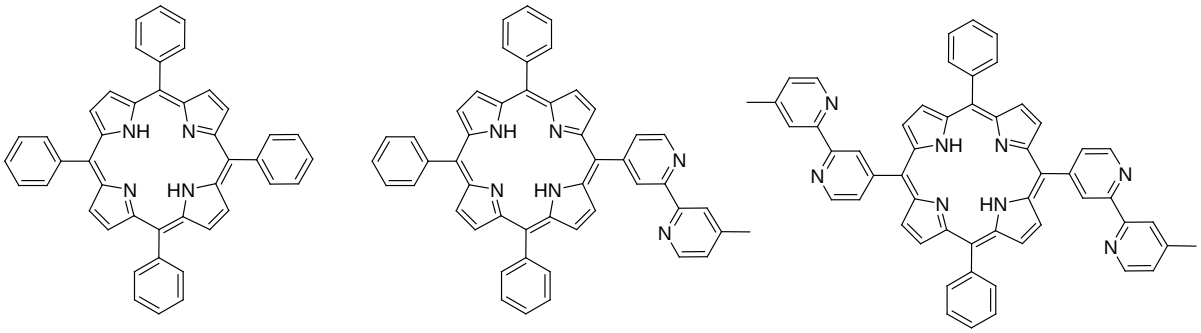

A3

Figure 3.2 The proposed structures of porphyrin derivatives from condensation reaction.

3.1.2 Synthesis and characterization of 5-(4′-methyl-bipyridine-4-yl)-10,15,20-triphenylporphyrinatozinc (A4)

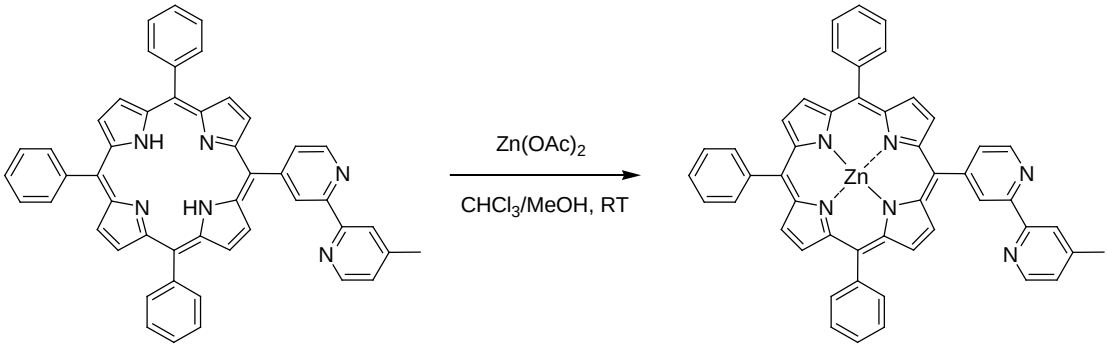

A3 **A4**

Scheme 3.2 Synthetic pathway of 5-(4′-methyl-bipyridine-4-yl)-10,15,20-triphenyl porphyrinatozinc (**A4**)

The synthesis of 5-(4′-methyl-bipyridine-4-yl)-10,15,20 triphenyl porphyrinatozinc (**A4**) was accomplished by treating bipyridylporphyrin **A3** with $Zn(OAc)_2$ at room temperature for 24 hours. After purification by a column chromatography (SiO_2, MeOH:CH_2Cl_2 = 5:95), zinc compound **A4** was successful to afford as a purple solid in 95% yield. The ^1H NMR spectrum of zinc-bipyridylporphyrin **A4** showed characteristic peaks of β-pyrrolic protons in porphyrin ring at 8.92-8.97 ppm, and the aromatic protons of meso position at 8.23, 7.73-7.76 ppm, respectively. The methyl group still appeared at 2.40 ppm. The upfield singlet proton of the free base of porphyrin-N***H*** in **A3** disappeared from spectrum of **A4**. It showed that the metalation of zinc complex was successful. In addition, the elemental analysis and MALDI-TOF mass spectrum confirmed in good agreement of structure; *m/z* = 770.371, correspondind to the molecular ion [M] as the major signal (Anal. Calcd. *m/z* = 770.21).

.

3.1.3 Synthesis and characterization of 5-(4′-carboxy-2,2′-bipyridine-4-yl)-10,15,20-triphenylporphyrin (A5)

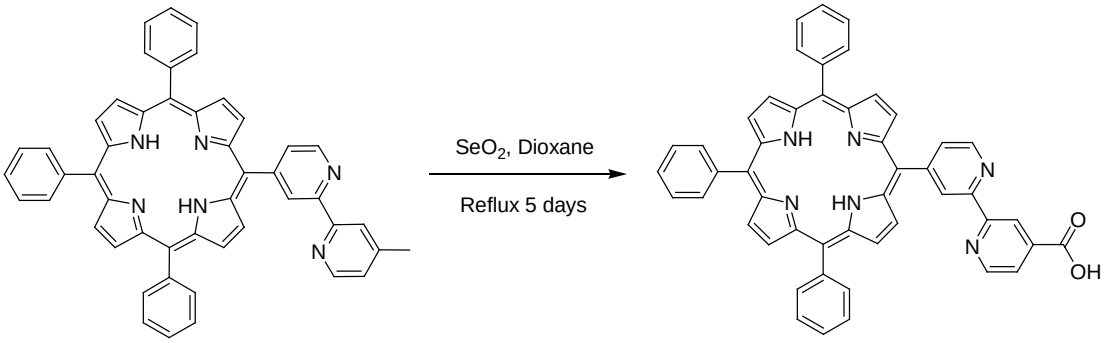

A3 **A5**

Scheme 3.3 Synthetic pathway of 5-(4′-carboxy-2,2′-bipyridine-4-yl)-10,15,20-triphenylporphyrin (**A5**)

5-(4′-carboxy-2,2′-bipyridine-4-yl)-10,15,20-triphenylporphyrin (**A5**) was synthesized by the oxidation of compound **A3** with SeO_2 in dioxane under nitrogen atmosphere for 5 days. The product was separated by column chromatography on siliga gel with MeOH/CH_2Cl_2 (5:95) as eluent to efford a purple solid in 45% yield. The ^{1}H NMR spectrum of compound **A5** showed the characteristic peaks of porphyrin in position of β-pyrrolic protons in porphyrin at 8.87-8.90 ppm, and the aromatic protons of meso position at 8.22-8.23, 7.76-7.78 ppm, respectively. The proton of the methyl group disappeared in spectrum, and ^{13}C NMR spectrum also exhibited carbon signal at 194.00 ppm. It is mentioning the methyl group should be transformed to carboxylic acid one. From the IR spectrum of **A5**, it exhited the significant signal of O-H stretching of carboxyl group at 3422 and C=O stretching 1713,which assigned to confirm in good agreement of carboxylic acid part.

3.1.4 Synthesis and characterization of 5-(4′-carboxy-2,2′-bipyridine-4-yl)-10,15,20-triphenylporphyrinatozinc (A6)

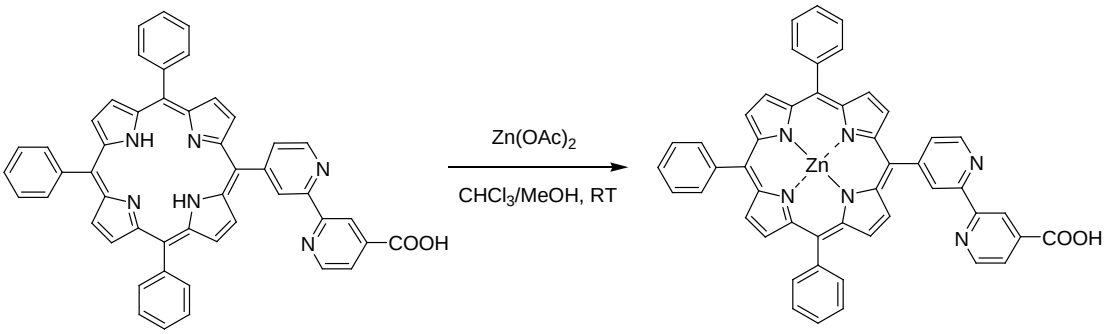

A5 **A6**

Scheme 3.4 Synthetic pathway of 5-(4′-carboxy-2,2′-bipyridine-4-yl)-10,15,20-triphenylporphyrinatozinc (**A6**)

The synthesis of 5-(4′-carboxy-2,2′-bipyridine-4-yl)-10,15,20-triphenyl porphyrinatozinc (**A6**) was performed by treating bipyridylporphyrin **A5** with $Zn(OAc)_2$ at room temperature for 24 hours. After purification by a column chromatography $MeOH/CH_2Cl_2$ (10:90), zinc compound **A6** was successful to afford as a purple solid in 95% yield. The ^1H NMR spectrum of zinc-bipyridylporphyrin **A6** showed characteristic peaks of β-pyrrolic protons in porphyrin ring at 8.78-8.86 (dd, $J_{H\text{-}H}$ = 4.8, 28.8 Hz) and 8.77 ppm, and the aromatic proton of meso position at 8.20, 7.78-7.79 ppm, respectively. The upfield singlet proton of the free base of porphyrin-N***H*** in **A5** disappeared from spectrum of **A4**. It showed that the metalation of zinc complex was successful. In addition, the elemental analysis and MALDI-TOF mass spectrum confirmed in good agreement of structure.

3.1.5 Synthesis and characterization of bipyridylporphyrin ruthenium complex (A7)

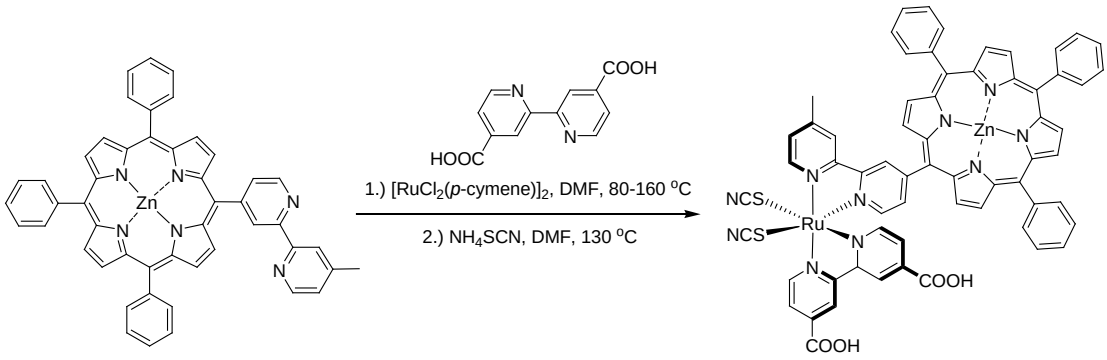

A4 **A7**

Scheme 3.5 Synthetic pathway of bipyridylporphyrin ruthenium complex (**A7**).

The complexation of **A7** was followed the general procudure of heteroleptic ruthenium complex [31, 37]. The first step, 5-(4′-methyl-bipyridine-4-yl)-10,15,20-triphenylporphyrinatozinc (**A4**) was reacted with dichloro(*p*-cymene)ruthenium(II) dimer with the ratio 1:1 equivalent in DMF at 80 °C under nitrogen for 6 hours resulting in a mononuclear complex. The progress of the reaction was monitored by TLC and then the heteroleptic dichloro complex was synthesized by reaction of the mononuclear complex with 4,4′-dicarboxyl-2,2′-bipyridine at higher temperature about 160°C over 6 hours under dark condition to avoid light induced *cis* to *trans* isomerisation. In the last step, the choro ligand was exchanged with a large excess of ammonium thiocyanate. From the highly hydrophobic complex, **A7** can be separated in the easy way by adding the water into the mix reaction and then the crude product precipitated. The bipyridylporphyrin ruthenium complex **A7** was purified by a Sephadex LH-20 column eluted with methanol. The red product of **A7** was collected in yield 58%.

3.1.6 Synthesis and characterization of bipyridylporphyrin ruthenium complex (A8)

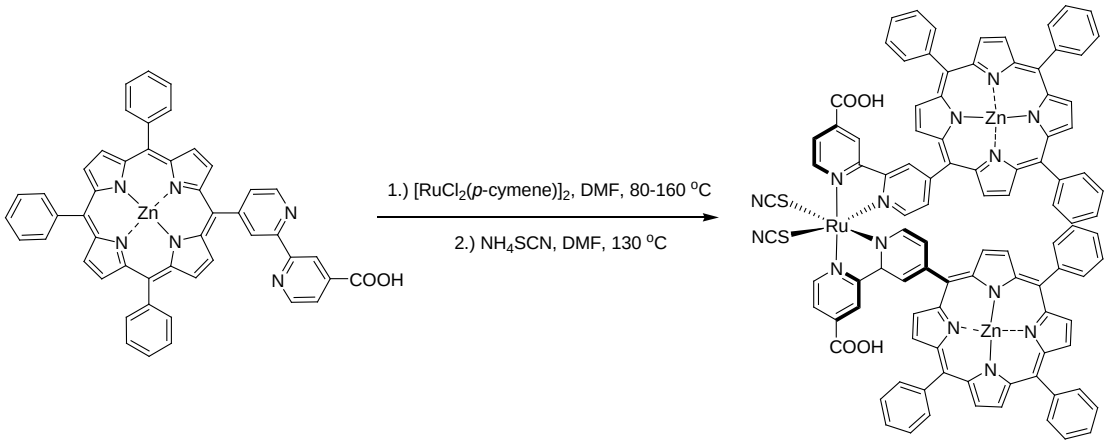

Scheme 3.6 Synthetic pathway of bipyridylporphyrin ruthenium complex (**A8**).

The complexation of **A8** was synthesized in one-pot synthesis. The first step, 5-(4′-carboxy-2,2′-bipyridine-4-yl)-10,15,20-triphenylporphyrina-tozinc (**A6**) was reacted with dichloro(*p*-cymene)ruthenium(II) dimer with the ratio 1:1 equivalent in DMF at 80 °C under nitrogen for 6 hours resulting in a mononuclear complex. Then the heteroleptic dichloro complex was synthesized by reaction of the mononuclear complex with another 1 equivalent of **A6** at higher temperature about 160°C over 6 hours under dark condition. In the last step, the choro ligand was exchanged with a large excess of ammonium thiocyanate ligand. From the highly hydrophobic complex, **A8** can be separated in the easy way by adding the water into the mix reaction and then the crude product precipitated. The bipyridylporphyrin ruthenium complex **A8** was purified by a Sephadex LH-20 column eluted with methanol. The red product of **A8** was collected in yield 52%.

3.2 Elemental analysis

Elemental analysis data were obtained by the facility of Scientific and Technological Research Equipment Centre (STREC) of Chulalongkorn University. The data shown in Table 3.1

Table 3.1 Elemental analysis data

Compound	Calculation			Found		
	C%	H%	N%	C%	H%	N%
A3	83.26	4.85	11.89	83.32	4.86	11.88
A4	76.41	4.19	10.91	76.10	4.19	10.92
A5	79.87	4.38	11.41	79.88	4.52	11.58
A6	73.55	3.78	10.50	73.50	3.79	10.65
A7	61.39	3.35	11.36	61.44	3.32	11.46
A8	66.04	3.38	10.78	-	-	-

3.3 ATR-FTIR spectroscopy

The ATR-IR spectra were performed by using Nicolet 6700 FT-IR spectrometer with solid sample. Bipyridylporphyrin **A3**, **A4**, **A5**, **A6**, **A7**, **A8** and **N719** show the significant signal at around 3300-3700 (broad), 3300, 2100 and 1500-1700 cm^{-1} which assigned to O-H stretching of carboxyl group, N-H stretching of porphyrin, C=N stretching of thiocyanate ligand (*cis*-configuration) and C=O stretching of carboxyl group, respectively.

From the spectra in Figure 3.3, **A3** and **A5** showed the significant signal of N-H stretching on the porphyrin ring, which were not observed in other Zn-porphyrin

compound **A4**, **A6**, **A7** and **A8.** The carboxylic acid as anchoring group in the dye-photosensitizers were also appeared the significant peaks of O-H stretching and C=O stretching of carboxyl group in the dye-photosensitizers **A5**, **A6**, **A7**, **A8** and **N719**. Moreover, the C=N stretching of thiocyanate ligand were showed in the ruthenium complexes of **A7**, **A8** and **N719**, respectively.

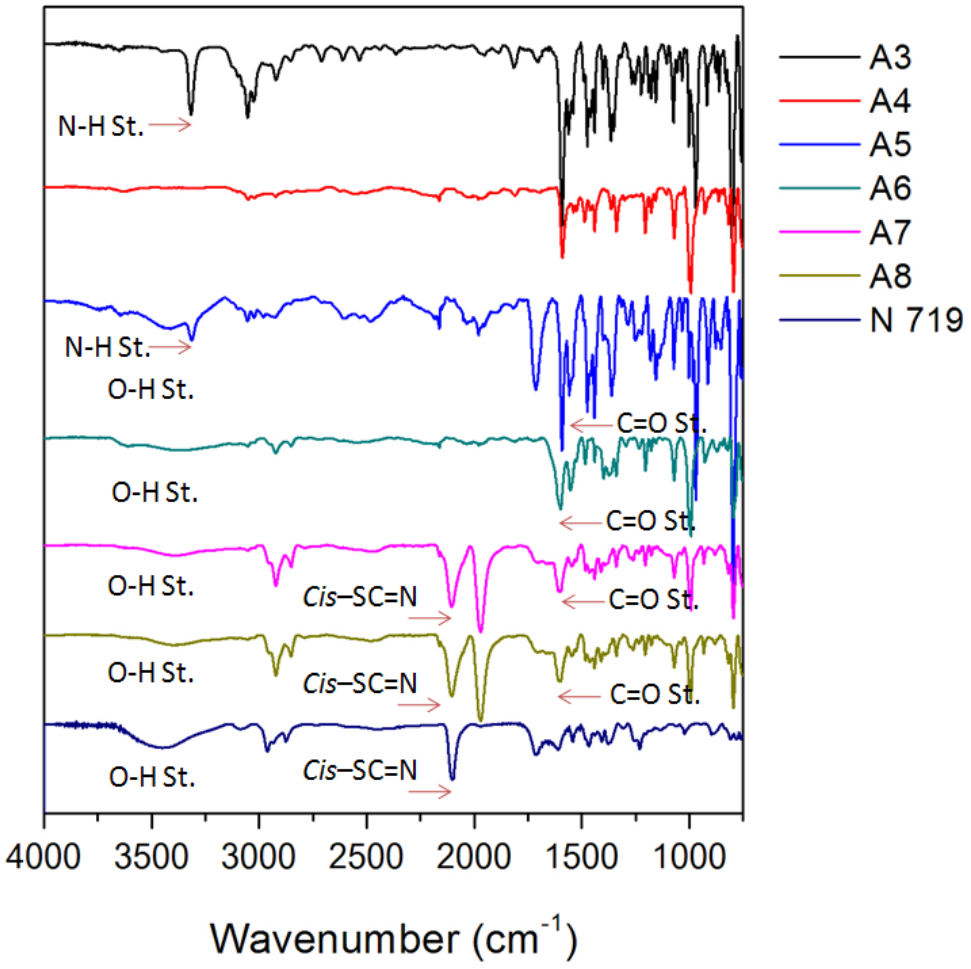

Figure 3.3 Relative ATR-IR spectra of bipyridylporphyrin **A3**, **A4**, **A5**, **A6**, **A7**, **A8** and **N719**.

3.4 Physical properties

The absorption spectra of the bipyridylporphyrin derivatives exhibited 2 major absorption bands of porphyrin. The Soret band around 420 nm, assigned to π - π^* transition to the second electronic exited state, and Q-bands around 500- 600 nm, corresponding to π - π^* transition to the first electronic exited state followed by Figure 3.3. In addition, the strong absorption band at 300 nm is due to $[Ru(bpy)_3]^{2+}$ moiety (bipy π - π^*), referred as ligand-based charge transfer (LC) transition.

The main absorption bands of bipyridylporphyrin ruthenium complex **A7** and **A8** display also a slight red shift and broad band, compared to the bipyridylporphyrin derivatives **A4-A6**, suggesting some interactions between the intramolecular porphyrin and $[Ru(bpy)_3]^{2+}$ moiety. In addition, the absorption spectra of Q-band in case of **A3** and **A5** showed the 4 Q-band characteristic of free base porphyrin and the absorption spectra of **A4** and **A6** also exhibited the 2 Q-band characteristic of Zn-porphyrin in fugure 3.4 and 3.5. In the case of the reference dye **N719**, the ligand-based charge transfer (LC) transition, MLCT I and MLCT II were exhibited around 311, 382 and 535 nm, respectively.

From the absorption spectra of dye-sensitizers **A5**, **A6**, **A7** and **A8**, the dyes can absorb the light in the range of solar wavelength and near-IR region, and considering that the dye-photosensitizer **A5**, **A6**, **A7** and **A8** could act like an antenna in plant to absorb the solar light in solar cells [38-41].

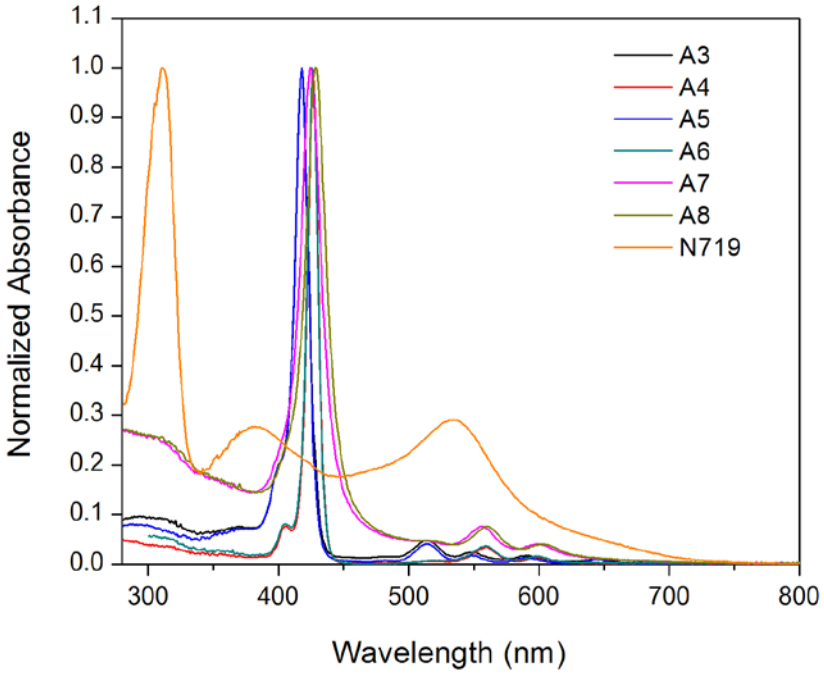

Figure 3.4 Normalized absorption spectra of bipyridyldiporphyrin derivatives and **N719** in DMF solvent.

The normalized emission spectra of all the bipyridyldiporphyrin derivatives and **N719** at in DMF are shown in Table 3.2. The emission spectra were performed by using excitation wavelength at Soret wavelength of each porphyrin. All dyes showed relatively strong emission with two emission maximum (λ_{em}) in the range of 612-717 nm. According to the excitation wavelength was overlab in the π-π* transition band, this emission band corresponded to the π*-π radiative decay.

According to absorption spectra, the energy gaps (E_g) calculated from the intersection between the absorption spectra and baseline (λ_{onset}) to the following equation.

$$E_g = 1240/ \lambda_{onset}.$$

The λ_{onset} can be converted to E_g (eV) which can further be used to define the electronic properties of a compound.

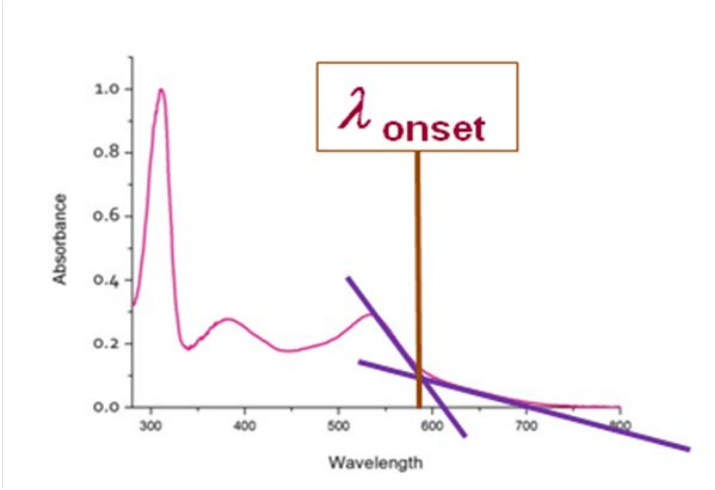

Figure 3.5 λ_{onset} of dye-sensitizer.

Table 3.2 The electronic absorption of the bipyridyldiporphyrin derivatives and **N719** altogether with E_g of corresponding compounds.

Dye	**Absorption (λ_{max}/nm) (ε/M^{-1} cm^{-1})**	**λ_{em} (nm)**	**λ_{onset} (V)**	**E_g (eV)**
A3	417(92603), 514 (46146), 549 (25015), 589 (18648), 644 (14220)	653, 717	663	1.87
A4	426 (1764354), 559 (53672), 600 (25759)	612, 659	612	2.03
A5	418 (87285), 514 (39213), 547 (17410), 592 (12343), 644 (7471)	614, 660	662	1.87
A6	426 (59830), 559 (24328), 600 (11497)	622, 660	614	2.02
A7	424 (5419), 555 (398), 530 (223)	624, 660, 723	651	1.90
A8	429 (5208), 560 (384), 535 (198)	626, 660, 728	656	1.89
N 719	311 (69737), 382 (19723), 535 (21013)	721	608	2.04

3.5 Electrochemical properties

All electrochemical data of bipyridyldiporphyrin derivatives and **N719** were collected by using the cyclic voltammetry on a μ-AUTOLAB potential using a glassy carbon working electrode, a Pt wire counter electrode and a $Ag/AgNO_3$ (Sat.) reference electrode at room temperature. The supporting electrolyte was 0.1 M $TBAPF_6$ in freshly distilled DMF and the concentration of analyzes were 1.0 mM. The solutions were purged with nitrogen. All samples were measured with a scan rate of 100 mV/sec.

The cyclic voltammogram of bipyridylporphyrin complex peaks showed the first and second oxidation of porphyrin unit in the bipyridyldiporphyrin derivatives **A5**, **A6**, **A7** and **A8**, and the oxidation peak of Ru^{II}/Ru^{III} part in **A7**, **A8** and **N719**, respectively. For the cyclic voltammogram shown in Figure 3.7, the first oxidation potential belongs at E_{onset} of 0.16, 0.29, 0.25, 0.15 and 0.22 V corresponding to **A5**, **A6**, **A7**, **A8** and **N719** as shown in Table 3.3.

From the cyclic voltammogram, the highest occupied molecular orbital (HOMO) energy level calculated by using data provided by a cyclic voltammogram as a parameter in Equation 1. First oxidation potential at E_{onset} can be obtained directly in this equation by using ferrocene as reference. The lowest unoccupied molecular orbital (LUMO) energy level can be calculated from the Equation 2 [42]. All electronic properties from the experimental calculation of bipyridyldiporphyrin derivatives and **N719** are illustrated in Table 3.3.

$$E_{HOMO}\,(eV) = -\,(E^{ox}_{onset} - E_{1/2\ fer} + 4.8) \qquad \textbf{Equation 1}$$

$$E_{LUMO}\,(eV) = E_{HOMO} + E_g \qquad \textbf{Equation 2}$$

Where $E_{1/2\ fer}$ in this experiment is -0.015 eV obtained from $E_{1/2}$ of reference ferrocene couple [43].

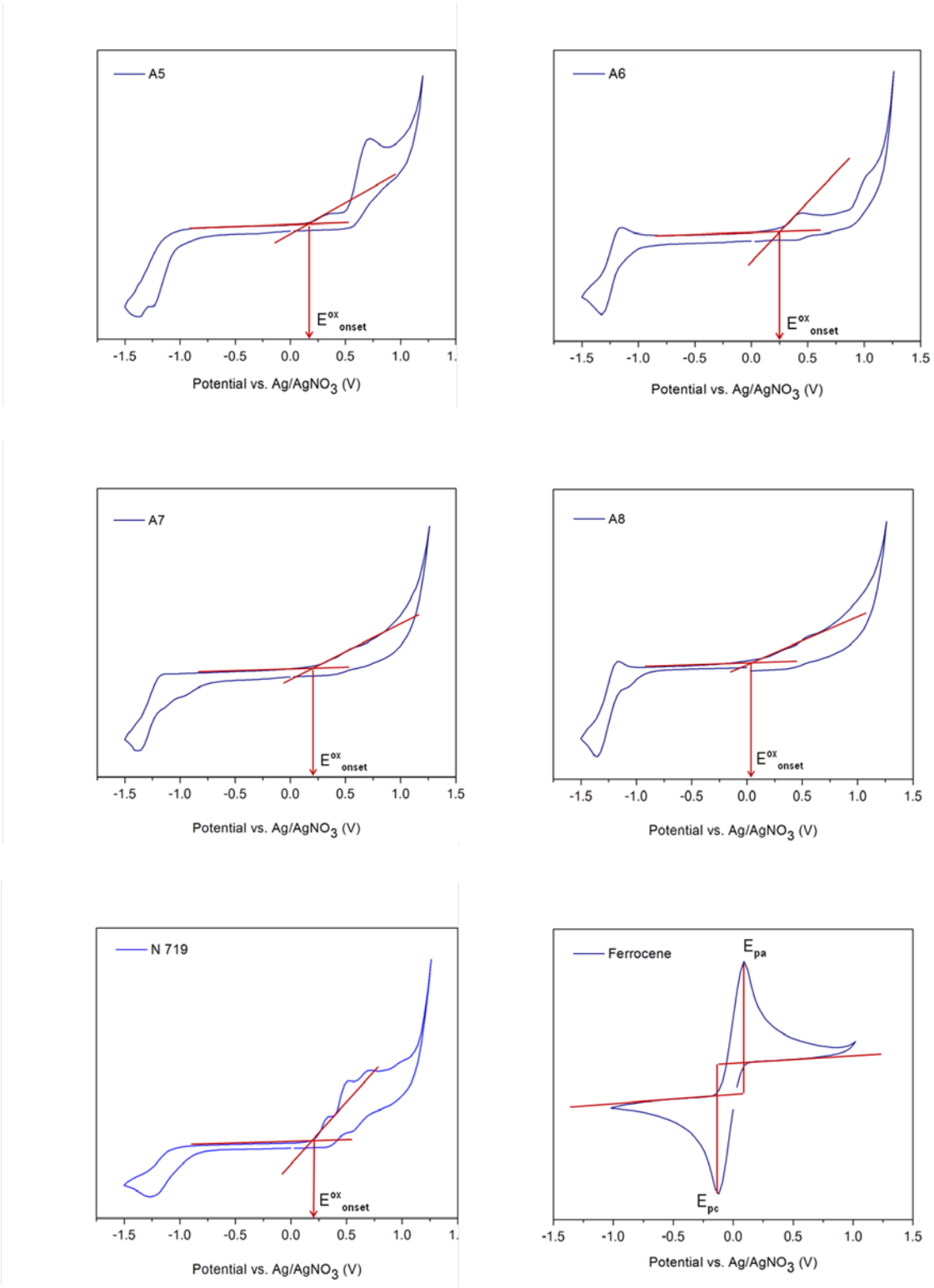

Figure 3.6 Cyclic voltammograms of bipyridyldiporphyrin derivatives and **N719**.

Table 3.3 Electronic properties of bipyridyldiporphyrin derivatives and **N719**.

Dye	E^{ox}_{onset} (V)	E_{HOMO} (eV)	E_g (eV)	E_{LUMO} (eV)
A5	0.16	-4.98	1.87	-3.10
A6	0.29	-5.10	2.02	-3.08
A7	0.25	-5.06	1.90	-3.16
A8	0.15	-4.96	1.89	-3.07
N719	0.22	-5.04	2.04	-3.00

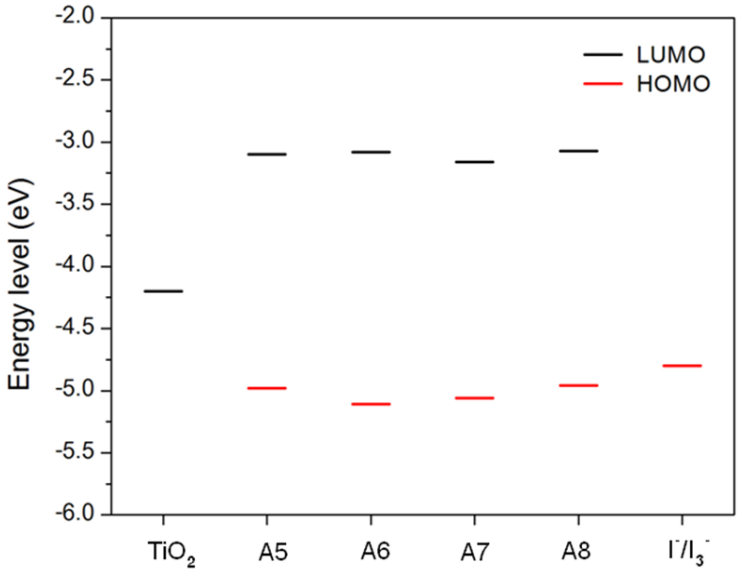

Figure 3.7 Energy diagram obtained from experimental.

The Figure 3.8 showed energy diagram obtained from experimental calculation. Considering the HOMO-LUMO energy level for use as dye-photosensitizer, the HOMO level of all dyes have to be lower than redox couple (I^-/I_3^-) to accept the electron from electrolyte to regenerate the dye (S^0) in system, and the LUMO lever of the dye have to be higher than the conduction band of titanium dioxide for suitable in the electron injection to the FTO electrode upon the illumination. The results indicated that bipyridylporphyrin **A5-A8** could be used as photosensitizer for dye-sensitized solar cell application, due to the LUMO and HOMO levels of all complexes are higher than the conduction band of TiO_2, -4.2 eV, and lower than HOMO level of redox couple (I^-/I_3^-), -4.8 eV, in electrolytic system, respectively [44].

3.6 Theoretical calculation

DFT calculations were employed to gain the equilibrium geometry and electronic structures for the frontier orbitals of the bipyridylporphyrin derivatives. Porphyrin generally showed two energetically degenerate LUMOs (LUMO+1, LUMO) and two nearly degenerate HOMOs (HOMO-1, HOMO). The calculation structure shown the electron distribution of **A5** at the ground state before the light irradiation (HOMO) and after light irradiation (LUMO) were delocalized mainly over porphyrin moiety.

For **A6**, which is zinc complex is shown the electron density at HOMO level over porphyrin moisty and at LUMO level, the electron density was moved to the bipyridyl unit due to their injected electron from porphyrin moisty at the ground state to the bipyridyl moisty on the excitate state.

For **A7**, The electron density located around only bipyridyl part for both HOMO and LOMO levels. The characteristics of the dyes are shown in Table 3.4.

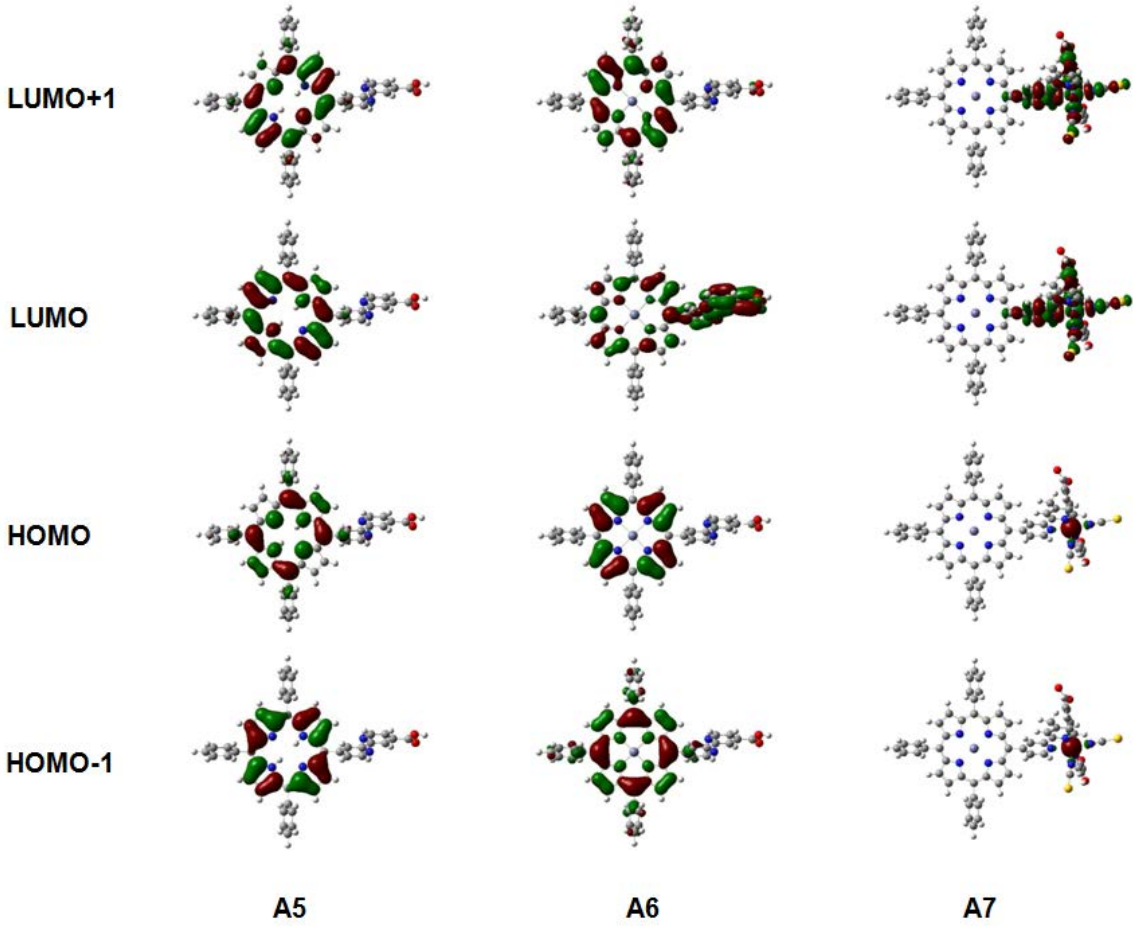

Figure 3.8 Plots of LUMO+1, LUMO, HOMO and HOMO-1 orbital for **A5**, **A6** and **A7**, which optimized at B3LYP/6-31G(d) (**A4** and **A5**) and LanL2DZ (**A7**) level theory.

Table 3.4 Molecular Orbital Energy Levels and energy gaps (in eV) of bipyridylporphyrin dyes, which optimized at B3LYP/ LanL2DZ for all dyes.

	A5	**A6**	**A7**	**A8**
LUMO+1	-2.57	-2.51	-3.37	-
LUMO	-2.60	-2.53	-3.73	-
HOMO	-5.23	-5.26	-5.61	-
HOMO-1	-5.61	-5.54	-5.97	-
$\mathbf{E_g^{cal}}$	2.63	2.73	1.88	-

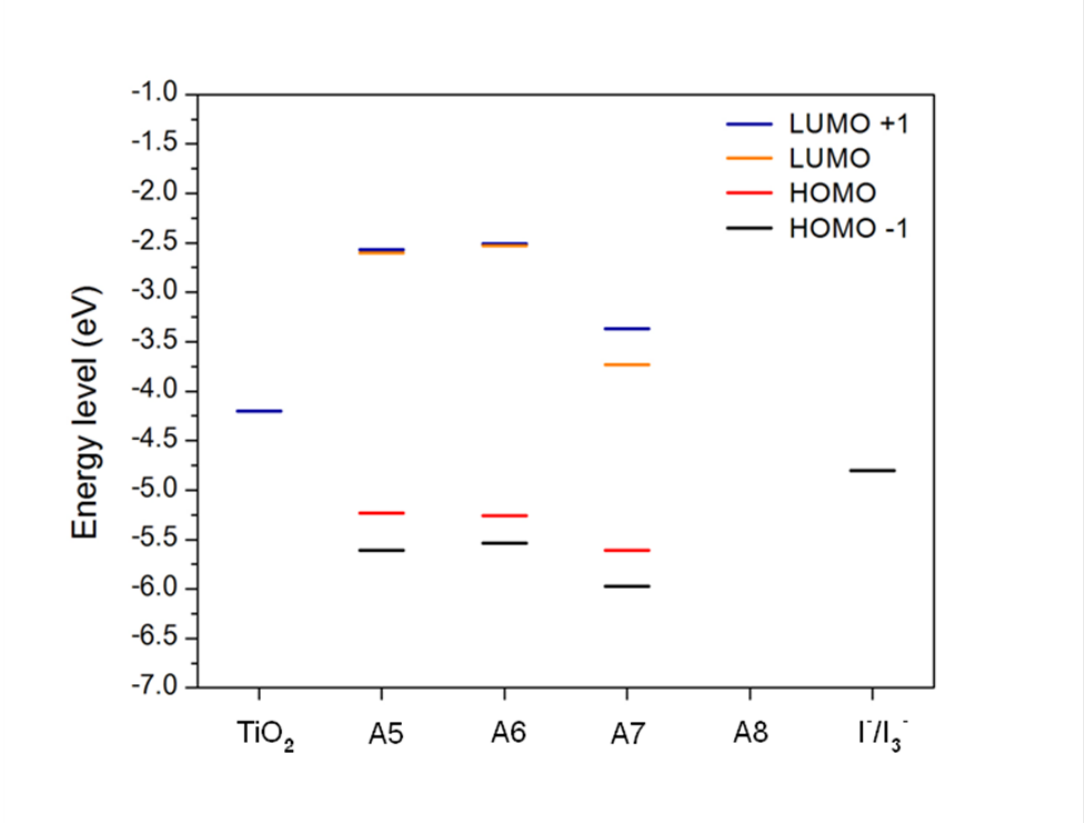

Figure 3.9 Energy diagram obtained from theoretical calculation.

The calculated LUMO levels are in range of -2.53 to –3.73 eV, which matched well with the CB band of TiO_2 favoring electron jumping from dyes to TiO_2. The

calculated HOMO levels are in range -5.23 to -5.61 eV, which matched well with the redox potential of the I^-/I_3^- electrolyte favoring electron jumping from electrolyte to dyes. This trend is supported with the photophysical and electrochemical HOMO-LUMO levels.

3.7 Preparation of DSSCs

The process of dye sensitized solar cells fabrication is described as follows:

1. The F-doped SnO_2 (FTO, purchased from Dyesol Industries Pty Ltd) glass was cut into 2×1.3 cm^2 size and then cleaned the surface by sonicated with the surfactant, water, aqua ligia, water, ethanol and acetone for 30 minutes in each step.

2. Screen printing the TiO_2 on the FTO glass.

First of all, the FTO glass plates were immersed into a $TiCl_4$ solution to prevent contact between the redox mediator in the electrolyte and the FTO. Two types of nanocrystalline-TiO_2 paste, nanocrystalline-TiO_2 20 nm for a light absorption layer that provides a large surface area for dye-sensitizer adsorption and good electron transport to the substrate, and submicronanocrystalline-TiO_2 70 μm for light-scattering layer were coated on corresponding glass electrode by using screen-printing technique. The working electrode was heated step by step at 325 °C to 450 °C to eliminate such as the solvent and the organic substances. Finally, the overcoating on

TiO_2 electrode was treated again with 40 mM $TiCl_4$ solution and sintered by heat treatment.

3. Dipping the FTO glass into the dye solution.

Before dipping into the dye solution, the working electrode was heated at 80 °C to avoid the absorption of water on TiO_2 surface, then the electrode was dipped into a dye solution and maintained under dark for 24 hours.

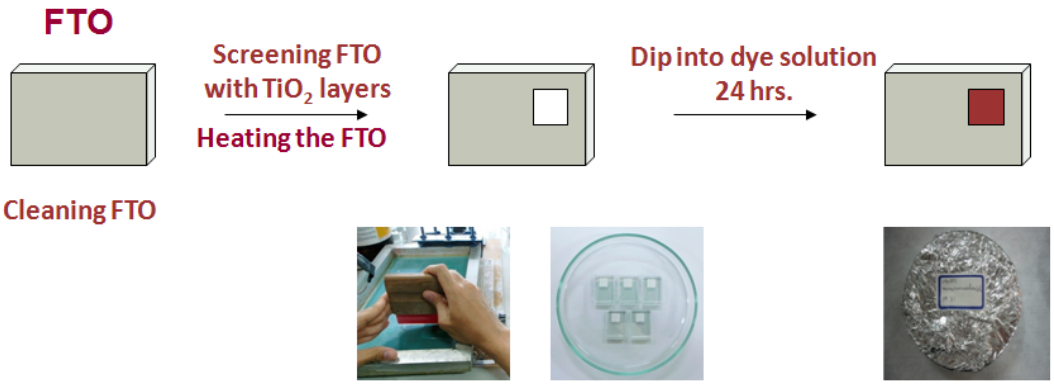

4. Counter electrode

For a counter electrode, FTO plates were drilled and cleaned by the previous method. After heating, the Pt catalyst was deposited on FTO by dropping of H_2PtCl_6 solution, and the solvent was dried at room temperature for 12 hrs.

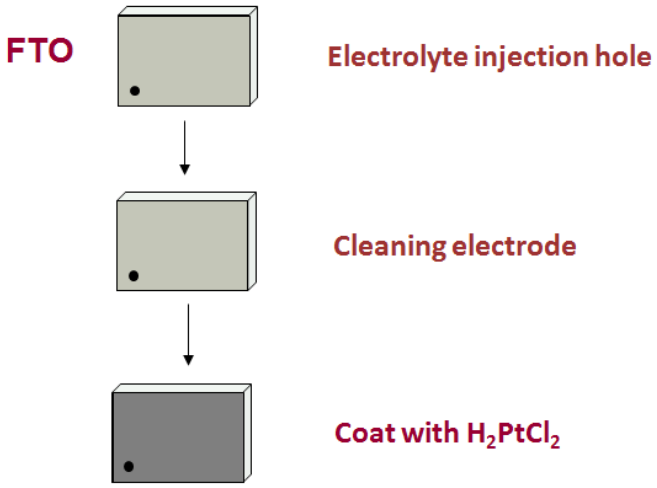

5. Attaching with Platinum electrode.

A sandwich cell was performed by assembly the counter Pt-electrode with the dye-coated working electrode, which separated by thin adhesive polymeric film sheets. The sandwiched electrodes were tightly held, and then heated around the thin film sheets to attach the two electrodes. The electrolyte was introduced into the inter-electrode space. Then, the cells were sealed with a cover glass to avoid leakage of the electrolyte solution. Pt foil was clipped onto the top of surface of the electrodes and silver paint was covered onto the conductive side for correcting electron.

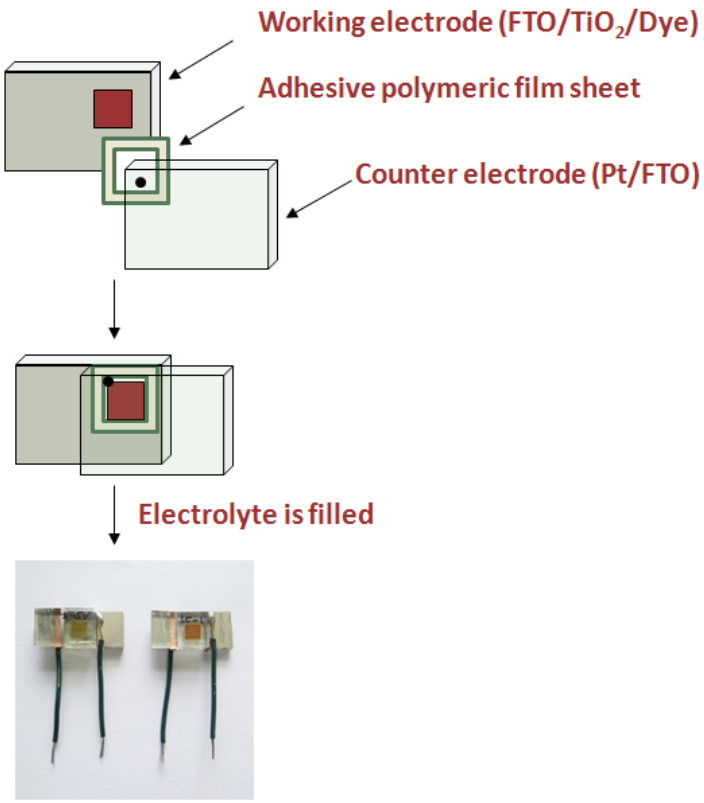

6. Measuring the photovoltaic performance of the cell using a 1000 W ozone free xenon light source that gives intensity at the cell surface of 100 mW/cm^2 equivalent to one sun at Air Mass (AM) 1.5.

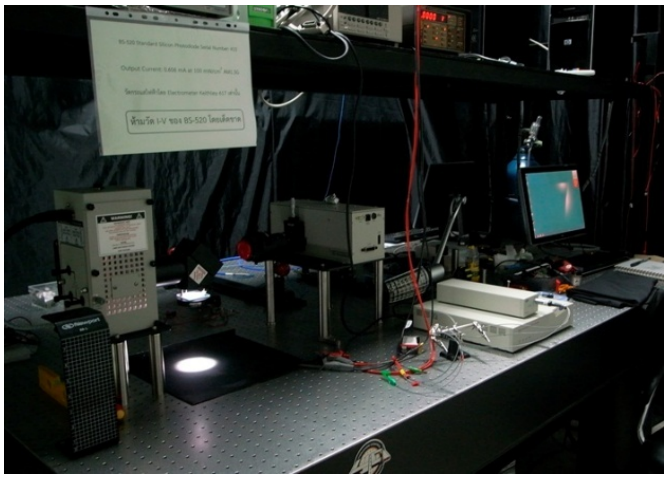

3.8 Photovoltaic performance

The photovoltaic performances of all experiments were showed in a relationship between current (mA/cm^2) and voltage (V). The photovoltaic parameters: short-circuit current density (J_{sc}), open-circuit voltage (V_{oc}), fill factor (*ff*), and overall conversion efficiency (η), were gained from experiments.

3.8.1 The photovoltaic properties of N719 with the various electrolytes

Fine tuning of the best electrolyte for using in all experiment in this thesis were investigated on reference dye **N719** and showed in Table 3.5.

First of all, the primary test was performed on DSSCs cell in difference electrolytic system. **E1** is general systematic of solvent, which optimized from The National Nanotechnology Institute, Bangkok and **E2** is general systematic of solvent from Center for Organic Electronic and Alternative Energy, Ubon Ratchatanee University. To find the best condition for all experiments, the result showed that **E2** retained the conversion efficiency better than electrolyte **E1** (η = 4.45 Vs 3.89%).

Although electrolyte **E1** gave the lower efficiency, but there was not optimize condition. Hence, we intended to try to improve the condition of **E1** in the future work to get it better the conversion efficiency than the modified **E2** electrolyte.

Next step, the comparison of ionic liquid effect as charge transfer intermediate in electrolytic system to improve the J_{sc} parameter in electron transfer process; **E2** as reference**, E3** in a present of ionic liquid PMII and **A4** in a present of ionic liquid TPAI, there showed that electrolyte **E4** perform the conversion efficiency better than electrolyte **E3** (η = 4.61 of **E4** Vs 3.66% of **E3**). The higher J_{sc} parameter in **E3** and **E4** presented that ionic liquid can be improved the electron transfer process in the system.

Furthermore, TBP and pyridine were use as additive to improve V_{oc} in this system. **E4** (pyridine) and **E5** (TBP) in a present of ionic liquid TPAI showed the higher efficiency in **E5** (η = 5.97 Vs 4.61% of **E4**) due to the improvement of V_{oc} in both cases.

The summary of this systematic variation of the electrolyte reflects the conversion efficiency, which decreased from **E5** (5.40%) > **E4** (4.61%) > **E1** (4.45)> **E2** (3.98) > **E3** (3.66%) as difference effects. From of the observation, **E5** (0.10 M LiI, 0.05 M I_2, 0.40 M pyridine and 0.60 M TPAI) was achieved the best performance via adjustment with the ionic liquid and additive, and used as electrolyte in all experiments.

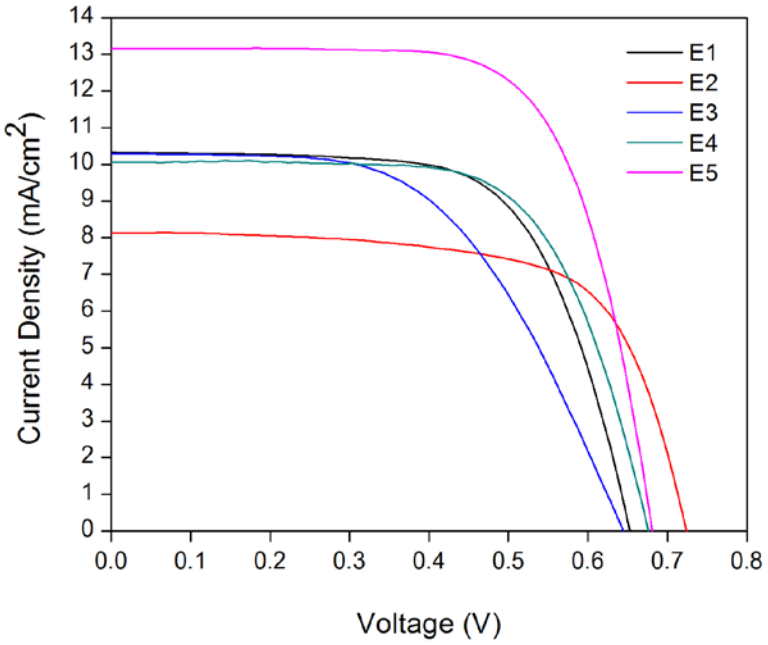

Figure 3.10 Photocurrent–voltage characteristics of representative TiO_2 electrodes sensitized with **N719** dye in the various electrolytes **E1**-**E5**.

Table 3.5 Photovoltaic performance of DSSCs based on **N719** dye with the various electrolytes **E1**-**E5**.

Electrolyte	V_{oc} (V)	J_{sc} (mA/cm^2)	fill factor (*FF*)	η (%)
E1	0.65	10.32	0.66	4.45
E2	0.72	8.13	0.68	3.98
E3	0.64	10.36	0.55	3.66
E4	0.68	10.18	0.67	4.61
E5	0.68	13.02	0.68	5.97

3.8.2 Solubility and dye adsorption on TiO_2

From the solubility test and the dye adsorption, EtOH solvent exhibited the good properties for use as a solvent by accelerated diffusion of dye into TiO_2 surface masked with more binding sites and dye adsorption was increased leading to increase in photocurrent and conversion efficiency.

The primary test of dye's solubility showed in this trend:

$$EtOH \approx DMF \approx THF > CHCl_3 > MeOH \approx Toluene.$$

And the dye adsorption followed by:

$$EtOH > THF > MeOH \approx CHCl_3 \approx Toluene \approx DMF$$

Table 3.6 Solubility and dye adsorption on TiO_2.

Solvent	Polarity	Solubility	Dye absorption on TiO_2
DMF	6.4	///	/
EtOH	5.2	///	///
MeOH	5.1	X	X
$CHCl_3$	4.1	//	//
THF	4.0	///	//
Toluene	2.4	X	X

* /// = Good solubility, // = fair solubility, / = poor solubility, X = insoluble

3.8.3 The photovoltaic properties of bipyridylporphyrin derivatives and N719

The photovoltaic properties of the solar cells constructed from organic dye-sensitized TiO_2 electrodes were measured under simulated AM 1.5 irradiation. The optimized evaluation conditions for all dyes were determined to be 5 x 10^{-4} M of dye in ethanol solution and used **E5 (**0.10 M LiI, 0.05 M I_2 0.40 M pyridine and 0.60 M TPAI in 50:50 ; CH_3CN:valeronitrile**)** as electrolyte. The photovoltaic performance of the bipyridylporphyrin derivatives are summarised in Table 3.7. Current density–voltage (I–V) characteristics and incident photon-to current conversion efficiencies (IPCE) of devices are shown in Figures 3.11 and 3.12, respectively. The data **A5** with free base porphyrin showed the lower conversion efficiency, according to the result of electron distribution from computational calculation over porphyrin at both HOMO and LUMO level. The bipyridylporphyrin ruthenium **A7** exhibited an excellent cell performance with $J_{sc,}$ 1.33 mA/cm^2, V_{oc} 0.45 V, *FF* 0.64 and η 0.38% due to the higher J_{sc} of **A7** over another bipyridylporphyrin dye, which showed that the D-A system of **A7** can be improved the electron injection in DSSCs cell. Although **A8** was the D-A system like the **A7** dye but the cell performance of **A8** was poorer than **A7**, there might be reducing of efficiency due to the steric hindrance effect of **A8** to cover on TiO_2. Moreover, the lower conversion efficiency of the porphyrin dye might be the cause of the aggregation between porphyrin dyes onto the TiO_2 surface.

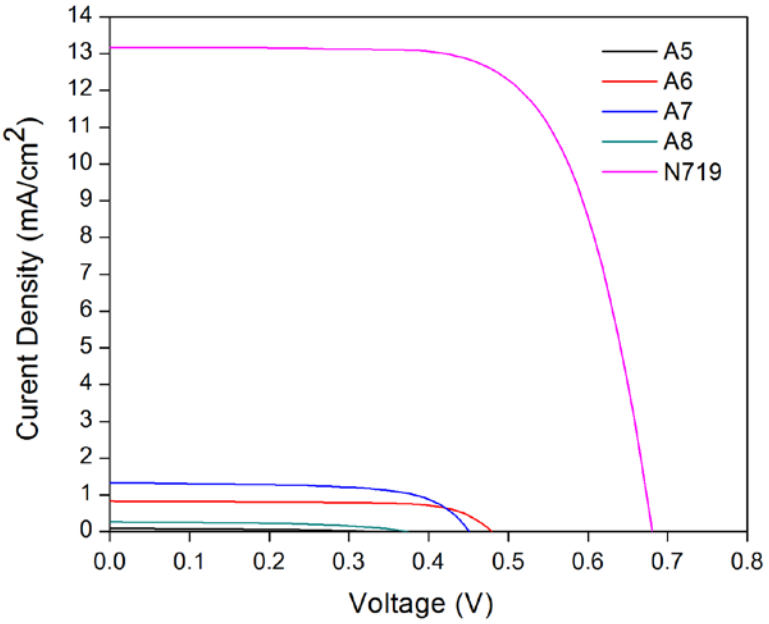

Figure 3.11 Photocurrent–voltage characteristics of representative TiO_2 electrodes sensitized with bipyridylporphyrin derivatives and **N719** with the electrolyte **E5**.

Table 3.7 Photovoltaic performance of DSSCs based on bipyridylporphyrin derivatives and **N719** dye with the electrolyte **E5**.

Dye	V_{oc} (V)	J_{sc} (mA/cm^2)	fill factor *(FF)*	η (%)
A5	0.33	0.09	0.47	0.05
A6	0.48	0.83	0.70	0.28
A7	0.45	1.33	0.64	0.38
A8	0.37	0.26	0.51	0.05
N719	0.68	13.02	0.68	5.97

According to incident photon-to-current conversion efficiency (IPCE) as a function of wavelength for the DSSCs based on bipyridylporphyrin derivatives with the electrolytes **E5** in Figure 3.12, the Soret band showed the higher IPCE value due to extinction coefficient of Soret band is frist order of magnitude larger than Q bands.

On the other hand, all bipyridylporphyrin derivatives showed the efficiency of 10-20% from 350 to 480 lower than IPCE of **N719** with the maximum of about 65% in range of visible light. The standard **N719** provides the best conversion efficiency because it can sufficiently harvest the light over the wide range of spectrum. The J_{sc} value of **N719** indicated that the electron injection was preferred and lead to the higher IPCE efficiency of **N719** sensitizer.

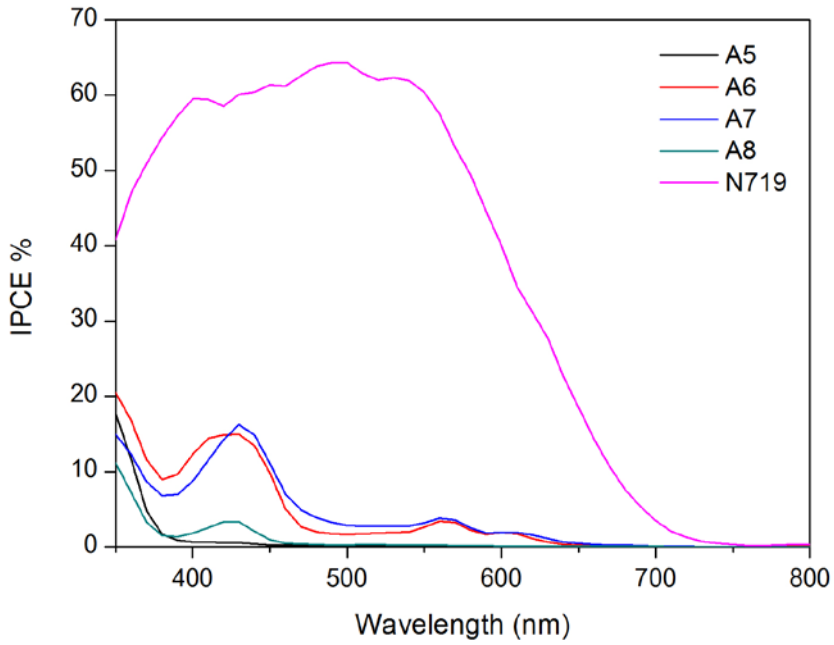

Figure 3.12 Incident photon-to-current conversion efficiency (IPCE) as a function of wavelength for the DSSCs based on bipyridylporphyrin derivatives and **N719** dye with the electrolytes **E5**.

3.8.4 The effect of CDCA concentration on photovoltaic performance

Chenodeoxycholic acid (CDCA) is used as a coabsorbate of the dye-sensitizer on the TiO_2 surface to dissociate the π-stacked dye aggregation between adjacent molecule. The ratios of the concentration of compound **A6** and CDCA were 1:0.5, 1:1, 1:2, 1:5 and 1;10. A power conversion efficiency of 0.28% was obtained for the DSSC based on **A6** as dye-sensitizer, which was significantly improved to 0.35% upon addition of CDCA into the **A6** solution for TiO_2 sensitization. The best cell performance of CDCA/Dye is for the cell ratio of 1:2. Coadsorption of CDCA decreased the dye adsorption, but significantly improved both short circuit current (J_{sc}) and open circuit voltage (V_{oc}). The breakup of π stacked aggregates might improve the electron injection yield and thus the increasing in J_{sc} has also been attributed to the reduction of the back reaction and the recombination of electrons with electrolyte.

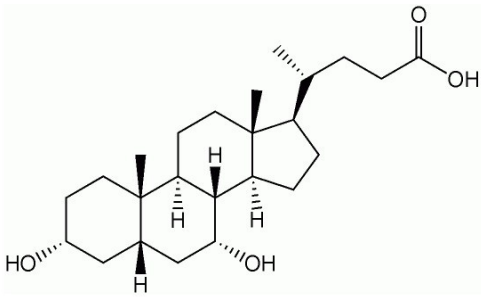

Figure 3.13 Structure of chenodeoxycholic acid.

Table 3.8 Photovoltaic performance of DSSCs based on bipyridylporphyrin derivative **A6** with a variety of CDCA concentrations**.**

Equivalent of CDCA/Dye	V_{oc} **(V)**	J_{sc} **(mA/cm^2)**	**fill factor (*FF*)**	η **(%)**
0.5	0.46	0.35	0.71	0.11
1.0	0.45	0.68	0.49	0.14
2.0	0.53	0.88	0.76	0.35
5.0	0.50	0.67	0.74	0.25
10.0	0.46	0.29	0.69	0.09

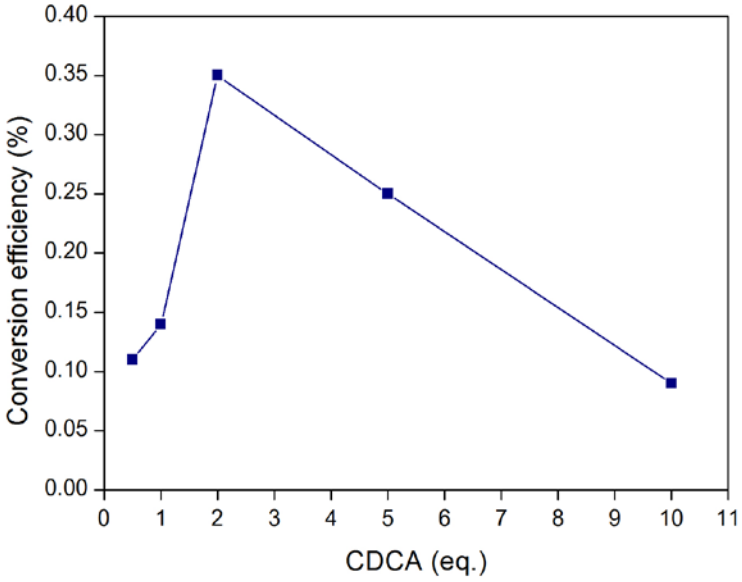

Figure 3.14 Solar-to-electricity conversion efficiency of TiO_2 electrodes sensitized with a variety CDCA concentrations**.**

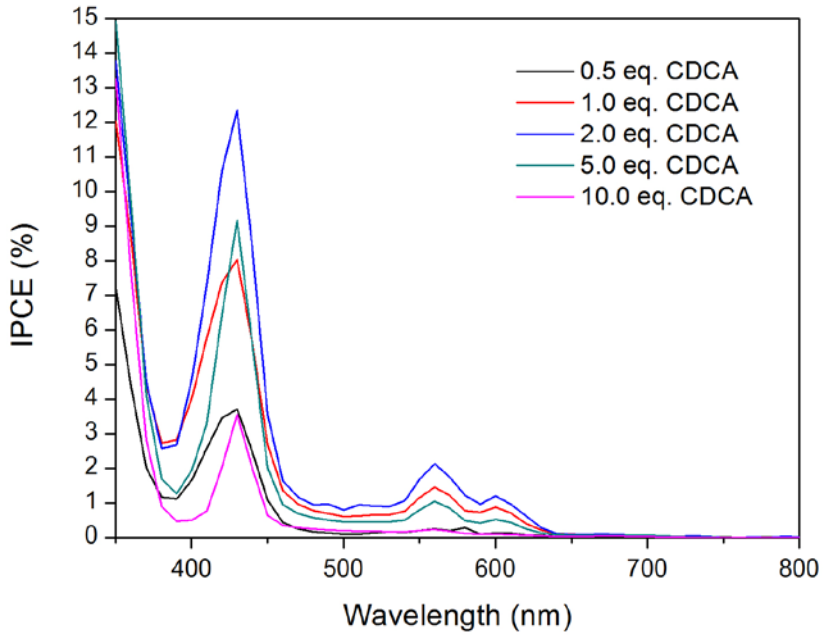

Figure 3.15 Incident photon-to-current conversion efficiency (IPCE) as a function of wavelength for the DSSCs based on bipyridylporphyrin derivative **A6** with a variety of CDCA concentrations**.**

CHAPTER IV

CONCLUSION

Bipyridylporphyrin derivatives were designed and synthesized for use as dye-sensitizer in dye-sensitized solar cells (DSSCs). Bipyridylporphyrin derivatives composed of Donor-Acceptor system (D-A) based on porphyrin moiety as the electron donor (D) and bipyridyl moiety as the electron-acceptor (A). The synthetic pathways of the bipyridylporphyrin derivetives for use as dye-sensitizer started from the compound 4,4′-dimethyl-2,2′-bipyridine was oxidized with SeO_2 to afford monoaldehyde **A1**. Bispyrrole **A2** was condensed between pyyrole and benzaldehyde in TFA. Then bipyridylporphyrin **A3** was obtained from condensation reaction between **A1**, **A2** and benzaldehyde in refluxing propionic acid/toluene using air-oxidation and used as the porphyrin-based for synthetic of the other bipyridylporphyrin derivatives in the next pathway. For the pathway 1 started from bipyridylporphyrin **A3**, which converted to zinc complex **A4** via metalation after that coupling with $[Ru(p\text{-cymene})Cl_2]_2$ complex then compound **A7** was occurred. For the pathway 2, the methyl group of **A3** was transformed to carboxylic acid one of **A5** using SeO_2 as oxidant. Treatment of **A5** with zinc acetate gave zinc porphyrin complex **A6**. Finally, the bipyridylporphyrin was transformed to bipyridylporphyrin ruthenium complex **A8** after that coupling with $[Ru(p\text{-cymene})Cl_2]_2$ complex. All compounds were characterized and confirmed structures by NMR, IR, Mass spectroscopy and Elemental Analysis. From the experimental and the theoretical calculation, the HOMO and LUMO energy levels of all compounds are in range, which match well with the CB band of TiO_2 favoring electron injection from the exited dyes (s*) to TiO_2 and the redox potential of the I^-/I_3^-electrolyte favoring electron injection from the electrolyte to the cationic dyes (S^+). Upon the studies of the photovoltaic performance measurements, a overall solar-to-electric conversion efficiency under AM 1.5 irradiation and use 0.10 M LiI, 0.05 M I_2, 0.40 M pyridine and 0.60 M TPAI as electrolytic system of 0.05, 0.28, 0.38 and 0.05 % was achieved based on the bipyridylporphyrin dyes **A5**, **A6**, **A7** and **A8**, respectively, which were

lower than the efficiency obtained from the standard dye **N719** (5.97%). From the short circuit photocurrent density of the bipyridylporphyrin dyes **A5**, **A6**, **A7** and **A8**, showed lower than the standard dye **N719**, possibly due to poorer electron injection from bipyridylporphyrin dyes onto the TiO_2 surface. In addition, the efficiency of the dye was improved by adding chenodeoxycholic acid (CDCA) as the coadsorbant.

REFERENCES

[1] Grätzel, M. Photoelectrochemical cells. *Nature* 414 (2001): 338-344.

[2] Grätzel, M. Solar energy conversion by dye-sensitized photovoltaic cells, *Inorg. Chem.* 44 (2005): 6841-6851.

[3] O'regan, B. and Grätzel, M. A low-cost, high-efficiency solar cell based on dye sensitized colloidal TiO_2 films. *Nature* 353 (1991): 737—740.

[4] Nazeeruddin, M. K.; De Angelis, F.; Fantacci, S.; Selloni, A.; Viscardi, G. and Grätzel, M. Combined experimental and DFT-TDDFT computational study of photoelectrochemical cell ruthenium sensitizers. *J. Am. Chem. Soc*. 127 (2005): 16835-16847.

[5] Choi, H., Lee, J. K., Song, H. K., Song, K., Kang, S. O. and Ko, J. Synthesis of new julolidine dyes having bithiophene derivatives for solar cell. *Tetrahedron* 63 (2007): 1553-1559.

[6] Boschloo, G. and Hagfeldt, A. Characteristics of the iodide/triiodide redox mediator in dye-sensitized solar cells. *Acc. Chem. Res.* 42 (2009): 1819-1826.

[7] Imahori, H., Umeyama, T. and Ito, S. Large π-aromatic molecules as potential sensitizers for highly efficient dye-sensitized solar cells. *Account. Chem. Res.* 42 (2009): 1809-1818.

[8] Ooyama, Y. and Harima, Y. Molecular Designs and syntheses of organic dyes for dye-sensitized solar cells Eur. *J. Org. Chem.* (2009): 2903–2934.

[9] Hagfeldt, A., Boschloo, G., Sun, L., Kloo, L. and Pettersson, H. Dye-sensitized solar cells. *Chem. Rev.* 110 (2010): 6595-6663.

[10] Bacsa, R. R. and Grätzel M. Rutile formation in hydrothermally crystallized nanosized titania. *J. Am. Ceram. Soc.* 79 (1996): 2185-1288.

[11] Zaban, A.; Ferrere, S. and Gregg, B. A. Relative energetics at the semiconductor sensitizing dye electrolyte interface *J. Phys. Chem. B 102* (1998): 452.

[12] Yan, S. G. and Hupp, J. T. Semiconductor-Based Interfacial Electron-Transfer Reactivity: Decoupling Kinetics from pH-Dependent Band Energetics in a Dye-Sensitized Titanium Dioxide/Aqueous Solution System *J. Phys. Chem.* 100 (1996): 6867-6870.

[13] Dabestani, R.; Bard, A. J.; Campion, A.; Fox, M. A.; Mallouk, T. E.; Webber, S. E.; White, J. M. Sensitization of titanium dioxide and strontium titanate electrodes by ruthenium(II) tris (2,2'- bipyridine-4,4'-dicarboxylic acid) and zinc tetrakis (4-carboxyphenyl) porphyrin: an evaluation of sensitization *J. Phys. Chem.* 92 (1988): 1872–1878.

[14] Weng, Y.-X.; Li, L.; Liu, Y.; Wang, L.; Yang, G.-Z. Surface-binding forms of carboxylic groups on nanoparticulate TiO_2 surface studied by the interface-sensitive transient triplet-state molecular probe. *J. Phys. Chem. B.* 107 **(**2003): 4356.

[15] Falaras, P.; Synergetic effect of carboxylic acid functional groups and fractal surface characteristics for efficient dye sensitization of titanium oxide. *Sol. Energy Mater. Sol. Cells*. 53 (1998): 163.

[16] Skoog, D. A. Principle of instrumental analysis, *Third Edition*: 684-688.

[17] Hagfeldt, A., Boschloo, G., Sun, L., Kloo, L. and Pettersson, H. Dye-sensitized solar cells. *Chem. Rev.* 110 (2010): 6595-6663.

[18] Nazeeruddin, M. K., Kay, A., Rodicio, I., Humphry-Baker, R., Mueller, E., Liska, P., Vlachopoulos, N. and Grätzel, M. Conversion of light to electricity by cis-X2bis (2,2'-bipyridyl-4,4'-dicarboxylate) ruthenium (II) charge-transfer sensitizers (X = Cl^-, Br^-, I^-, CN^-, and SCN^-) on nanocrystalline titanium dioxide electrodes. *J. Am. Chem. Soc.* 115 (1993): 6382-6390.

[19] Nazeeruddin, M. K., Zakeeruddin, S. M., Humphry-Baker, R., Jirousek, M., Liska, P., Vlachopoulos, N., Shklover, V., Fischer, C. H. and Grätzel, M. Acid−base equilibria of (2,2′-bipyridyl-4,4′-dicarboxylic acid)ruthenium(II)

complexes and the effect of protonation on charge-transfer sensitization of nanocrystalline titania. *Inorg. Chem.* 38 (1999): 6298-6305.

[20] Kay, A., Grätzel, M. Artificial photosynthesis. 1. Photosensitization of titania solar cells with chlorophyll derivatives and related natural porphyrins *J. Phys. Chem.* 97 (1993): 6272–6277.

[21] Tachibana, Y.; Haque, S. A.; Mercer, I. P.; Durrant, J. R.; Klug, D. R. Electron injection and recombination in dye sensitized nanocrystalline titanium dioxide films: a comparison of ruthenium bipyridyl and porphyrin sensitizer dyes. *J. Phys. Chem. B.* 2000,*104*, 1198.

[22] Gervaldo, M.; Fungo, F.; Durantini, E. N.; Silber, J. J.; Sereno, L.; Otero, L. Carboxyphenyl melalloporphyrins as photosensitizers of semiconductor film Electrodes. A study of the effectof different central metals. *J. Phys. Chem. B* 109 (2005): 20953–20962.

[23] Rochford, J.; Chu, D.; Hagfeldt, A.; Galoppini, E. Tetrachelate porphyrin chromophores for metal oxide semiconductor sensitization: effect of the spacer length and anchoring group position. *J. Am. Chem. Soc*. 1 29 (2007): 4655.

[24] Campbell, W. M.; Jolley, K. W.; Wagner, P.; Wagner, K.; Penny J. Walsh, P. J.; Gordon, K. C.; Schmidt-Mende, L.; Nazeeruddin, M. K.; Wang, Q.; Gra1tzel, M. and Officer, D. V.; Highly efficient porphyrin sensitizers for dye-sensitized solar cells *J. Phys. Chem. C*, 111 (2007): 11760-11762.

[25] Hasobe, T.; Imahori. H.; Kamet, P. V.; Ahn, T. K.; Kim, S, K.; Kim, D.; Fujimoto, A.; Hirakawa, T.; Fukuzumi, S. Photovoltaic cells using composite nanoclusters of porphyrins and fullerenes with gold nanoparticles. *J. Am. Chem. Soc*. 127 (2005): 1226.

[26] Lee, C-W.; Lu, H-P.; Lan, C-M.; Huang, Y-L.; Liang, Y-R.; Yen, W-N.; Liu, Y-C.; Lin, Y-S.; Diau, E. W-G. and Yeh, C-Y. Novel zinc porphyrin sensitizers for dye-sensitized solar cells: Synthesis and spectral, electrochemical, and photovoltaic properties *Chem. Eur. J.* 15 (2009): 1403 – 1412.

[27] Seo, K. D.; Lee, M. J.; Song, H. M.; Kang, H. S.; Kim, H. K. Novel D-π-A system based on zinc porphyrin dyes for dye-sensitized solar cells: Synthesis, electrochemical, and photovoltaic properties. *Dyes and Pigments* 94 (2012): 143-149.

[28] Lee, M. J.; Seo, K. D.; Song, H. M.; Kang, M. S.; Kang, H. S.; Kim, H. K. Novel D-π-A system based on zinc-porphyrin derivatives for highly efficient dye-sensitised solar cells. *Tetrahedron Lett* 52 (2011): 3879-3882.

[29] Liu, X.; Liu, J.; Pan, J.; Andersson, S.; Sun, L. Synthesis, electrochemical, and photophysical studies of multicomponent systems based on porphyrin and ruthenium (II) polypyridine complexes. *Tetrahedron*. 63 (2007): 9195.

[30] LeGourriérec, D.; Andersson, M.; Davidsson, J.; Mukhtar, E.; Sun, L.; Hammarström, L. Photoinduced electron transfer from a higher excited state of a porphyrin in a zinc porphyrin-ruthenium(II) *tris*-bipyridine dyad. *J. Phys. Chem. A.* 103 (1999): 557.

[31] Jung, I.; Choi, H.; Lee, J. K.; Song, K. H.; Kang, S. O.; Ko, J. New ruthenium sensitizers containing styryl and antenna fragments. *Inorg. Chimi. Acta.* 360 (2007): 3518-3524.

[32] Lo, C-F.; Shun-Ju Hsu, S-J.; Wang, C-L.; Cheng, Y-H.; Lu, H-P.; Diau, E. W-G. and Lin, C-Y. Tuning spectral and electrochemical properties of porphyrin-sensitized solar cells *J. Phys. Chem. C* 114 (2010): 12018–12023.

[33] Zhou, W.; Zhao, B.; Shen, P.; Jiang, S.; Huang, H.; Deng, L. and Tan, S. Multi-alkylthienyl appended porphyrins for efficient dye-sensitized solar cells *Dyes and Pigments* 91 (2011): 404-412.

[34] Eu, S.; Hayashi, S.; Umeyama, T.; Oguro, A.; Kawasaki, M.; Kadota, N.; Matano, Y. and Imahori, H. Effects of 5-membered heteroaromatic spacers on structures of porphyrin films and photovoltaic properties of porphyrin-sensitized TiO_2 cells *J. Phys. Chem. C* 111 (2007): 3528-3537.

[35] Khan, S. I.; Beilstein, A. E.; Smith, G. D.; Sykora, M.; Grinstaff, M. W. Synthesis and excited-state properties of a novel ruthenium nucleoside: 5-$[Ru(bpy)_2(4\text{-m-}4'\text{-pa-bpy})]^{2+}$-2'-deoxyuridine. *Inorg. Chem*. 38 (1999): 2411.

[36] Sagyam, R. R., Padi, P. R., Ghanta, M. R. and Vurimidi, H. An efficient synthesis of highly substituted pyrrole and bis pyrrole derivatives *J. Heterocyclic Chem.* 44 (2009): 923-926.

[37] Fan, S.H., Zhang, A.G., Ju, C.C., Gao, L.H. and Wang, K.Z. A triphenylamine-grafted imidazo[4,5-f][1,10]phenanthroline ruthenium(II) complex: acid-base and photoelectric properties. *Inorg. Chem.* 49 (2010): 3752-3763.

[38] Han, W. S.; Han, J. K.; Kim, H. Y.; Choi, M. J.; Kang, Y. S.; Pac, C. and Kang, S. O. Electronic optimization of heteroleptic Ru(II) bipyridine complexes by remote substituents: synthesis, characterization and application to dye-sensitized solar cells. *Inorg. Chem.* 50 (2011): 3271-3280.

[39] Jiang, K.J.; Masaki, N.; Xia, J.B.; Noda, S. and Yanagida, S. A novel ruthenium sensitizer with a hydrophobic 2- thiophen-2-yl-vinyl-conjugated bipyridyl ligand for effective dye sensitized TiO_2 solar cells. *Chem. Commun.* (2006): 2460-2462.

[40] Chen, C.Y.; Lu, H.C.; Wu, C.G.; Chen, J.G. and Ho, K.C. New Ruthenium complexes containing oligoalkylthiophen-substituted 1,10-phenanthroline for nanocrystalline dye-sensitized solar cells. *Adv. Funct. Mater.* 17 (2003): 29-36.

[41] Chen, C.Y.; Chen, J.G.; Wu, S.J.; Li, J.Y.; Wu, C.G. and Ho, K.C. Multifunctionalized ruthenium-based supersensitizers for highly efficient dye-sensitized solar cells. *Angew. Chem. Int. Ed.* 47 (2008): 7342-7345.

[42] Zhu, R.; Jiang, C.Y.; Liu, B. and Ramakrishna, S. Highly efficient nanoporous TiO_2-polythiophene hybrid solar cells based on interfacial modification using a metal-free organic dye. *Adv. Matet.* 21 (2009): 994-1000.

[43] Hallett, A.J. and Jones, J.E. Purification-free synthesis of a highly efficient ruthenium complex for dye-sensitized solar cells (DSSCs). *Dalton. Trans*. 40 (2011): 3871-3876.

[44] Preat, J.; Michaux, C.; Jacquemin, D. and Perpe`te, E.A. Enhanced efficiency of organic dye-sensitized solar cells: triphenylamine derivatives *J. Phy. Chem. C* 113 (2009): 16821-16833.

APPENDIX A

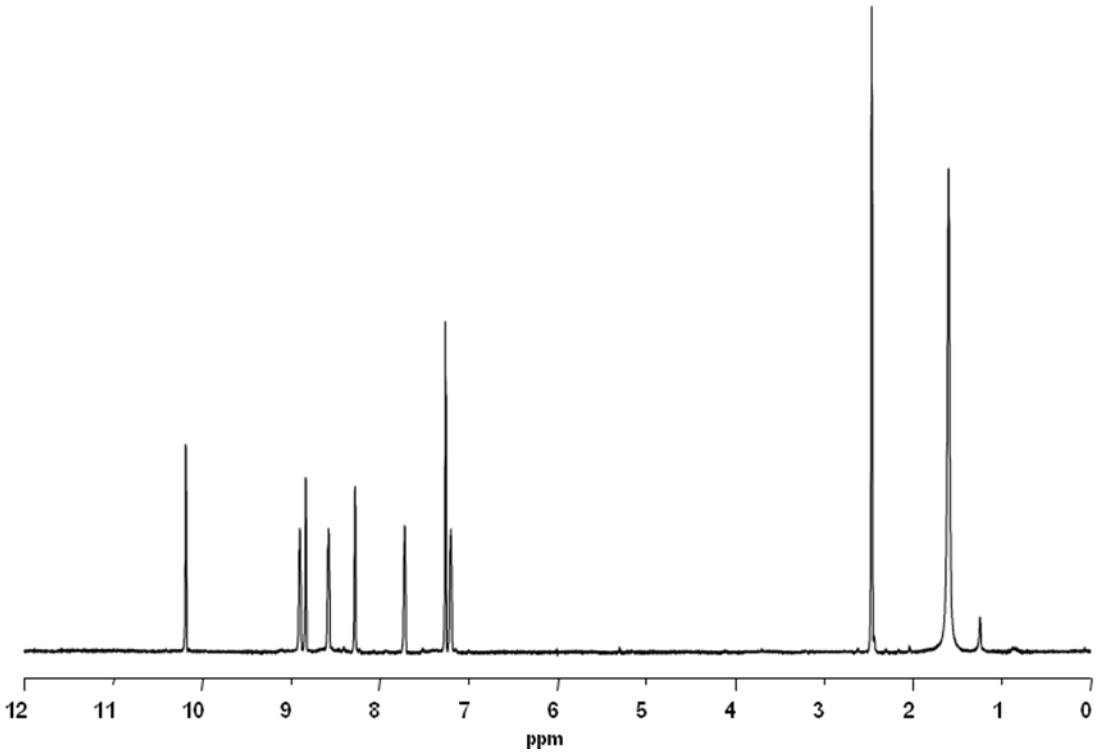

Figure A1. ^{1}H NMR spectrum of 4′-methyl-2,2′-bipyridine-4-carboxaldehyde **(A1)**

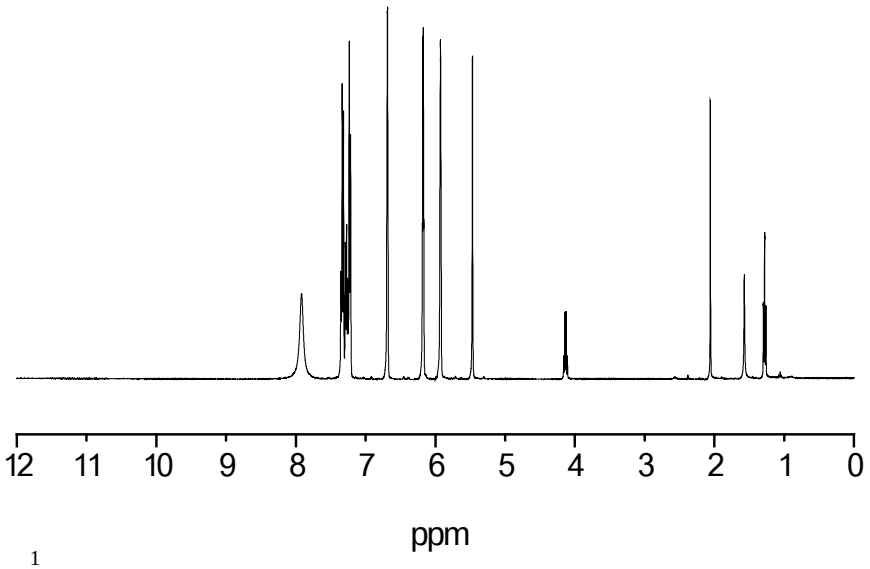

Figure A2. ^{1}H NMR spectrum of Phynyldipyrromethane **(A2)**

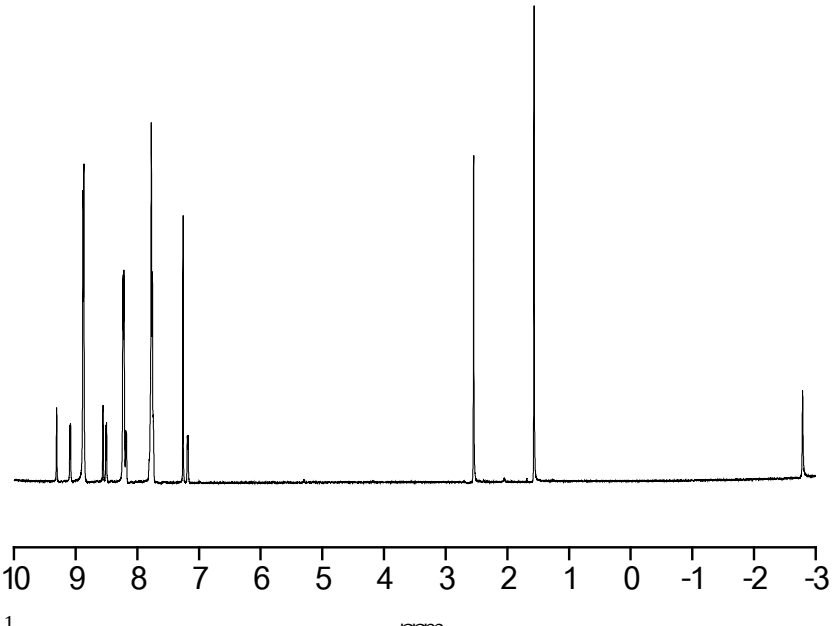

Figure A3. ^{1}H NMR spectrum of 5-(4′-methyl-bipyridine-4-yl)-10,15,20-triphenylporphyrin **(A3)**

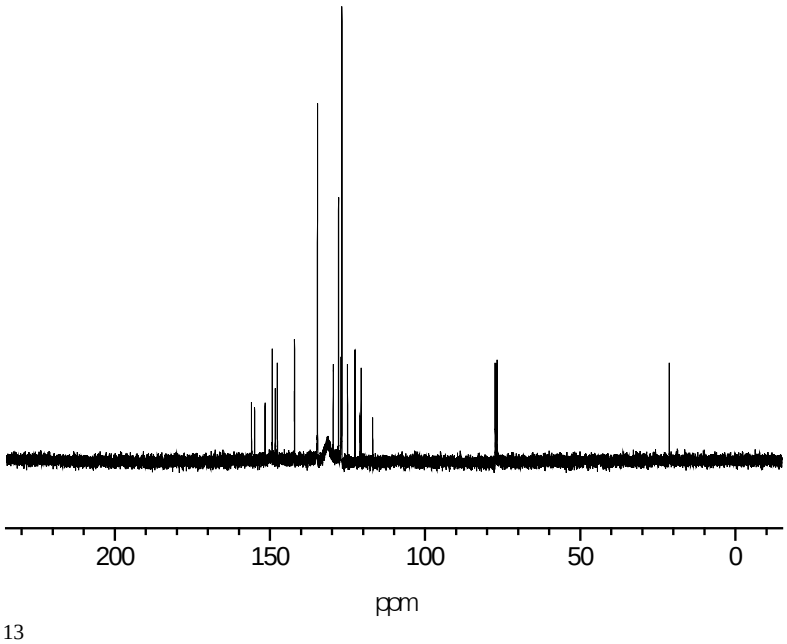

Figure A4. ^{13}C NMR spectrum of 5-(4′-methyl-bipyridine-4-yl)-10,15,20-triphenylporphyrin **(A3)**.

Figure A5. ^{1}H NMR spectrum of 5-(4′-methyl-bipyridine-4-yl)-10,15,20-triphenylporphyrinatozinc **(A4)**.

Figure A6. ^{13}C NMR spectrum of 5-(4′-methyl-bipyridine-4-yl)-10,15,20-triphenylporphyrinatozinc **(A4)**.

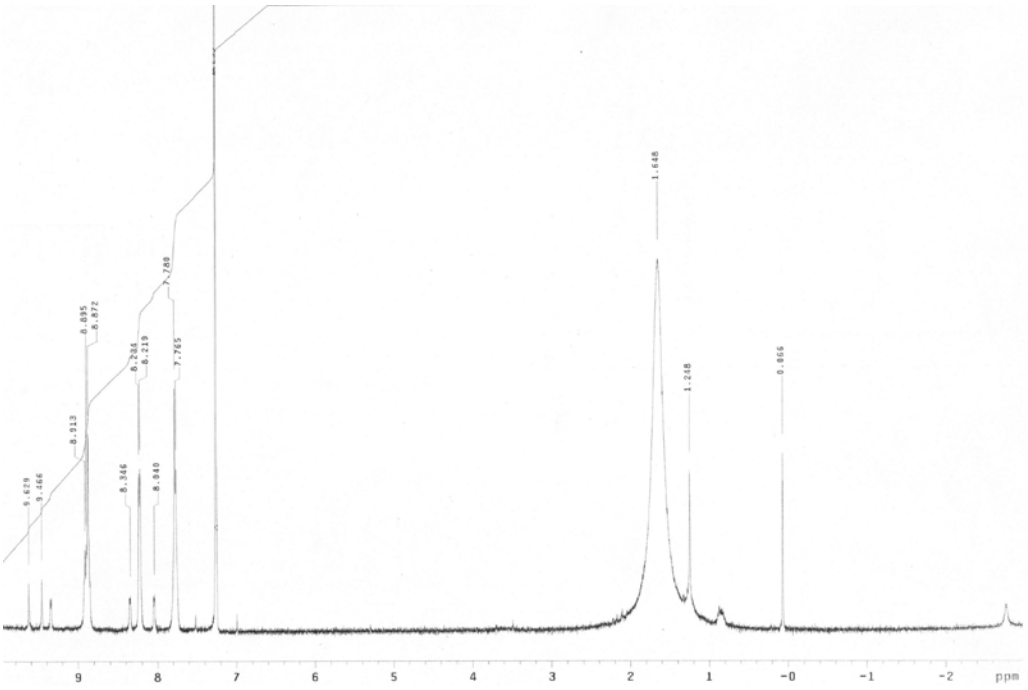

Figure A7. ^{1}H NMR spectrum of 5-(4′-carboxy-2,2′-bipyridine-4-yl)-10,15,20-triphenylporphyrin **(A5)**.

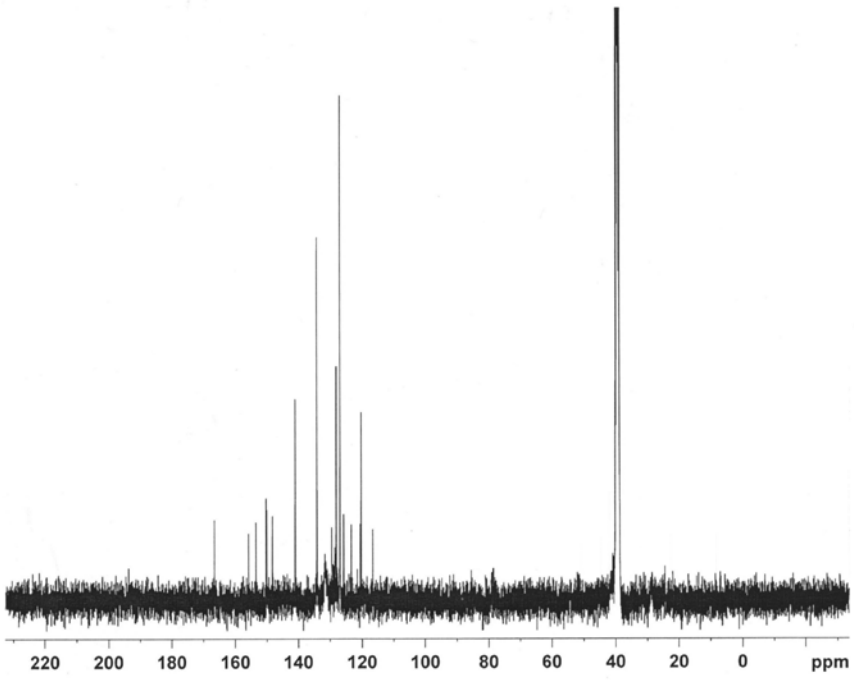

Figure A8. ^{13}C NMR spectrum of 5-(4′-carboxy-2,2′-bipyridine-4-yl)-10,15,20-triphenylporphyrin **(A5)** in DMSO-$_{d6}$.

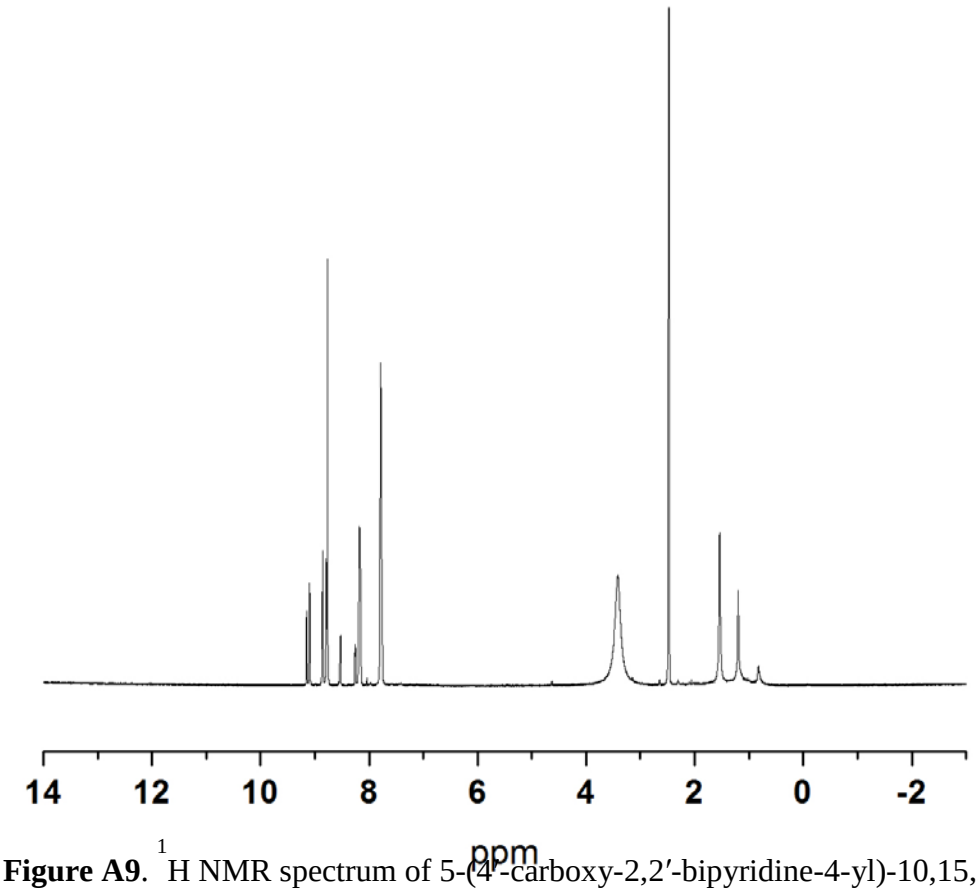

Figure A9. ^{1}H NMR spectrum of 5-(4′-carboxy-2,2′-bipyridine-4-yl)-10,15,20-triphenylporphyrina-tozinc **(A6)**.

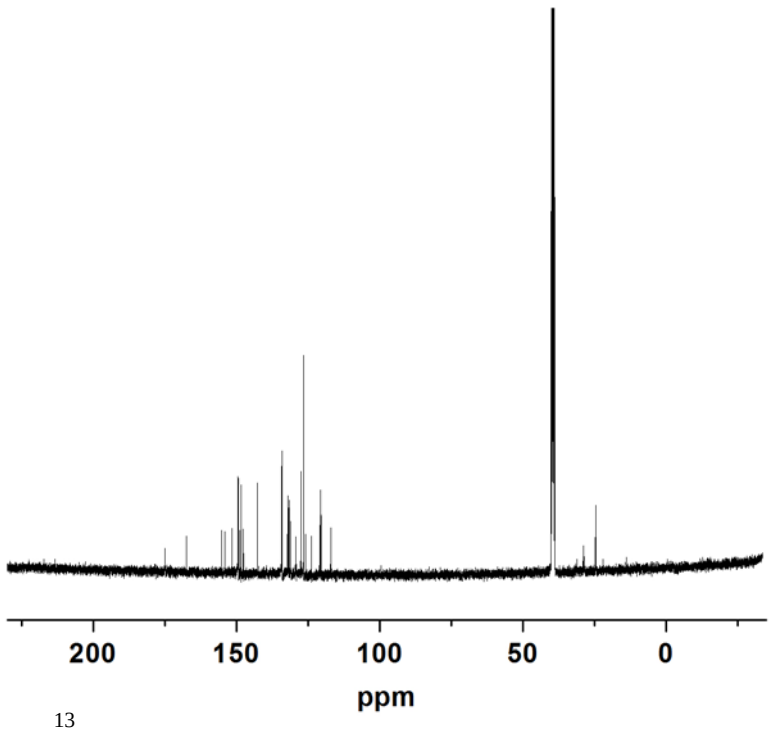

Figure A10. ^{13}C NMR spectrum of 5-(4′-carboxy-2,2′-bipyridine-4-yl)-10,15,20-triphenylporphyrina- tozinc **(A6)**.

APPENDIX B

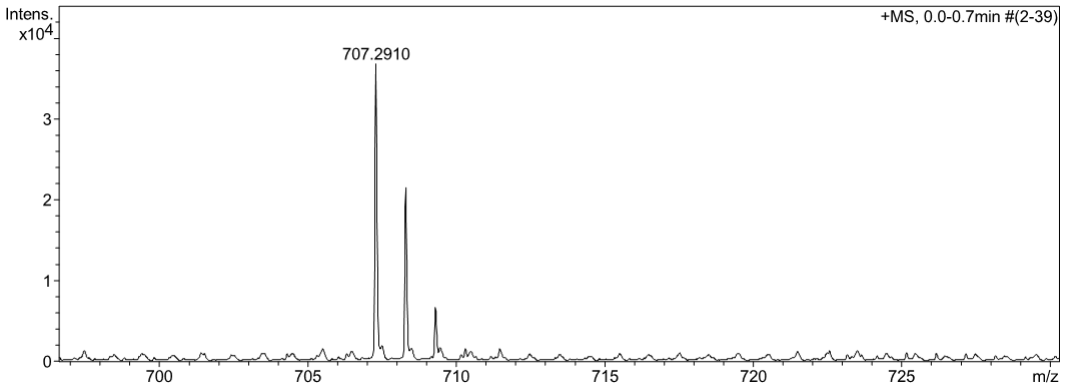

Figure B1. Mass spectrum of 5-(4′-methyl-bipyridine-4-yl)-10,15,20-triphenyl porphyrin **(A3)**.

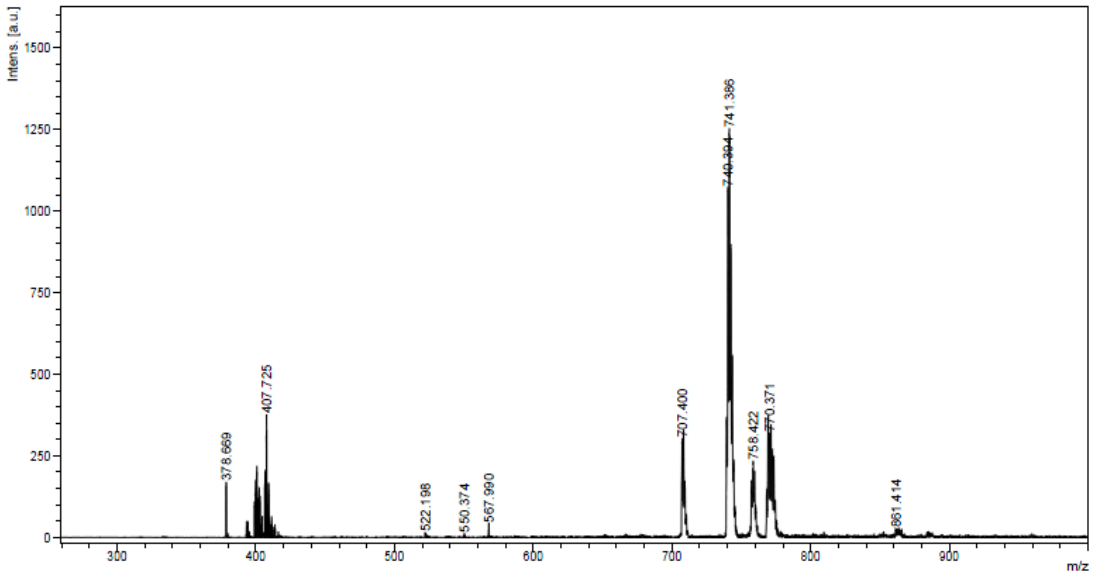

Figure B2. Mass spectrum of 5-(4′-methyl-bipyridine-4-yl)-10,15,20-triphenyl porphyrinatozinc **(A4)**.

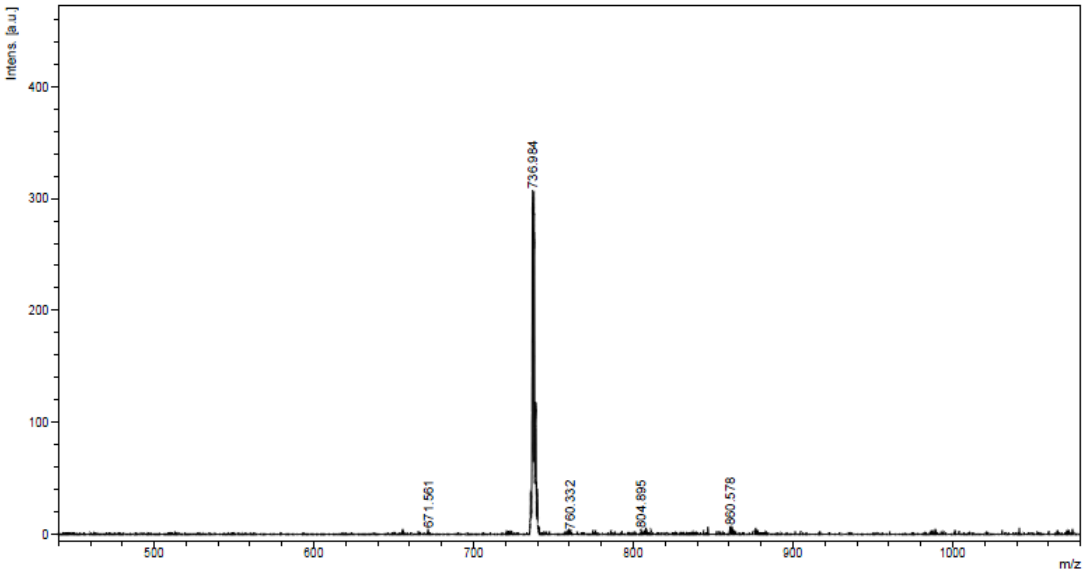

Figure B3. Mass spectrum of 5-(4′-carboxy-2,2′-bipyridine-4-yl)-10,15,20-triphenyl porphyrin **(A5)**.

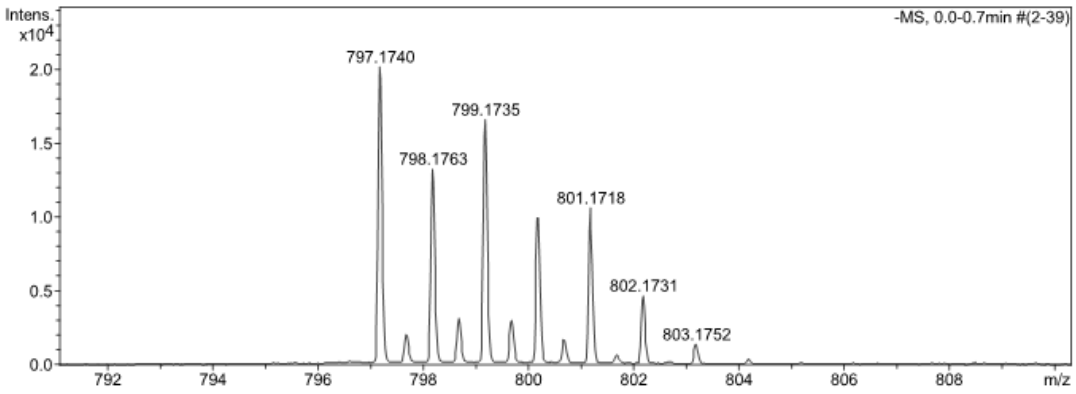

Figure B4. Mass spectrum of 5-(4′-carboxy-2,2′-bipyridine-4-yl)-10,15,20-triphenylporphyrina-tozinc **(A6)**.

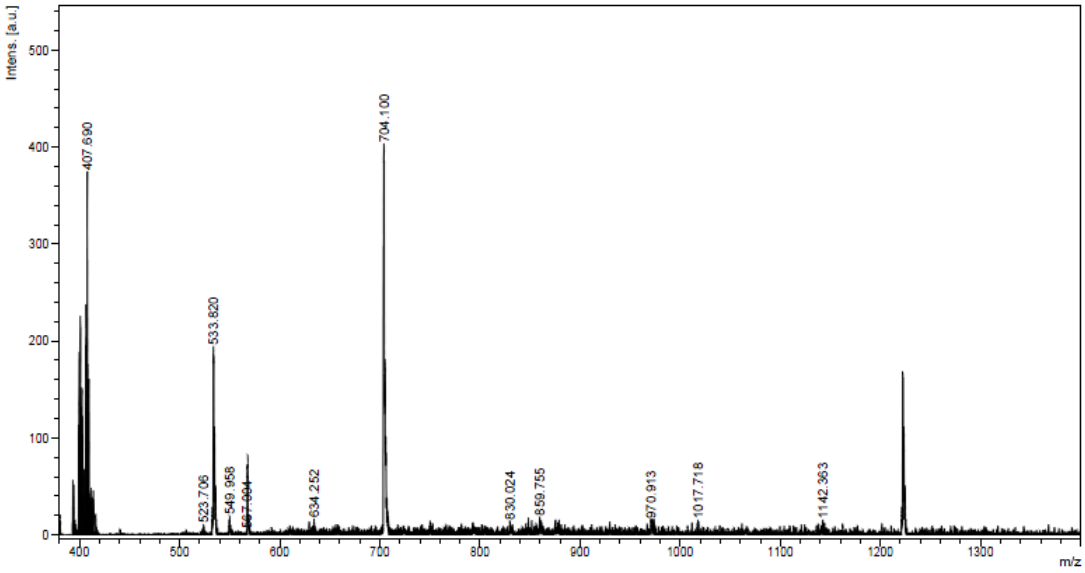

Figure B5. Mass spectrum of bipyridylporphyrin ruthenium complex **(A7)**.

APPENDIX C

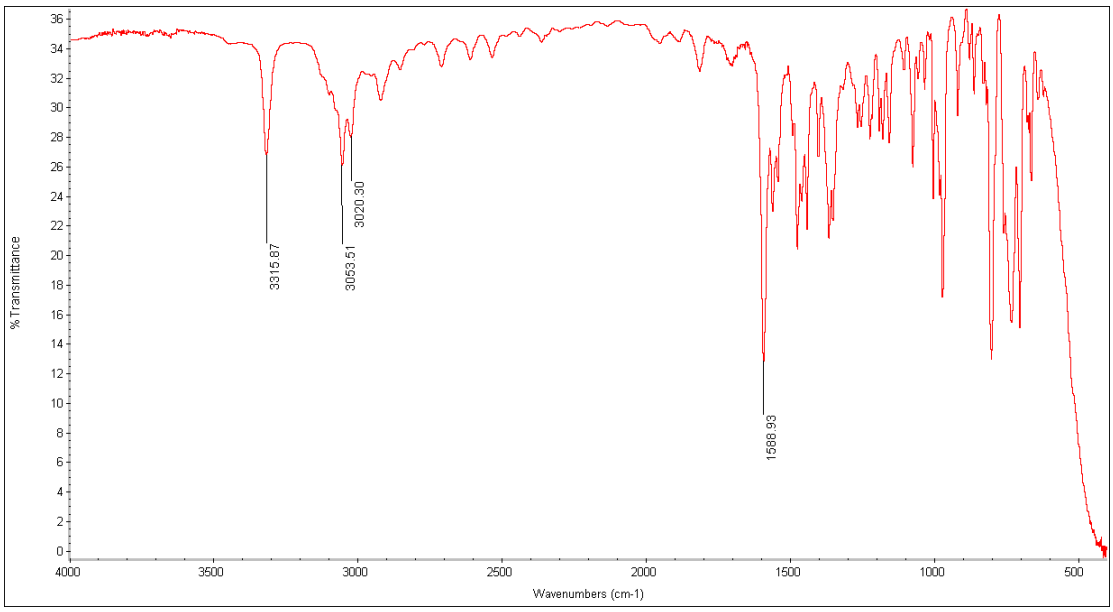

Figure C1. IR spectrum of 5-(4′-methyl-bipyridine-4-yl)-10,15,20-triphenylporphyrin **(A3)**.

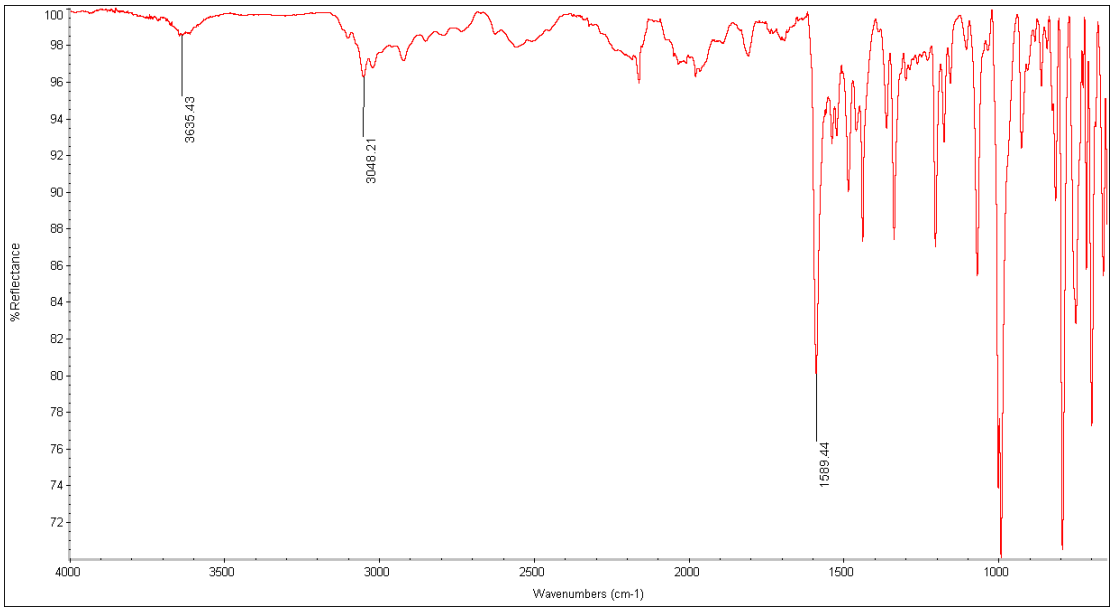

Figure C2. IR spectrum of 5-(4′-methyl-bipyridine-4-yl)-10,15,20-triphenyl porphyrinatozinc **(A4)**.

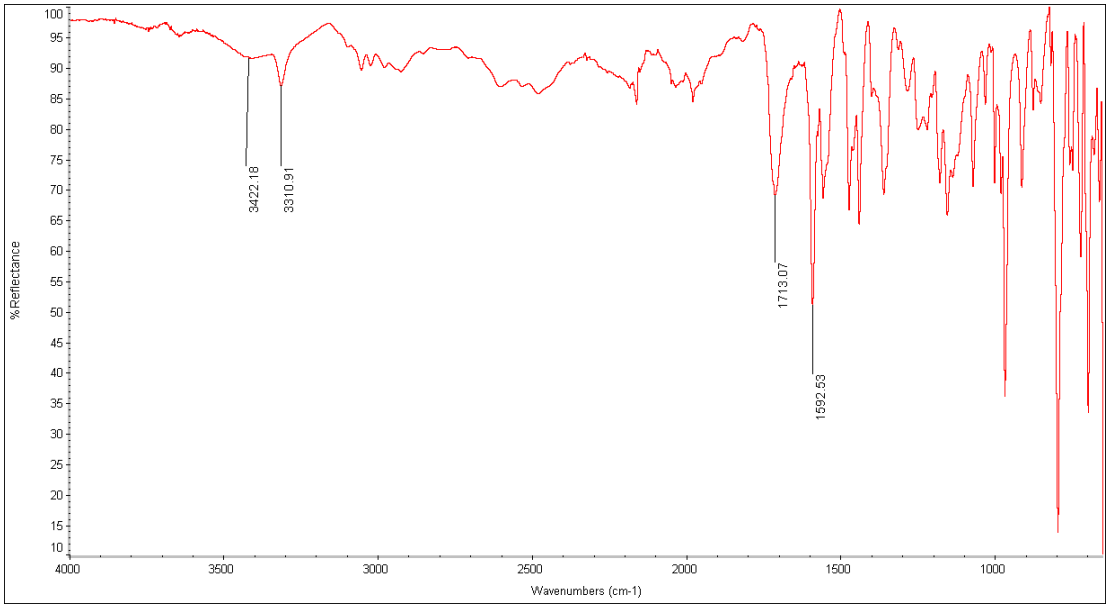

Figure C3. IR spectrum of 5-(4′-carboxy-2,2′-bipyridine-4-yl)-10,15,20-triphenyl porphyrin **(A5)**.

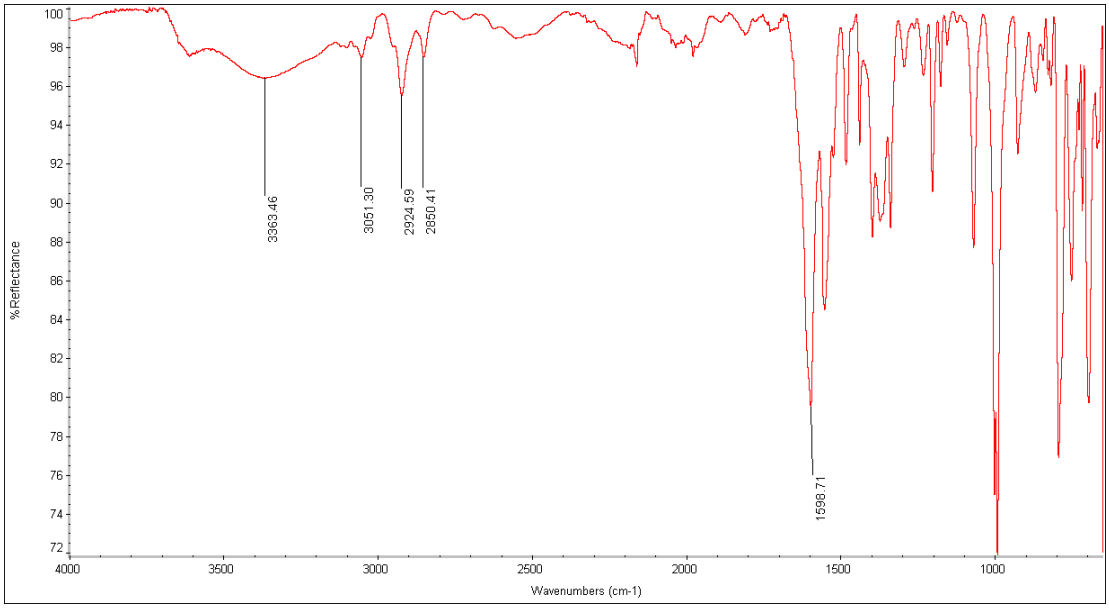

Figure C4. IR spectrum of 5-(4′-carboxy-2,2′-bipyridine-4-yl)-10,15,20-triphenyl porphyrina-tozinc **(A6)**.

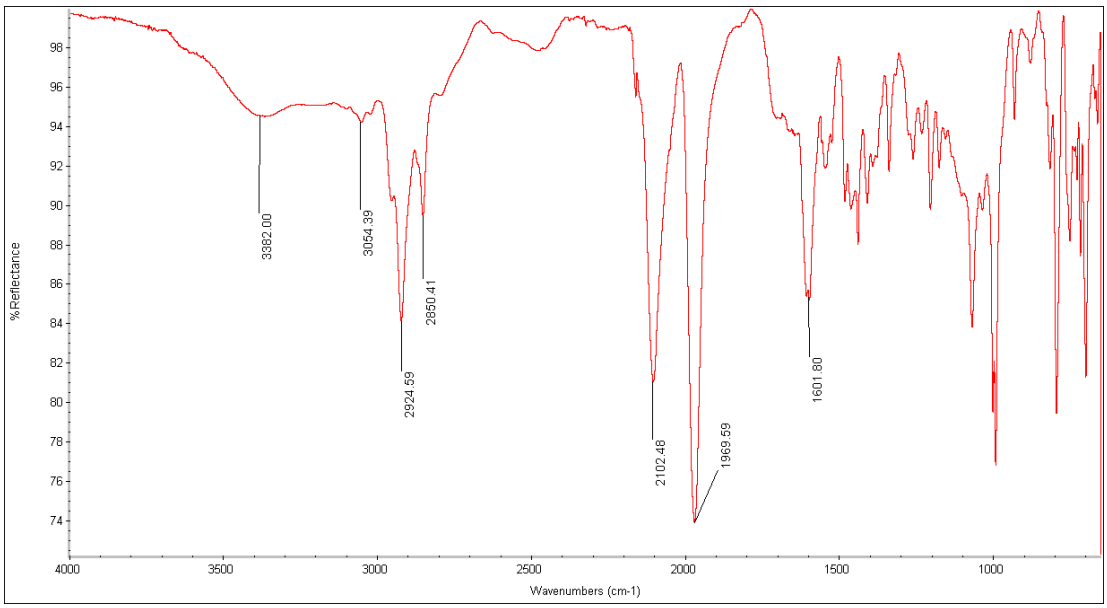

Figure C5. IR spectrum of bipyridylporphyrin ruthenium complex **(A7)**.

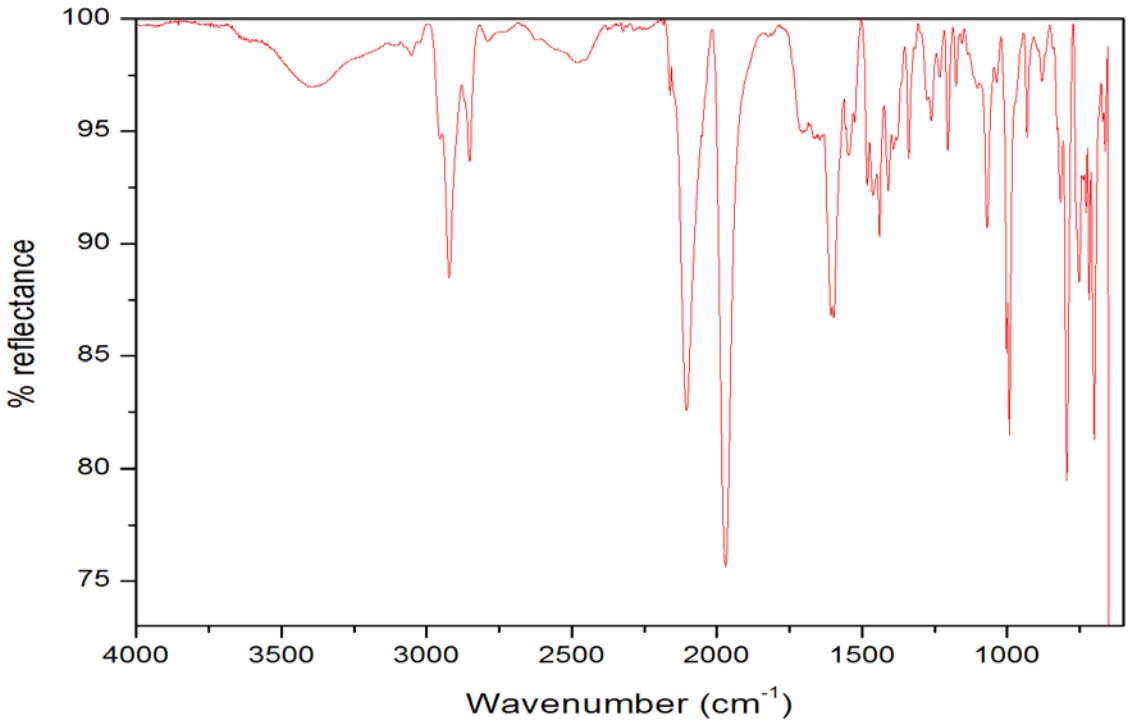

Figure C6. IR spectrum of bipyridylporphyrin ruthenium complex **(A8)**.

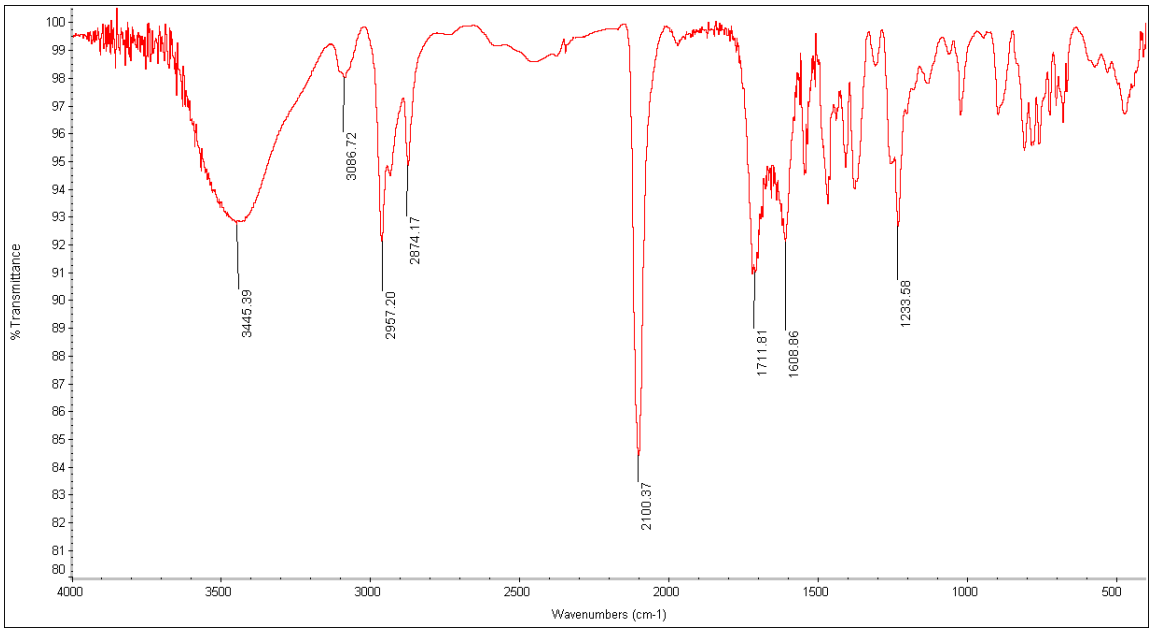

Figure C7. IR spectrum of **N719**.

APPENDIX D

Table D1. Molecular Orbital Energy Levels and energy gaps (in eV) of bipyridylporphyrin dyes, which optimized at B3LYP/ LanL2DZ/6-31 G(d).

	A5	**A6**	**A7**	**A8**
LUMO+1	-2.29 / -2.56	-2.27 / -2.51	-3.37	-
LUMO	-2.31 / -2.60	-2.29 / -2.53	-3.73	-
HOMO	-5.02 / -5.23	-5.12 / -5.26	-5.61	-
HOMO-1	-5.30 / -5.61	-5.34 / -5.54	-5.97	-
$\mathbf{E_g^{cal}}$	2.71 / 2.63	2.83 / 2.73	1.88	-

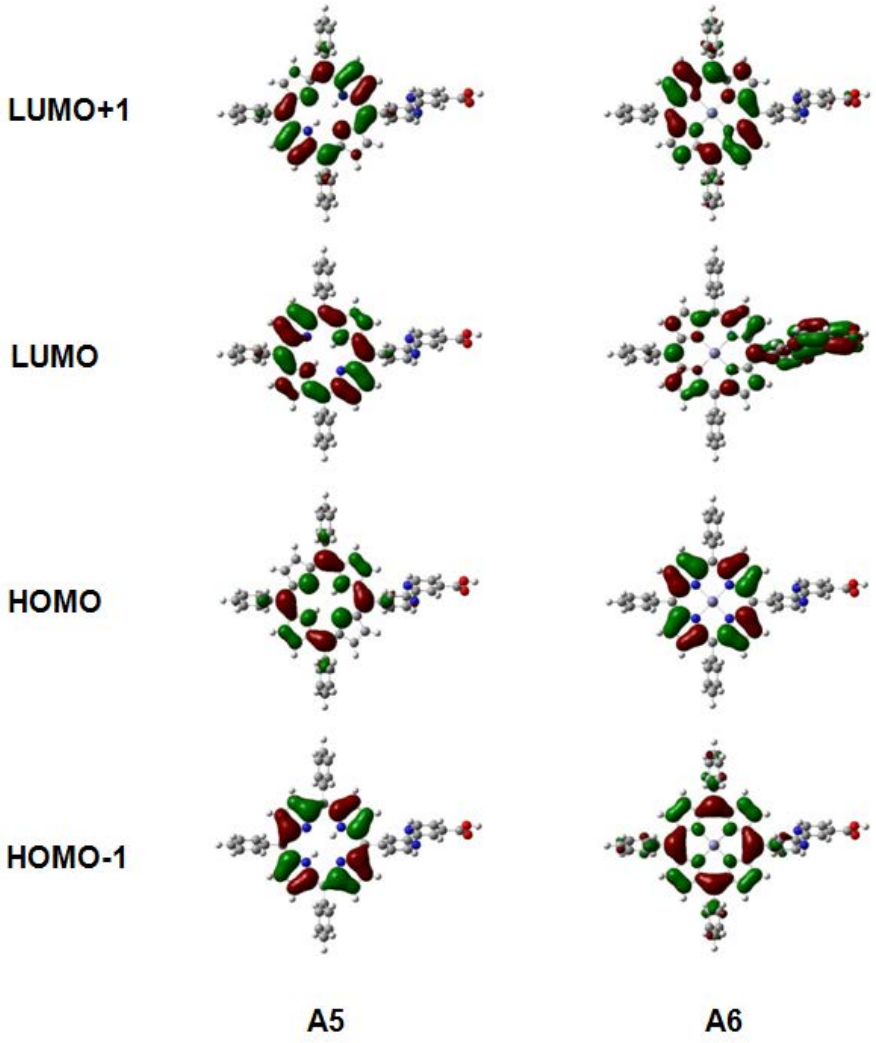

Figure D1. Plots of LUMO+1, LUMO, HOMO and HOMO-1 orbital for **A5** and **A6**, which optimized at B3LYP/6-31G(d) level theory.

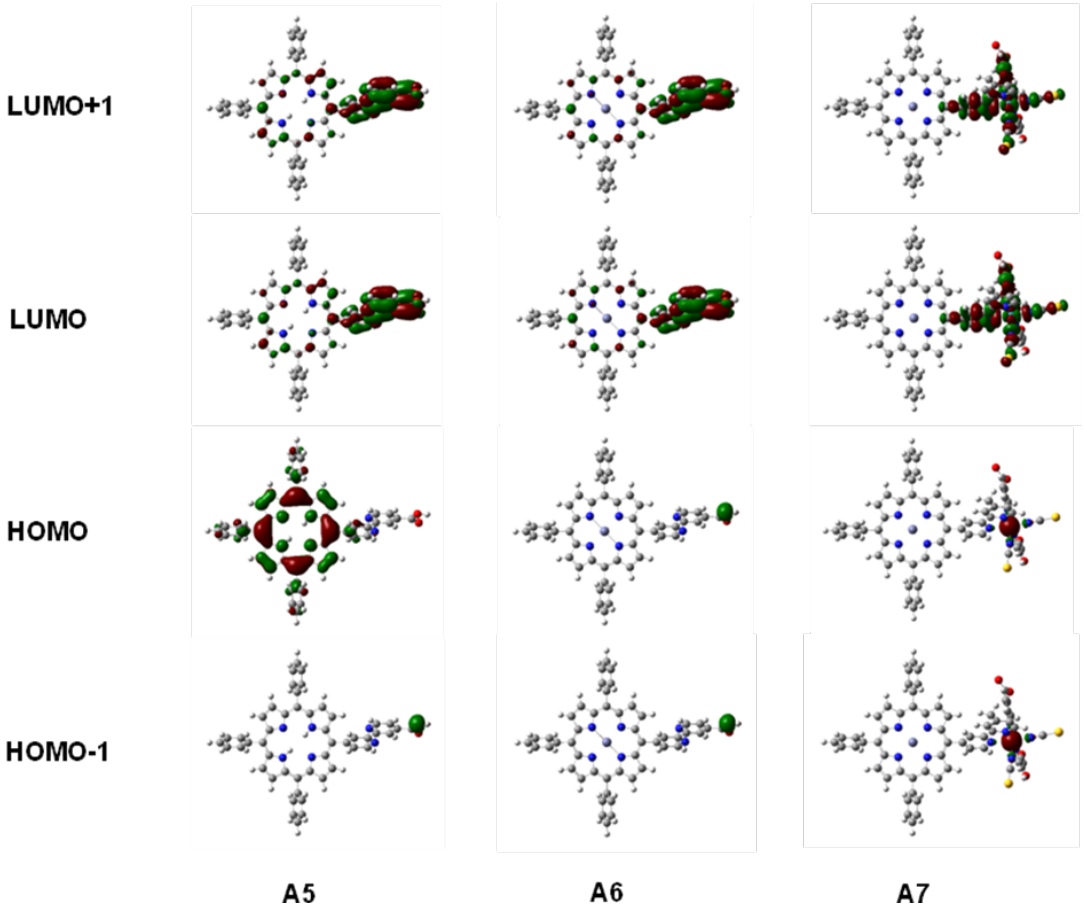

Figure D2. Plots of LUMO+1, LUMO, HOMO and HOMO-1 orbital for **A5**, **A6** and **A7**, which optimized at B3LYP/LanL2DZ level theory.

Molecular structures and total energies of A5, A6 and A7.

Compound: **A5**

Basic set: B3LYP/6-31 G(d) level

Total energy: -2365.45914479 A.U.

Alpha occ. Eigenvalues: -0.19485 and -0.18456

Alpha virt. Eigenvalues: -0.08508 and -0.08400

Table D2. Cartesian coordinates (in angstrom) of **A5** computed at the B3LYP/6-31 G(d) level.

Atoms	x	y	z
C	4.62238200	0.86885000	0.28428600
C	5.06836500	-0.46162500	0.36120100
C	4.25550800	-1.60484400	0.20577700
C	4.77682400	-2.96696600	0.27371100
H	5.80855300	-3.24168000	0.43857400
C	3.71775000	-3.78954100	0.08870900
H	3.71007900	-4.86984100	0.08544600
C	2.55701600	-2.92621600	-0.10904500
C	1.25653800	-3.42713600	-0.33643400
C	0.10431600	-2.64428100	-0.51502800
C	-1.21233500	-3.11579500	-0.83315700
H	-1.47562000	-4.15521000	-0.95863200
C	5.39958100	2.04973000	0.52525200
H	6.44693400	2.04911200	0.78715600

C	6.52613100	-0.65886600	0.64917800
C	6.94925500	-1.19391000	1.87607600
H	6.20592400	-1.46334900	2.62112900
C	8.30633800	-1.37390500	2.14573500
H	8.61468900	-1.78593600	3.10303000
C	9.26436500	-1.02165600	1.19314000
C	1.06880000	-4.91280900	-0.40849500
C	1.58870200	-5.65222100	-1.48244200
H	2.13030300	-5.13461600	-2.26924000
C	1.40972600	-7.03441400	-1.54948700
H	1.81618600	-7.58943400	-2.39091400
C	0.70732400	-7.70123600	-0.54380600
C	0.18450800	-6.97699800	0.52895300
H	-0.36006400	-7.48790600	1.31869200
C	0.36297900	-5.59449500	0.59515000
H	-0.03891200	-5.03395500	1.43469200
N	2.90917200	-1.60833900	-0.03133100
N	3.34316000	1.29393000	0.00637500
C	-1.25577800	-0.84743800	-0.73581300
C	-1.69610000	0.48369000	-0.82139300
C	-0.88463300	1.62933200	-0.67239300
C	-1.40511600	2.99198500	-0.74498700
H	-2.43549500	3.27071300	-0.91228600
C	-0.34656400	3.81406400	-0.55539800

H	-0.33909200	4.89434200	-0.55270900
C	0.81285000	2.95068400	-0.35152500
C	2.11140400	3.45073200	-0.11899500
C	3.26362200	2.66647900	0.06305500
C	4.57803300	3.13683800	0.39091000
H	4.83964800	4.17582800	0.52357600
C	-2.03474200	-2.02994300	-0.96701400
H	-3.08416800	-2.03421100	-1.22042700
C	2.29936300	4.93614300	-0.04324900
C	3.01135900	5.61937000	-1.04151700
H	3.41801600	5.06007400	-1.87961100
C	3.18950900	7.00173100	-0.97224800
H	3.73848200	7.51390700	-1.75812500
C	2.66032400	7.72440200	0.09848100
C	1.95195400	7.05610900	1.09895700
H	1.54033400	7.60989200	1.93867500
C	1.77327300	5.67400600	1.02877100
H	1.22697500	5.15526000	1.81154900
N	0.45932100	1.63208500	-0.42965800
N	0.02462500	-1.27076000	-0.46399300
H	10.32129800	-1.16217100	1.40309800
H	0.56830000	-8.77775000	-0.59606200
H	2.79885300	8.80086300	0.15303200
C	7.49904800	-0.30737600	-0.29955200

C	8.85649500	-0.48806900	-0.03063000
H	7.18385700	0.10081600	-1.25590200
H	9.59468300	-0.21553300	-0.78036200
C	-3.15080100	0.68257300	-1.11487900
C	-3.58048800	1.23791700	-2.32859100
C	-4.13574400	0.31723100	-0.19104900
C	-4.94811700	1.39850800	-2.55100800
H	-2.86106300	1.53296000	-3.08593300
C	-5.48675400	0.51741200	-0.50478900
H	-3.87317900	-0.11019200	0.76925500
N	-5.88991600	1.05150200	-1.67110200
H	-5.30346800	1.82470800	-3.48790300
C	-6.55564600	0.14229900	0.46332500
N	-6.16239700	-0.40109200	1.62960000
C	-7.90611700	0.35435100	0.15432800
C	-7.09983100	-0.74493000	2.51575500
C	-8.87442500	-0.01027800	1.08908700
H	-8.18716000	0.79387400	-0.79432400
C	-8.46751200	-0.57445000	2.30305100
H	-6.74037500	-1.18035700	3.44642800
C	-10.31042800	0.21904600	0.75155400
H	-9.19017000	-0.86983800	3.05453300
O	-11.14964700	-0.17380600	1.74236100
O	-10.70978800	0.70143800	-0.28660800

H	-12.04982700	0.01893600	1.42038000
H	2.55817300	0.67749000	-0.17884000
H	0.80994600	-0.65363400	-0.28234700

Compound: **A6**

Basic set: B3LYP/6-31 G(d) level

Total energy: -4142.86814527 A.U.

Alpha occ. Eigenvalues: -0.19634 and -0.18810

Alpha virt. Eigenvalues: -0.08424 and -0.08327

Table D3. Cartesian coordinates (in angstrom) of **A6** computed at the B3LYP/6-31 G(d) level.

Atoms	**x**	**y**	**z**
C	4.49282800	0.83409700	0.32940700
C	4.95493700	-0.49182100	0.40079400
C	4.14856800	-1.63167400	0.23682100
C	4.62672500	-2.99851100	0.29804600
H	5.65008500	-3.29031000	0.46942700
C	3.55065900	-3.81626000	0.10106100
H	3.53788500	-4.89400500	0.09466400
C	2.39385200	-2.96746800	-0.10385600
C	1.08918900	-3.43443700	-0.34396700
C	-0.03410000	-2.61123100	-0.53217100
C	-1.36542300	-3.09152100	-0.84516500

H	-1.63911900	-4.12740400	-0.96275600
C	5.31102100	2.00659200	0.56711200
H	6.35836000	1.99026400	0.82159300
C	6.41385600	-0.70418800	0.68196500
C	6.83754500	-1.26380600	1.90211700
H	6.09587400	-1.53720300	2.64579200
C	8.19775200	-1.45908800	2.16429100
H	8.50679100	-1.88720600	3.11280300
C	9.15733500	-1.09919500	1.21079000
C	0.88024600	-4.91942800	-0.40789400
C	1.41479400	-5.67842500	-1.46596400
H	1.97870800	-5.17700800	-2.24601900
C	1.21668600	-7.06213300	-1.52349600
H	1.63182800	-7.63113300	-2.34954700
C	0.48152700	-7.71039600	-0.52405100
C	-0.05519400	-6.96623400	0.53306200
H	-0.62349100	-7.46162400	1.31413100
C	0.14176900	-5.58241600	0.59037500
H	-0.27059400	-5.00805500	1.41375800
N	2.77999300	-1.63419900	-0.01448900
N	3.18686400	1.23135100	0.05990600
Zn	1.57080100	0.00524800	-0.21267600
C	-1.35269500	-0.82474200	-0.75022000
C	-1.80967400	0.50207000	-0.82907900

C	-1.00510000	1.64394100	-0.67058300
C	-1.48244800	3.01147500	-0.73534600
H	-2.50451800	3.30770300	-0.90756300
C	-0.40670600	3.82848900	-0.53484500
H	-0.39400300	4.90623100	-0.52862800
C	0.74897800	2.97947900	-0.32492100
C	2.05207100	3.44567000	-0.08073900
C	3.17539400	2.62137400	0.11023100
C	4.50469900	3.10069000	0.43250000
H	4.77681200	4.13622900	0.55710200
C	-2.17268600	-1.99854900	-0.97880200
H	-3.22231800	-1.98751100	-1.22396400
C	2.26124500	4.93045000	-0.01372500
C	3.00467300	5.59463500	-1.00753600
H	3.42078300	5.02120300	-1.82969200
C	3.20139500	6.97835600	-0.94772500
H	3.77311300	7.47477700	-1.72565500
C	2.65962900	7.72130100	0.10769900
C	1.91973400	7.07188200	1.10286900
H	1.50050300	7.63992400	1.92749500
C	1.72179900	5.68823700	1.04275100
H	1.15419300	5.18592900	1.81953600
N	0.36164900	1.64562400	-0.41479900
N	-0.04582500	-1.22027400	-0.48673900

H	10.21262200	-1.25101800	1.41429600
H	0.32810500	-8.78395900	-0.56896900
H	2.81261300	8.79484400	0.15445800
C	7.38815100	-0.34556800	-0.26852300
C	8.74825700	-0.54214200	-0.00648300
H	7.07276500	0.08070300	-1.21547800
H	9.48568200	-0.26427700	-0.75312400
C	-3.26535400	0.71521700	-1.11553900
C	-3.69246500	1.29284200	-2.32568900
C	-4.25081400	0.34392100	-0.18778900
C	-5.06010900	1.47117300	-2.55087400
H	-2.96974000	1.58863600	-3.07754100
C	-5.60382800	0.55647300	-0.49008900
H	-3.98845800	-0.09879800	0.76431500
N	-6.00500300	1.11444500	-1.65983700
H	-5.41795600	1.91024100	-3.47644900
C	-6.67122000	0.18010700	0.46596800
N	-6.28158200	-0.38111900	1.63862800
C	-8.02359200	0.39815500	0.16311700
C	-7.22462000	-0.73639900	2.53351200
C	-8.99386100	0.02468200	1.09921800
H	-8.30011000	0.84793400	-0.78117400
C	-8.59168700	-0.55548100	2.31279900
H	-6.86451000	-1.18023400	3.45539100

C	-10.42039400	0.25642600	0.77396700
H	-9.32339400	-0.85215400	3.05233200
O	-11.27283800	-0.15481800	1.77916900
O	-10.84627700	0.75995700	-0.27157500
H	-12.20238900	0.01821300	1.51790100

Compound: **A5**

Basic set: B3LYP/LanL2DZ level

Total energy: -2365.06354028 A.U.

Alpha occ. Eigenvalues: -0.20616 and -0.19219

Alpha virt. Eigenvalues: -0.09564 and -0.09428

Table D5. Cartesian coordinates (in angstrom) of **A4** computed at the B3LYP/ LanL2DZ level.

Atoms	**x**	**y**	**z**
C	4.66084800	0.86292100	0.28445300
C	5.10997500	-0.47321000	0.36472500
C	4.28743600	-1.61584400	0.20984900
C	4.79750100	-2.99313500	0.27850200
H	5.82721100	-3.27261700	0.44417800
C	3.72542000	-3.82014300	0.08705300
H	3.71491700	-4.89982800	0.08468800
C	2.55356400	-2.95497200	-0.11332700
C	1.24747800	-3.45592200	-0.34129300

C	0.09632000	-2.65958500	-0.51813200
C	-1.23471300	-3.12994600	-0.82880700
H	-1.50305800	-4.16810900	-0.94983200
C	5.45098700	2.05065200	0.51603200
H	6.49926900	2.04642000	0.77235500
C	6.57204000	-0.67889700	0.65152200
C	6.99502100	-1.22826000	1.88352700
H	6.25144600	-1.49684400	2.62978800
C	8.36295100	-1.41491400	2.15531000
H	8.67026000	-1.83223000	3.11137100
C	9.33112000	-1.06107100	1.19540400
C	1.05645700	-4.94622100	-0.41315200
C	1.59322000	-5.69262000	-1.48706200
H	2.14333000	-5.17751800	-2.27067300
C	1.40879600	-7.08588300	-1.55677700
H	1.82261000	-7.64293000	-2.39408800
C	0.68946600	-7.75705800	-0.54871400
C	0.15301600	-7.02292700	0.52682100
H	-0.39975900	-7.53210000	1.31284800
C	0.33191900	-5.62850500	0.59086000
H	-0.07743600	-5.06665500	1.42698600
N	2.91857600	-1.61692700	-0.03307300
N	3.36577600	1.29344400	0.01340100
C	-1.26918900	-0.84144700	-0.74153000

C	-1.71274800	0.49523200	-0.82958900
C	-0.89219400	1.64030300	-0.67679400
C	-1.40206000	3.01842600	-0.74548100
H	-2.43045700	3.30300200	-0.91149000
C	-0.33065000	3.84467600	-0.54810000
H	-0.32067200	4.92433000	-0.54278400
C	0.84037100	2.97936900	-0.34519400
C	2.14446800	3.47947800	-0.11266000
C	3.29632700	2.68183300	0.06449700
C	4.62572200	3.15087300	0.38268000
H	4.89257900	4.18851400	0.51170400
C	-2.06045600	-2.03129600	-0.96426600
H	-3.11066600	-2.03346000	-1.21253100
C	2.33519600	4.96943700	-0.03384600
C	3.06315900	5.65628300	-1.03228000
H	3.47541800	5.09813600	-1.86946900
C	3.24119600	7.05048900	-0.96183100
H	3.79611000	7.56336800	-1.74395200
C	2.70056900	7.77988800	0.11487600
C	1.97805300	7.10418200	1.11758200
H	1.56079500	7.65754000	1.95561200
C	1.79450600	5.71111600	1.04139100
H	1.24195700	5.19247000	1.82093100
N	0.47416100	1.64050400	-0.42921500

N	0.02635900	-1.27010900	-0.47378000
H	10.38826100	-1.20782700	1.40386300
H	0.54935900	-8.83419200	-0.60065200
H	2.83966100	8.85690600	0.17161900
C	7.55170200	-0.32289900	-0.30342300
C	8.91993000	-0.51606700	-0.03645200
H	7.23817400	0.09015400	-1.25918500
H	9.65901600	-0.24486200	-0.78669900
C	-3.17056800	0.70298500	-1.12331600
C	-3.59639700	1.27894600	-2.34189800
C	-4.16558800	0.32762400	-0.19826800
C	-4.97289100	1.44965400	-2.57737000
H	-2.87314800	1.57617100	-3.09478400
C	-5.52580700	0.53622100	-0.50943000
H	-3.91338700	-0.10945700	0.76087800
N	-5.92679600	1.09108900	-1.68825000
H	-5.32658100	1.88529200	-3.50821200
C	-6.59872900	0.15388700	0.45160200
N	-6.20959800	-0.41140900	1.63032300
C	-7.95865000	0.37329700	0.14289000
C	-7.15900800	-0.76920600	2.52562300
C	-8.93607100	-0.00354300	1.08089300
H	-8.22719100	0.82499500	-0.80454400
C	-8.53514200	-0.58767800	2.30113800

H	-6.80074500	-1.21453500	3.44969000
C	-10.37161900	0.22714500	0.75597700
H	-9.26921300	-0.88593000	3.04003600
O	-11.22237800	-0.19263400	1.77209400
O	-10.80547000	0.73338100	-0.29104400
H	-12.16028000	-0.02641100	1.52578200
H	2.57290900	0.67757900	-0.15886600
H	0.81923400	-0.65351500	-0.30409500

Compound: **A6**

Basic set: B3LYP/LanL2DZ level

Total energy: -2429.56006389 A.U.

Alpha occ. Eigenvalues: -0.20343 and -0.19337

Alpha virt. Eigenvalues: -0.09304 and -0.09220

Table D6. Cartesian coordinates (in angstrom) of **A5** computed at the B3LYP/ LanL2DZ level.

Atoms	**x**	**y**	**z**
C	4.51837700	0.84656600	0.32877000
C	4.98385500	-0.48838100	0.40572400
C	4.17520700	-1.63892100	0.24266000
C	4.65856200	-3.01220400	0.30804300
H	5.68391900	-3.30271800	0.48111000
C	3.57780300	-3.83735500	0.10639200

H	3.56703300	-4.91695400	0.10189400
C	2.41348600	-2.98584600	-0.10121900
C	1.10013400	-3.45728100	-0.34380100
C	-0.03366900	-2.63196800	-0.53335600
C	-1.37128700	-3.11802900	-0.84771200
H	-1.64321100	-4.15609100	-0.96699300
C	5.33922700	2.02686500	0.56726300
H	6.38711900	2.01247400	0.82739400
C	6.44548800	-0.69816300	0.69135800
C	6.86891200	-1.25456900	1.92000000
H	6.12589200	-1.52420700	2.66660000
C	8.23673000	-1.44536100	2.18995300
H	8.54402600	-1.86717800	3.14407500
C	9.20470700	-1.08944000	1.23071600
C	0.89427900	-4.94576600	-0.40912500
C	1.43442300	-5.70536300	-1.47197900
H	1.99695100	-5.20155200	-2.25426800
C	1.23627200	-7.09716500	-1.53471400
H	1.65233200	-7.66389100	-2.36442300
C	0.49994600	-7.75414500	-0.52966600
C	-0.03965100	-7.00704800	0.53537900
H	-0.60646900	-7.50498300	1.31861700
C	0.15301400	-5.61422900	0.59195100
H	-0.26084300	-5.04218900	1.41884400

N	2.80294400	-1.64922500	-0.01162300
N	3.20998800	1.24741100	0.05462600
Zn	1.57857200	0.00509700	-0.21640500
C	-1.36242900	-0.83779100	-0.75660300
C	-1.82262300	0.49802900	-0.84008400
C	-1.01616700	1.65063300	-0.68208800
C	-1.49856000	3.02476400	-0.75188600
H	-2.52241500	3.32000500	-0.92673200
C	-0.41800500	3.84909600	-0.54745800
H	-0.40703900	4.92868100	-0.54404900
C	0.74515400	2.99738400	-0.33441100
C	2.05683800	3.46802800	-0.08814100
C	3.19082600	2.64152100	0.10417200
C	4.52604300	3.12655000	0.42932900
H	4.79612000	4.16419100	0.55678100
C	-2.18546600	-2.01961400	-0.98429800
H	-3.23627200	-2.01119000	-1.23286500
C	2.26300200	4.95626700	-0.01939900
C	3.01022700	5.62599900	-1.01521200
H	3.42839200	5.05498600	-1.84065000
C	3.20270900	7.01870200	-0.95579500
H	3.77360600	7.51777300	-1.73535700
C	2.65715800	7.76447300	0.10718000
C	1.91515200	7.10626000	1.10720300

H	1.49429000	7.67194700	1.93517900
C	1.71713300	5.71455800	1.04150300
H	1.15020000	5.20979600	1.81997700
N	0.35416900	1.66009900	-0.42348600
N	-0.05306200	-1.23679700	-0.48946800
H	10.26178200	-1.23896800	1.43755800
H	0.34869400	-8.83002300	-0.57611900
H	2.80794800	8.84032100	0.15571800
C	7.42522800	-0.34054300	-0.26286400
C	8.79322200	-0.53794700	0.00178800
H	7.11168600	0.07975100	-1.21540100
H	9.53216500	-0.26401700	-0.74763200
C	-3.28127000	0.70864800	-1.12823600
C	-3.71256600	1.27819400	-2.34770300
C	-4.27209800	0.34345200	-0.19472900
C	-5.08996000	1.45124300	-2.57684800
H	-2.99310700	1.56782300	-3.10729500
C	-5.63338100	0.55444800	-0.49921600
H	-4.01535800	-0.08972000	0.76492600
N	-6.03969700	1.10200500	-1.67978300
H	-5.44767300	1.88115600	-3.50885400
C	-6.70208500	0.18235900	0.47050600
N	-6.30786600	-0.36639200	1.65532700
C	-8.06360500	0.39432700	0.16338300

C	-7.25360000	-0.71504100	2.55810800
C	-9.03712100	0.02716800	1.10921700
H	-8.33620100	0.83304000	-0.78898000
C	-8.63089300	-0.54013700	2.33565000
H	-6.89130000	-1.14750200	3.48671300
C	-10.47425000	0.24977600	0.78578300
H	-9.36188200	-0.83082600	3.08059000
O	-11.32081800	-0.15875500	1.81007300
O	-10.91288000	0.74099400	-0.26638500
H	-12.25986800	0.00152300	1.56422900

Compound: **A7**

Basic set: B3LYP/LanL2DZ level

Total energy: -3451.21872543 A.U.

Alpha occ. Eigenvalues: -0.21942 and -0.20615

Alpha virt. Eigenvalues: -0.13714 and -0.12397

Table D7. Cartesian coordinates (in angstrom) of **A7** computed at the B3LYP/ LanL2DZ level.

Atoms	**x**	**y**	**z**
C	-7.36108600	1.18510300	0.22976300
C	-7.95574800	-0.09995600	0.26416100
C	-7.24367100	-1.32421600	0.21899000
C	-7.85640300	-2.64404800	0.28019500

H	-8.91505800	-2.83471800	0.37012100
C	-6.84224700	-3.56974000	0.21115800
H	-6.93208300	-4.64540600	0.21777400
C	-5.58960100	-2.83291400	0.12109900
C	-4.30550200	-3.42968800	0.03753700
C	-3.08821600	-2.71783000	-0.06678800
C	-1.76945500	-3.33373800	-0.06295300
H	-1.57759300	-4.39247400	0.02509000
C	-8.09968600	2.44019700	0.20427100
H	-9.17558100	2.52847000	0.20908200
C	-9.45455400	-0.16902800	0.35101400
C	-10.21723600	-0.67044800	-0.72855200
H	-9.71165400	-0.99817300	-1.63362500
C	-11.62065300	-0.72946500	-0.64851300
H	-12.19298000	-1.10871500	-1.49158400
C	-12.28253700	-0.29814100	0.51753500
C	-4.23073900	-4.93045500	0.07893000
C	-4.56391500	-5.63463300	1.25861000
H	-4.86898800	-5.08177500	2.14369200
C	-4.48111200	-7.03832000	1.30299800
H	-4.72770000	-7.56370800	2.22223400
C	-4.07509900	-7.76057100	0.16402700
C	-3.74717600	-7.06804300	-1.01758800
H	-3.43723300	-7.61781300	-1.90299800

C	-3.81901500	-5.66330100	-1.05741900
H	-3.57035600	-5.13305300	-1.97370000
N	-5.85861400	-1.46556900	0.12403500
N	-5.99297600	1.45682700	0.17529200
Zn	-4.47033700	0.06466500	0.02871400
C	-1.57994600	-1.06203500	-0.19545700
C	-0.98897400	0.22938900	-0.22242800
C	-1.69494700	1.45990200	-0.15827200
C	-1.08720600	2.78517500	-0.22109200
H	-0.03352500	2.99699600	-0.32423500
C	-2.10407400	3.70554900	-0.14346600
H	-2.01569800	4.78129300	-0.14561000
C	-3.35482100	2.96571500	-0.05344700
C	-4.63483100	3.55862500	0.03556900
C	-5.85641300	2.84240900	0.12783800
C	-7.17654700	3.45705000	0.14246600
H	-7.36871700	4.51798300	0.08933700
C	-0.84378300	-2.32087800	-0.13954700
H	0.23052000	-2.42643900	-0.10707800
C	-4.71158400	5.05998200	0.02352900
C	-5.12404800	5.76688200	1.17610300
H	-5.37633600	5.21647800	2.07922300
C	-5.19127100	7.17223500	1.16938400
H	-5.49946300	7.70114600	2.06787400

C	-4.85782800	7.89192800	0.00549600
C	-4.45279400	7.19578600	-1.14990400
H	-4.19879800	7.74249000	-2.05474000
C	-4.37568100	5.79090800	-1.13891900
H	-4.06989100	5.25812400	-2.03613600
N	-3.07647000	1.59475400	-0.06312300
N	-2.94440500	-1.32826500	-0.14053200
H	-13.36671800	-0.34778800	0.58150100
H	-4.01303200	-8.84538100	0.19786500
H	-4.91207000	8.97770900	-0.00074400
C	-10.12796000	0.26762900	1.51478800
C	-11.53063400	0.19818500	1.60009100
H	-9.55174800	0.64542700	2.35584900
H	-12.03223100	0.52851700	2.50637900
C	5.01307500	-1.66158600	-4.67027000
C	3.61579400	-1.81666400	-4.82117800
C	2.79822300	-1.34926900	-3.77324400
C	3.36601700	-0.75554700	-2.63230800
C	5.53022700	-1.06458200	-3.51631600
C	2.58167500	-0.21460400	-1.50018300
C	1.18413400	-0.27894300	-1.41324400
C	0.49759800	0.29447700	-0.31857500
C	1.28546600	0.92556800	0.67404500
C	2.67669700	0.94532600	0.55189100

H	5.69655100	-1.99688000	-5.44428100
H	6.59435000	-0.92478000	-3.37274600
H	0.82142300	1.37123500	1.54658900
H	3.29761300	1.40950000	1.30738600
N	4.72737500	-0.62577200	-2.51219500
N	3.32099700	0.38842000	-0.50719400
Ru	5.38806200	0.34884800	-0.77775700
N	5.40043000	-1.30273000	0.47297500
N	5.89372600	1.23561400	1.04092800
C	5.14680300	-2.58129400	0.07649600
C	5.09852200	-3.63992800	0.98264900
C	5.32502300	-3.38227500	2.35117900
C	5.61915600	-2.06727800	2.75551800
C	5.64767900	-1.03582600	1.80503600
C	5.93699700	0.37794100	2.11906000
C	6.24239800	0.85647300	3.40194300
C	6.51632000	2.22333400	3.58633200
C	6.49349300	3.08021100	2.46996700
C	6.18277600	2.55332800	1.21098100
C	5.23610900	-4.51823300	3.36379100
C	6.83197600	2.76684700	4.97709700
O	4.61106200	-5.57522800	2.97555600
O	5.78186800	-4.32073800	4.50956600
O	7.08027400	4.02629300	5.06971800

O	6.81400400	1.92548600	5.95104400
H	4.98588000	-2.73528500	-0.98312000
H	4.87553800	-4.65303100	0.66557200
H	5.82374500	-1.88663800	3.80500300
H	6.27612600	0.20817400	4.27129100
H	6.71506500	4.13360700	2.60522400
H	6.15403200	3.16845400	0.32060200
N	7.32002900	0.10024100	-1.15555900
N	5.23794100	2.07161000	-1.78972100
C	8.49465800	-0.07294300	-1.32828500
C	5.01134600	3.06119100	-2.42838300
S	10.11316300	-0.31499500	-1.59824000
S	4.71623400	4.44423400	-3.30064000
H	1.72110500	-1.44360000	-3.85627600
H	0.61041500	-0.75236900	-2.20071700
C	3.02767200	-2.43691300	-6.06821700
H	3.09434500	-1.73845900	-6.91361300
H	3.57176800	-3.34484700	-6.35435600
H	1.97308200	-2.69787500	-5.93350500

VITAE

Miss Preeyanut Duanglaor was born on August 17th, 1982 in Saraburi Province, Thailand. She finished secondary School at Bodindecha (Sing Singhaseni) School. She was a student under The Development and Promotion of Science and Technology Talent Project (DPST) from 1998-2003. She graduated and received a Bachelor's degree from Department of Chemistry, Faculty of Science, Chulalongkorn University in 2004. After that she continued her docterate degree in major of Organic Chemistry at Department of Chemistry, Faculty of Science, Chulalongkorn University and completed the program in 2012. During this period, her financial support is granted by The Royal Jubilee Ph. D. Program (RGJ) (Grant No. PHD/0226/2549; 3.C.CU/49/W.1) from the Thailand Research Fund (TRF). Her address is 45/1 Moo 4, Pokaoton, Muang District, Lopburi, Thailand 10500.